Brookhaven National Laboratory

From Heavy Ion Physics to the Electron Ion Collider

The 2022 CFNS Summer School on the Physics of the Electron-Ion Collider

Björn Schenke, Brookhaven National Laboratory

07/15/2022

U.S. DEPARTMENT OF ENERGY | Office of Science

Three lectures

- Lecture 1: Introduction to saturation - theory basics, experimental observables
  based heavily on "*Mining for Gluon Saturation at Colliders*"
  by Astrid Morreale and Farid Salazar, Universe 7 (2021) 8, 312
- Lecture 2: The Color Glass Condensate and applications to heavy ion collisions
- Lecture 3: Applications to physics in ultra-peripheral HICs and at the Electron Ion Collider

Science goals of the Electron Ion Collider

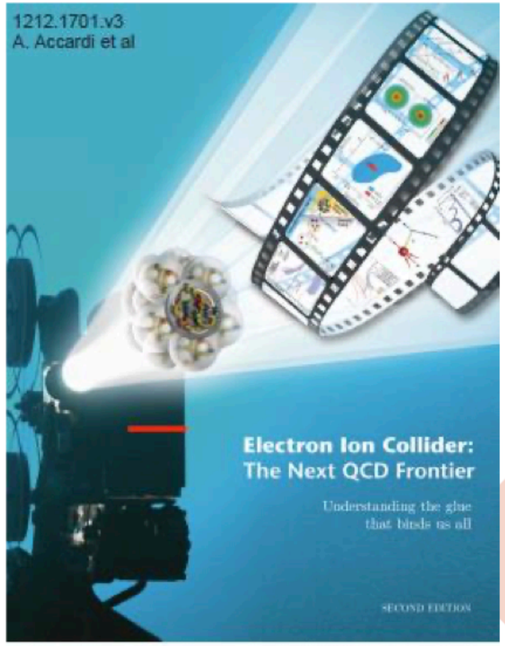

White paper
arXiv:1212.1701

Origin of nucleon mass

Origin of nucleon spin

Gluon saturation

Nucleon tomography

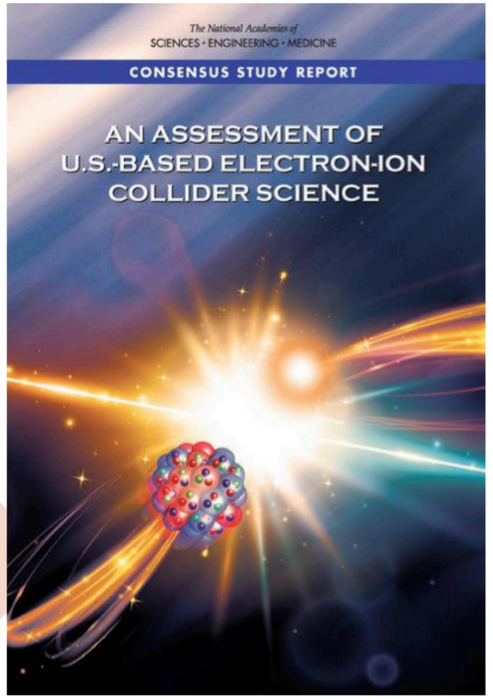

NAS report
July 2018

Science goals of the Electron Ion Collider

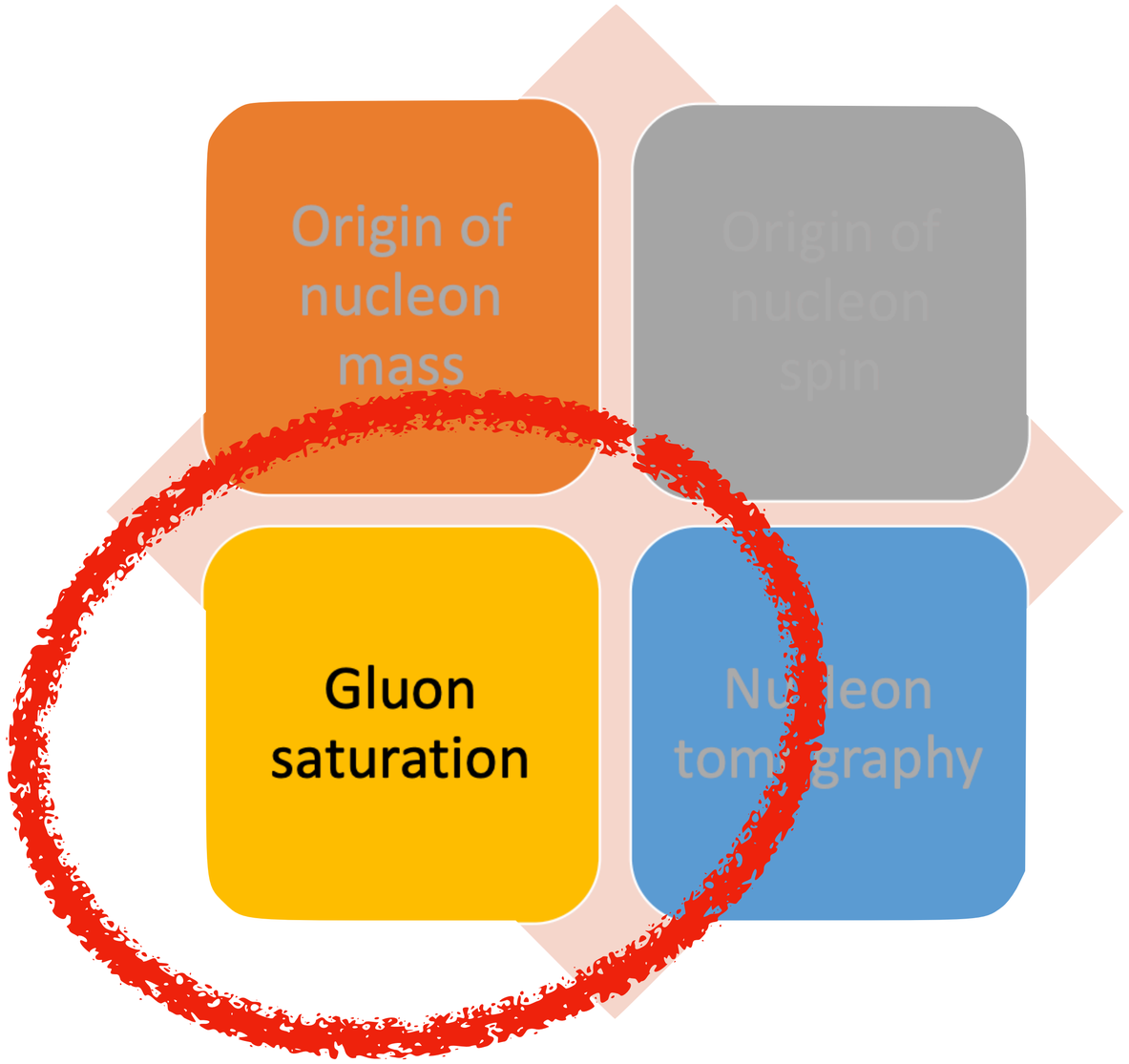

The boosted proton

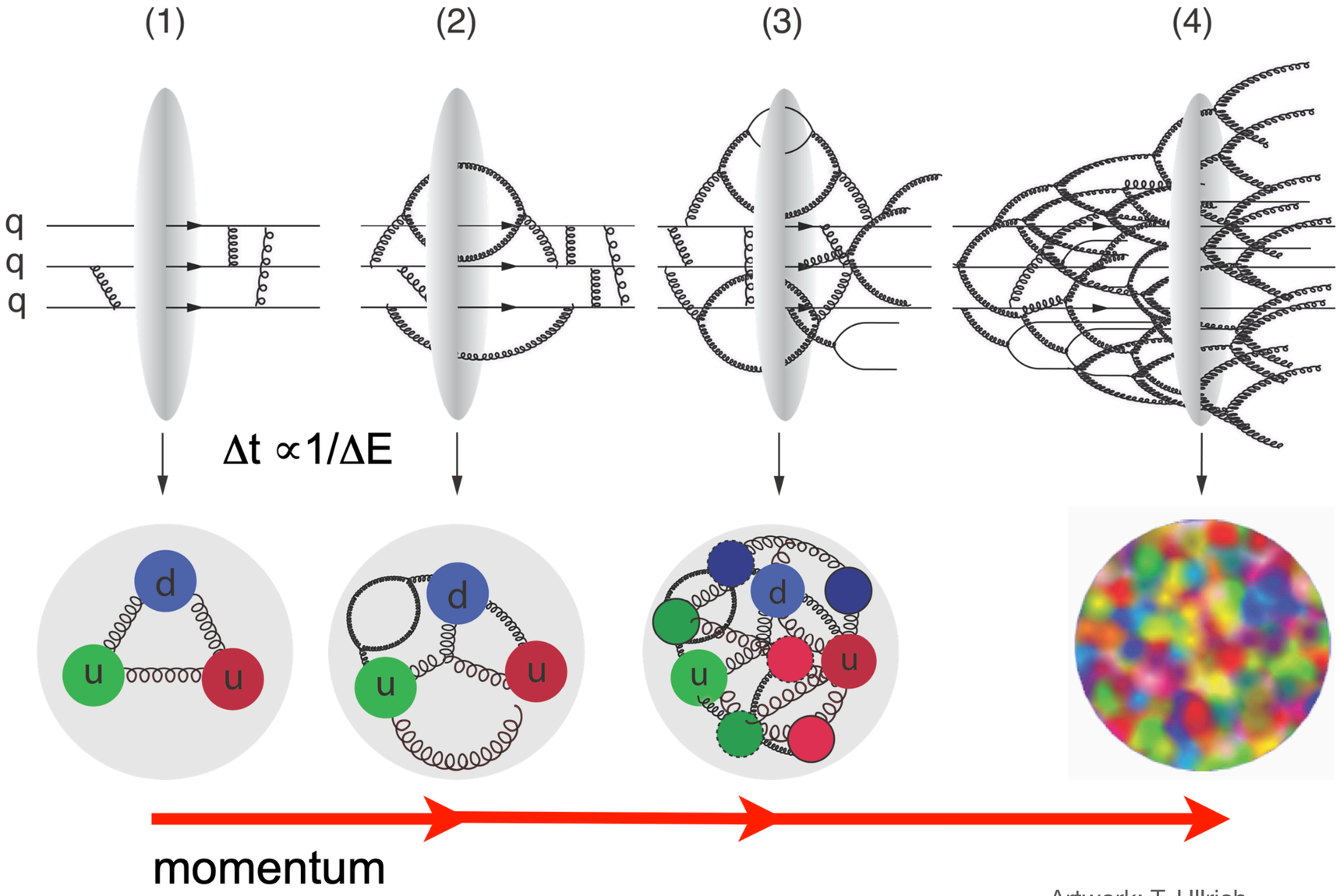

Artwork: T. Ullrich

Saturation

Explosive growth of gluon density violates unitarity

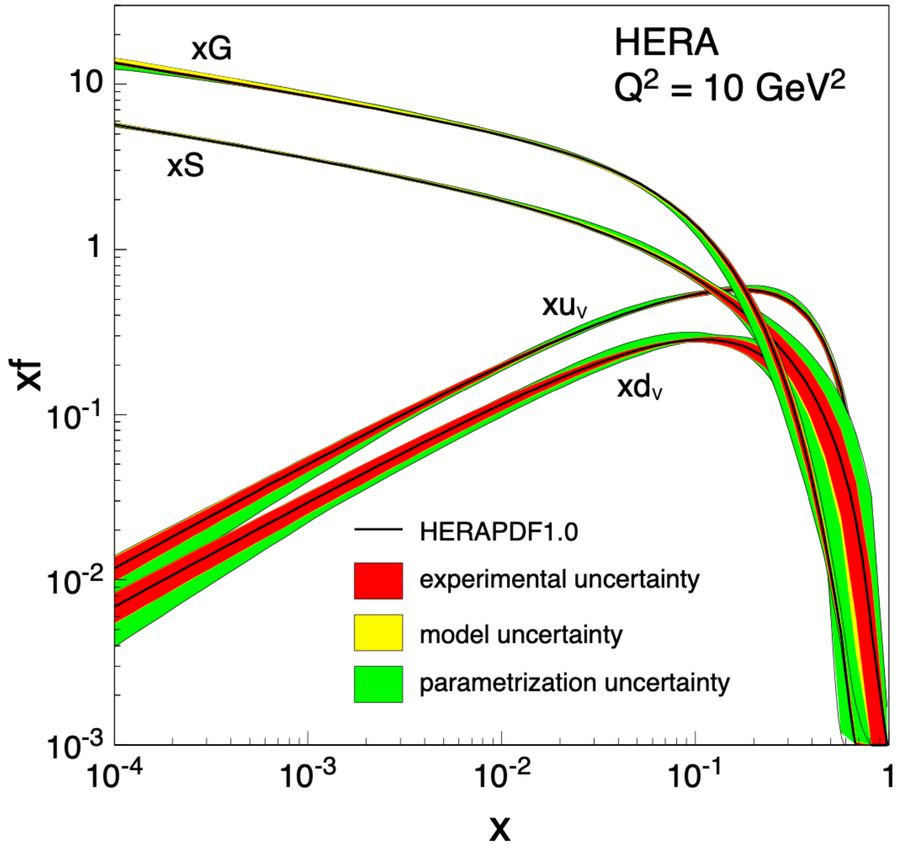

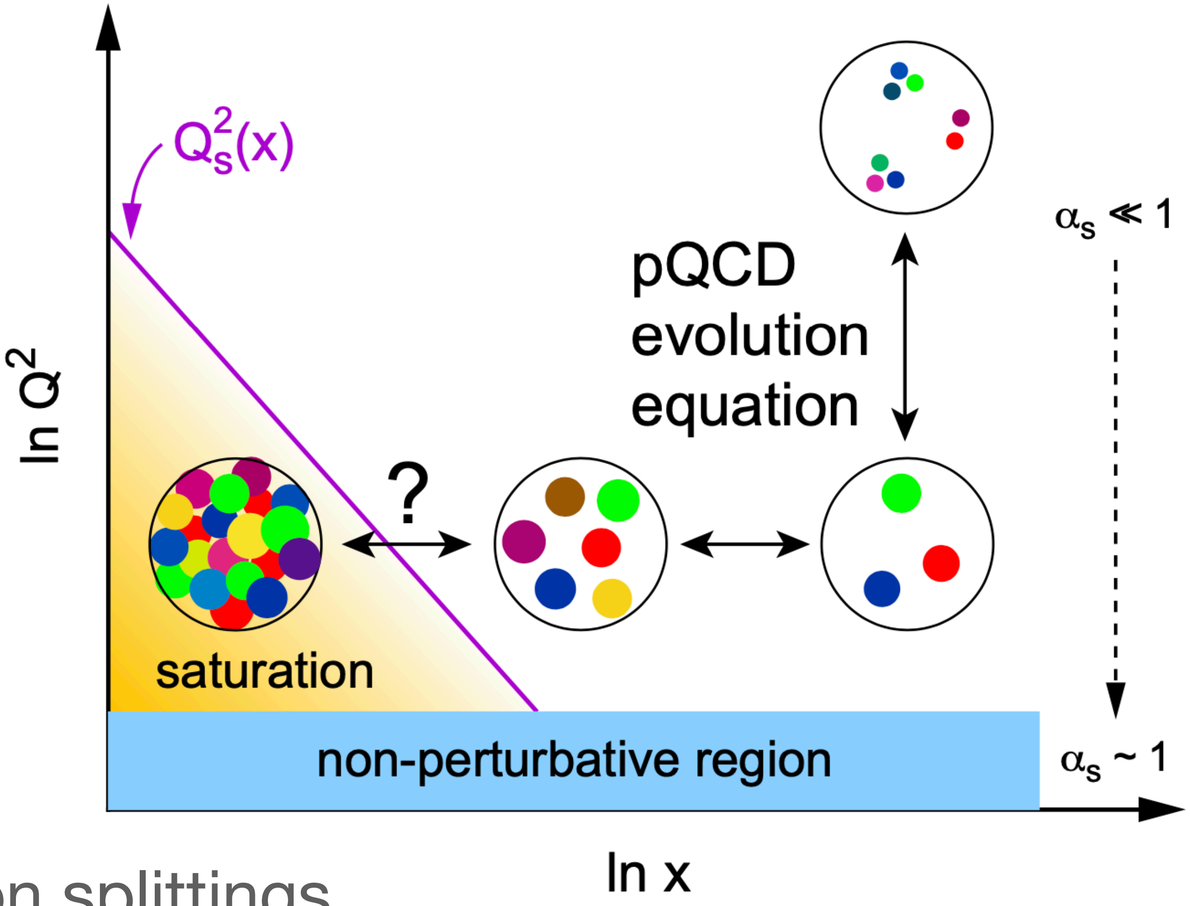

BUT: Recombination will balance gluon splittings

Need non-linear evolution equations at low *x* and low to moderate Q^2

Saturation of gluon densities is characterized by the scale $Q_s(x)$

The boosted proton

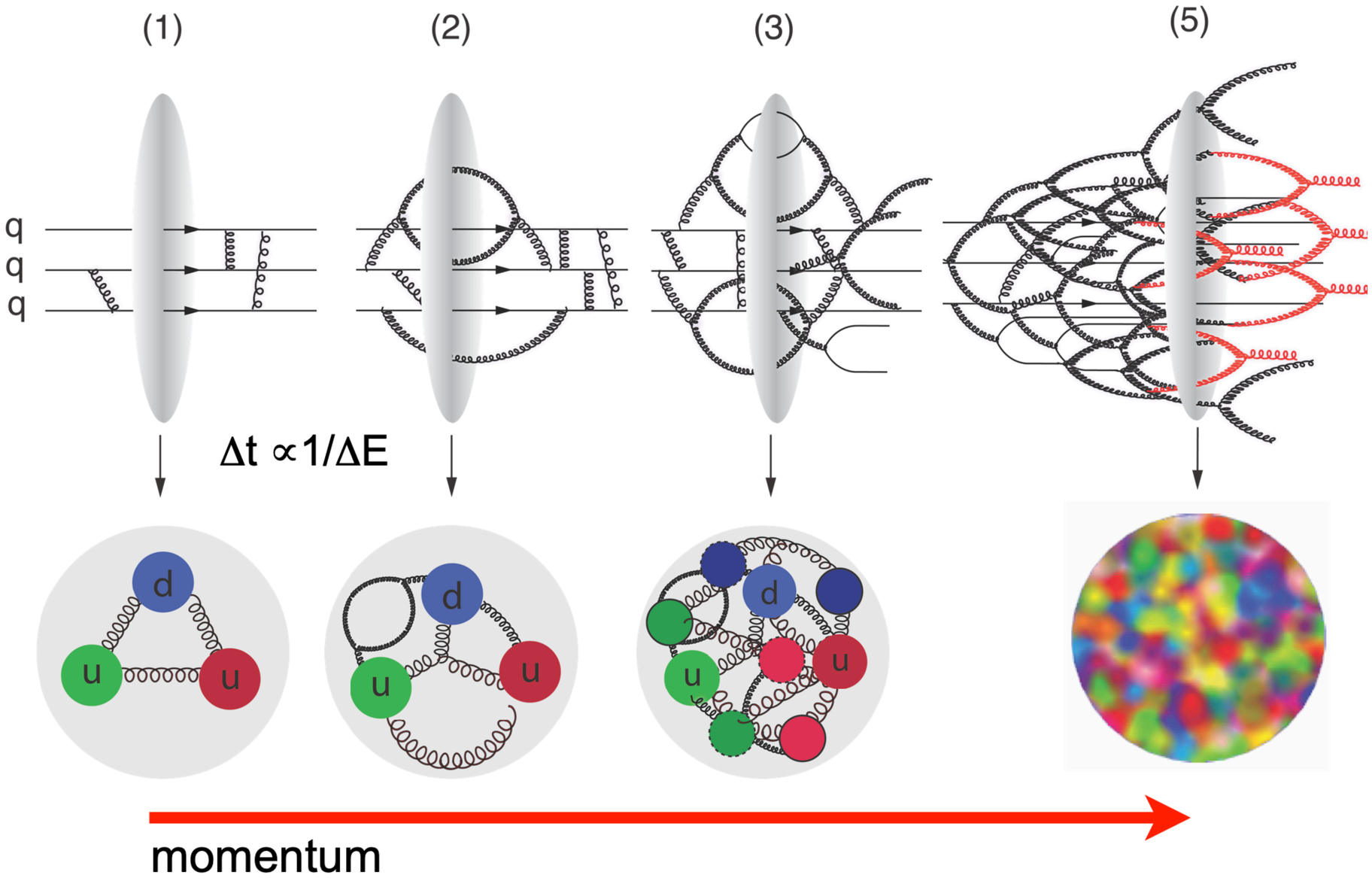

Light cone

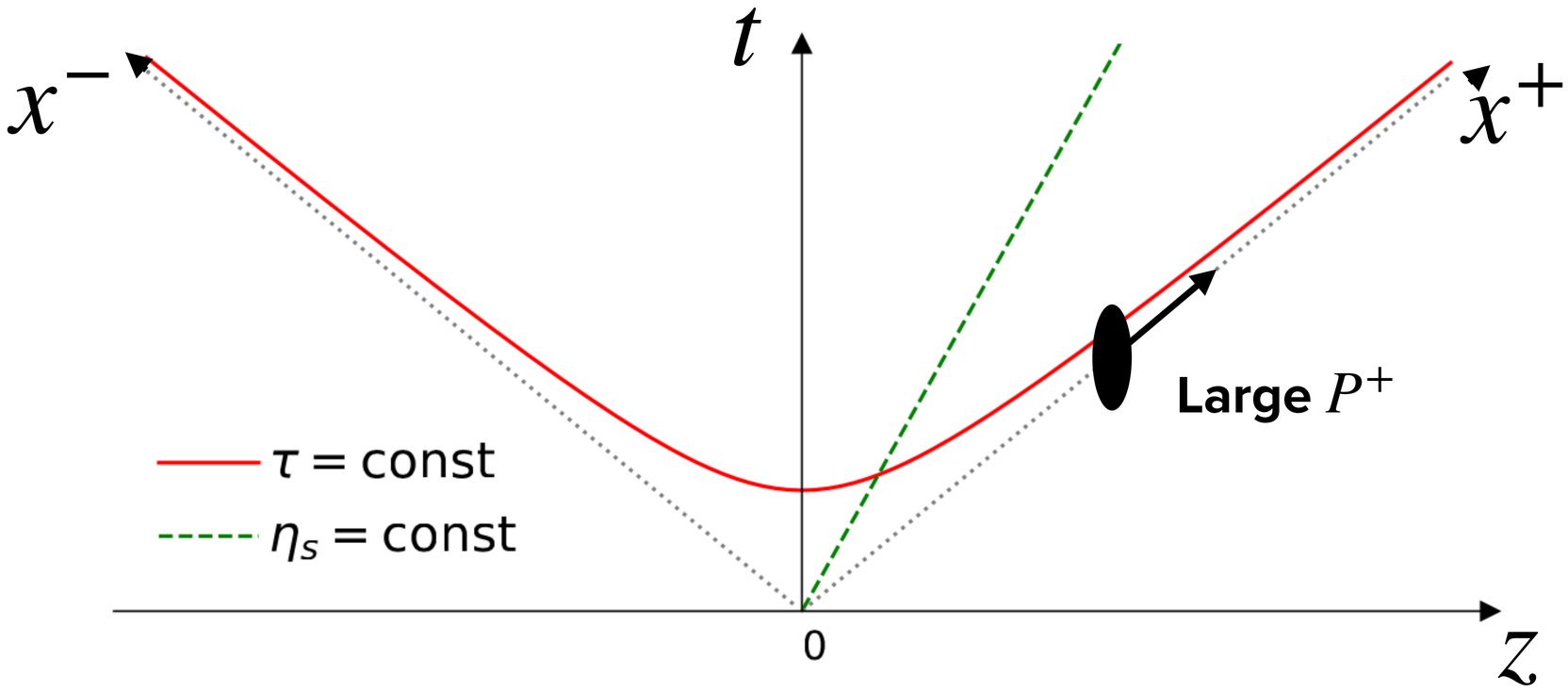

Light cone coordinates $v^{\pm} = (v^0 \pm v^3)/\sqrt{2}$

In the future light cone define $x^+ = \dfrac{\tau}{\sqrt{2}} e^{+\eta}$, and $x^- = \dfrac{\tau}{\sqrt{2}} e^{-\eta}$

or inverted $\tau = \sqrt{2x^+x^-}$, and $\eta = \dfrac{1}{2} \ln\left(\dfrac{x^+}{x^-}\right)$.

Light cone

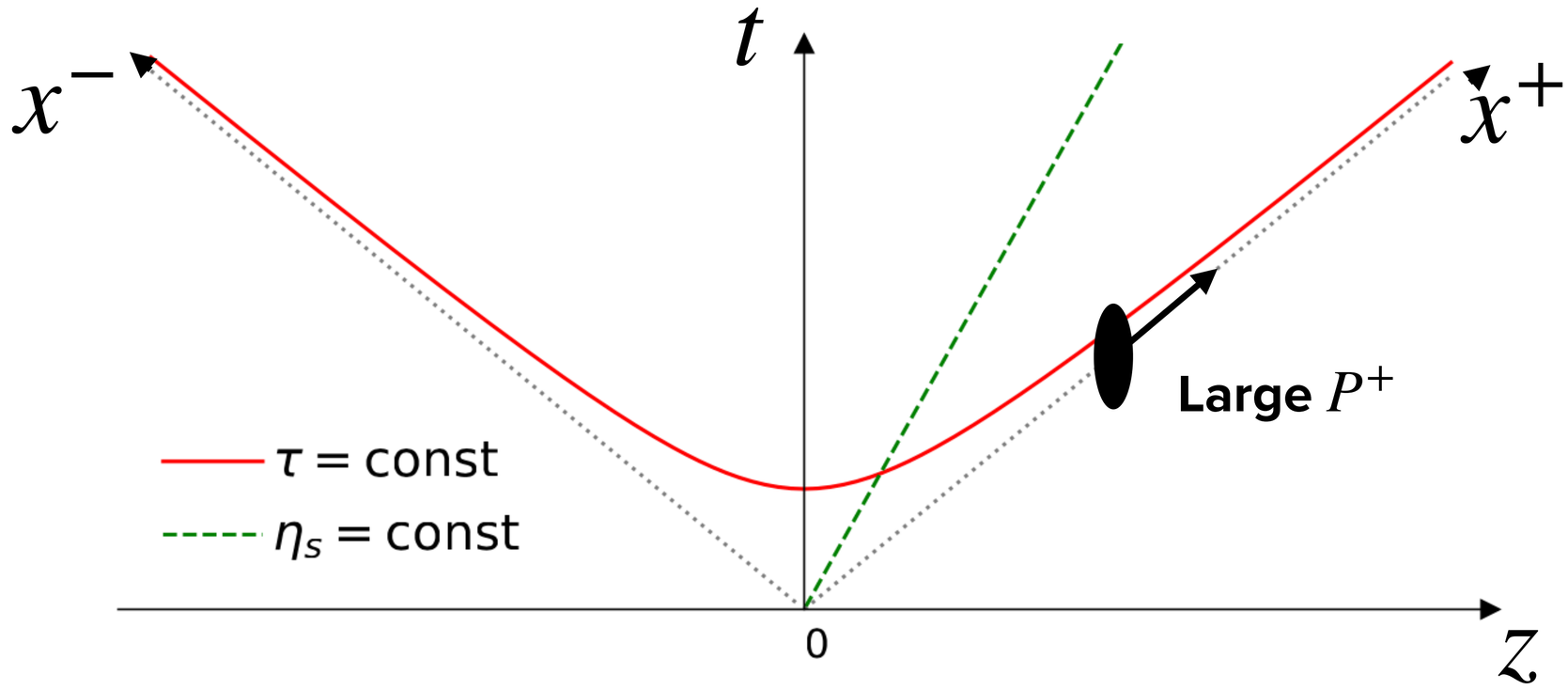

Probe hadron (or nucleus) moving with large P^+ at scale $x_0 P^+$ with $x_0 \ll 1$

Separate partonic content based on longitudinal momentum $k^+ = xP^+$

Large $x > x_0$: Static and localized color sources ρ

Color sources

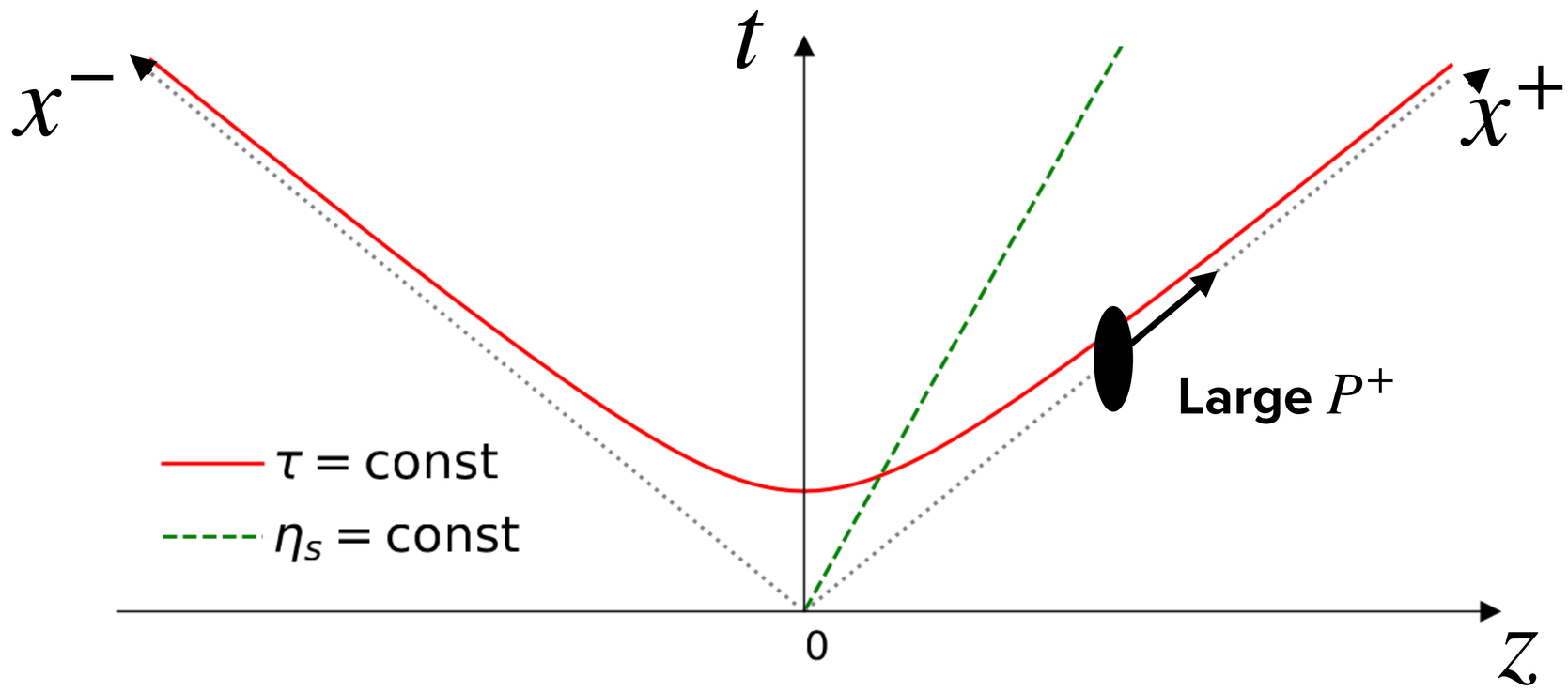

How localized are these sources? $\Delta z^- \sim \frac{1}{k^+} = \frac{1}{xP^+}$

What is the resolution scale of the probe? $\frac{1}{x_0 P^+} > \frac{1}{xP^+}$ **for** $x > x_0$

→Look fully localized in z^- **to the probe**

Color sources

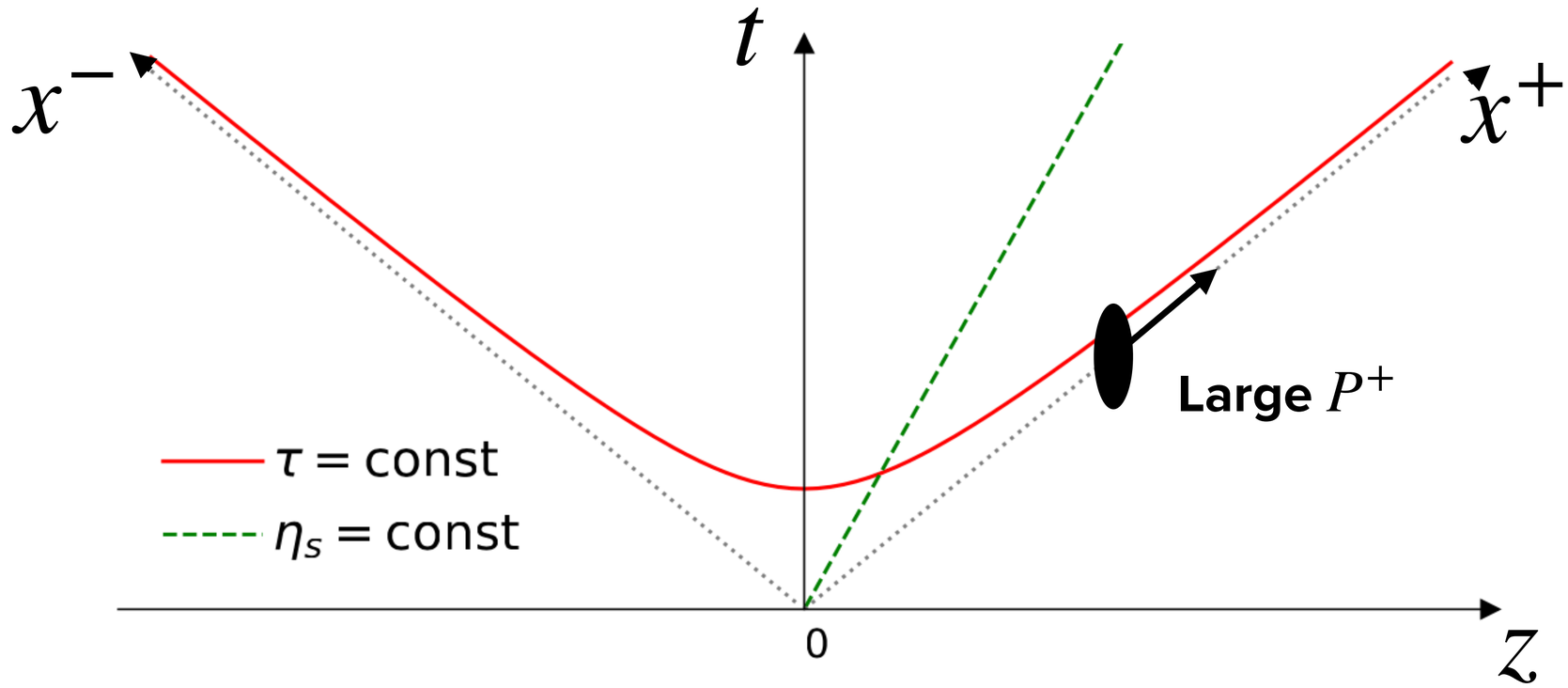

How fast do they evolve? $\Delta z^+ \sim \frac{1}{k^-} = \frac{2k^+}{k_T^2} = \frac{2xP^+}{k_T^2}$ **(because** $a_\mu b^\mu = a^+b^- + a^-b^+ - \vec{a}_T \cdot \vec{b}_T$**)**

What is the time scale of the probe? $\tau \approx \frac{2x_0P^+}{k_T^2} < \frac{2xP^+}{k_T^2}$

→Look static in light cone time z^+ **to the probe**

Dynamic color fields

The moving color sources generate a current, independent of light cone time z^+:

$$J^{\mu,a}(z) = \delta^{\mu+}\rho^a(z^-, z_T)$$

a is the color index of the gluon
the name “color” comes from this

This current generates delocalized dynamical fields $A^{\mu,a}(z)$ described by the Yang-Mills equations

$$[D_\mu, F^{\mu\nu}] = J^\nu$$

with $D_\mu = \partial_\mu + igA_\mu$ and $F_{\mu\nu} = \frac{1}{ig}[D_\mu, D_\nu] = \partial_\mu A_\nu - \partial_\nu A_\mu + ig[A_\mu, A_\nu]$

These fields are the small $x < x_0$ degrees of freedom

They can be treated classically, because their occupation number is large $\langle AA \rangle \sim 1/\alpha_s$

the name “condensate” comes from this scaling

Color Glass Condensate: Sources and fields

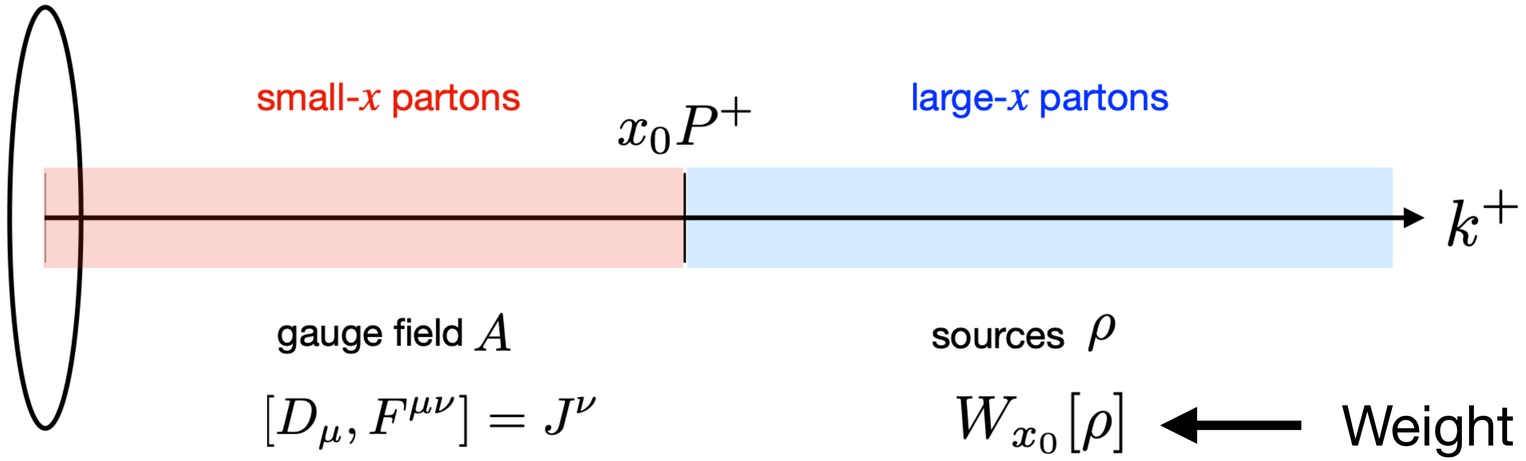

Two steps to compute expectation value of an observable $\mathcal{O}$:

1) Compute quantum expectation value $\mathcal{O}[\rho] = \langle \mathcal{O} \rangle_\rho$ for sources drawn from a given $W_{x_o}[\rho]$

2) Average over all possible configurations given the appropriate gauge invariant weight functional $W_{x_o}[\rho]$ this situation is similar to spin glasses - the name “glass” comes from this

When $x \lesssim x_0$ the path integral $\langle \mathcal{O} \rangle_\rho$ is dominated by classical solution and we are done

For smaller x we need to do quantum evolution

Weight functional

https://arxiv.org/pdf/hep-ph/0406169.pdf

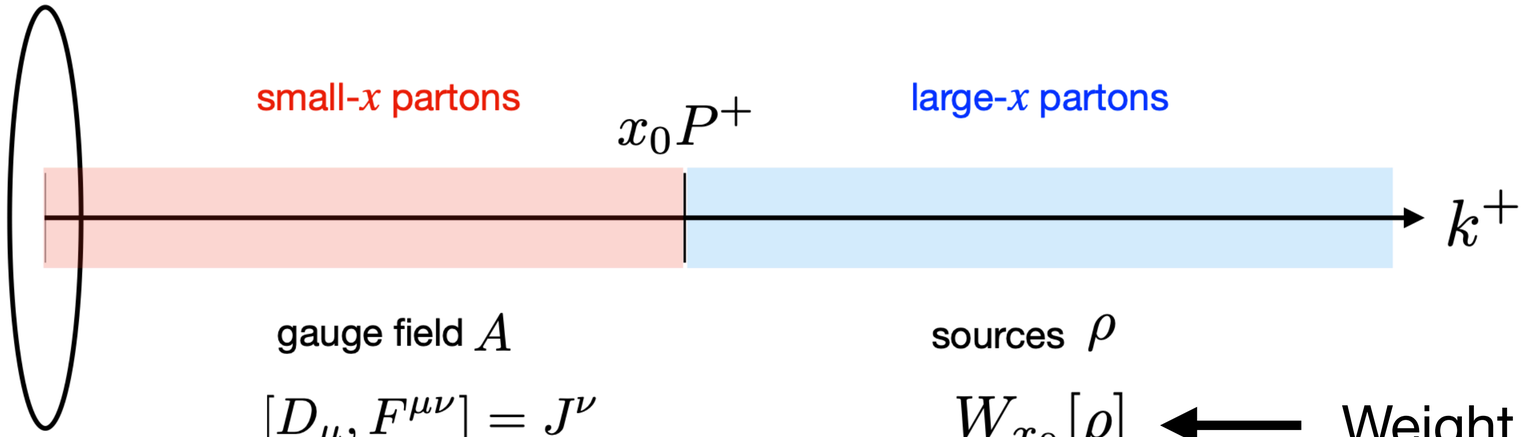

What is the weight functional?

Need to model. E.g. the McLerran-Venugopalan model:

Assume a large nucleus, invoke central limit theorem. All correlations of ρ^a are Gaussian

$$W_{x_0}[\rho] = \mathcal{N} \exp\left(-\frac{1}{2} \int dx^- d^2x_T \frac{\rho^a(x^-, x_T)\rho^a(x^-, x_T)}{\lambda_{x_0}(x^-)} \right)$$

where $\lambda_{x_0}(x^-)$ is related to the transverse color charge density distribution of the nucleus

Weight functional

https://arxiv.org/pdf/hep-ph/0406169.pdf

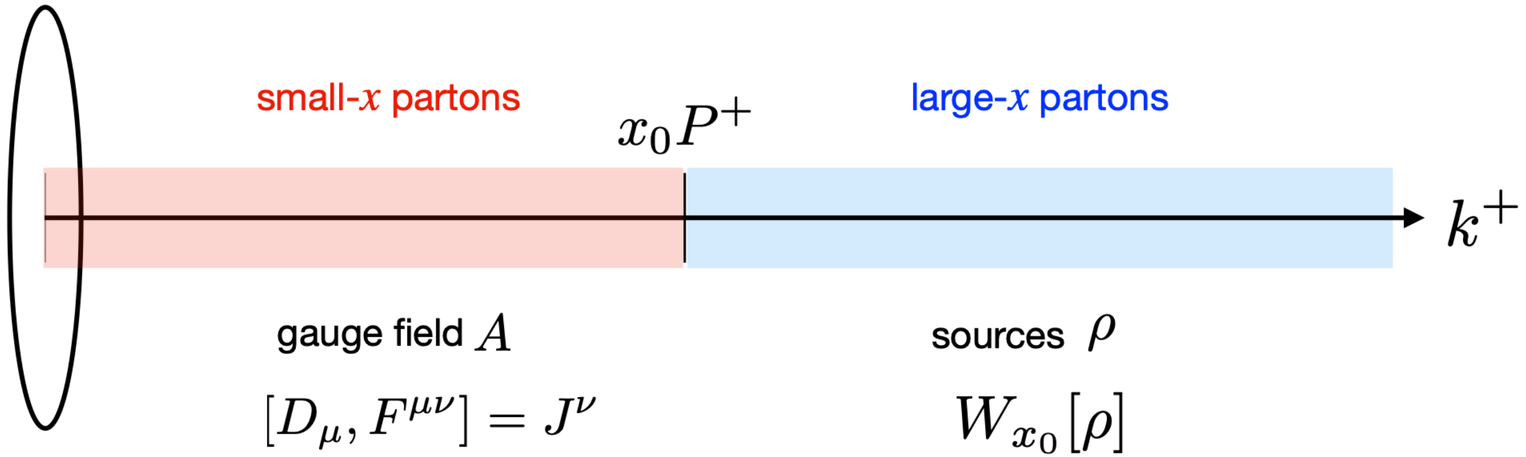

…where $\lambda_{x_0}(x^-)$ is related to the transverse color charge density distribution of the nucleus

$$\mu^2 = \int dx^- \lambda_{x_0}(x^-) = \frac{(g^2 C_F)(A N_c)}{\pi R_A^2} \frac{1}{N_c^2 - 1} = \frac{g^2 A}{2\pi R_A^2} \sim A^{1/3}$$

That color charge density is related to Q_s, the saturation scale.

normalized per color degree of freedom

Wilson lines

Interaction of high energy color-charged particle with large k^- momentum (and small $k^+ = \dfrac{k_T^2}{2k^-}$)

with a classical field of a nucleus can be described in the **eikonal approximation:**

The scattering rotates the color, but keeps k^-, transverse position $\overrightarrow{x}_T$, and any other quantum numbers the same.

The color rotation is encoded in a light-like Wilson line, which for a quark reads

$$V_{ij}(\overrightarrow{x}_T) = \mathscr{P}\left(ig \int_{-\infty}^{\infty} A^{+,c}(z^-, \overrightarrow{x}_T)\, t^c_{ij}\, dz^- \right)$$

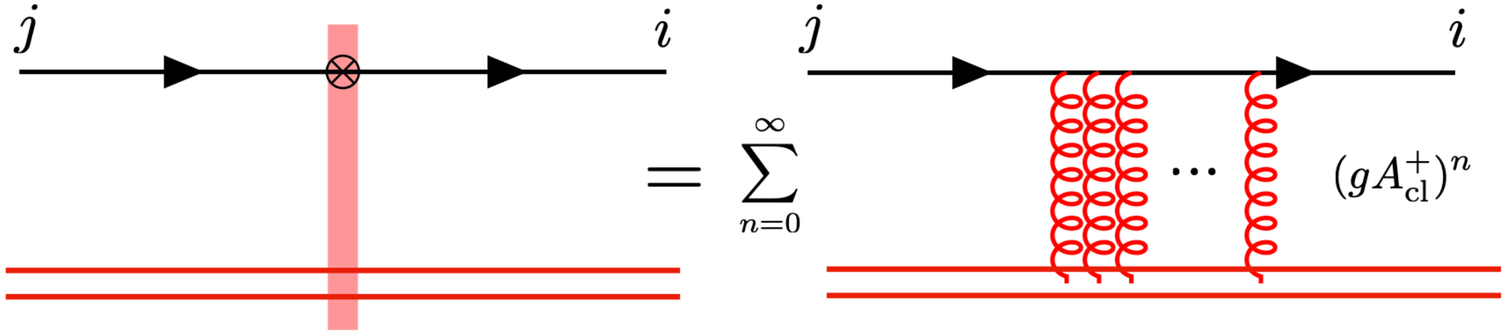

MULTIPLE INTERACTIONS NEEDED TO BE RESUMMED, BECAUSE $A^+ \sim 1/g$

Wilson lines

Interaction of high energy color-charged particle with large k^- momentum (and small $k^+ = \frac{k_T^2}{2k^-}$)

with a classical field of a nucleus can be described in the **eikonal approximation:**

The scattering rotates the color, but keeps k^-, transverse position $\overrightarrow{x}_T$, and any other quantum numbers the same.

The color rotation is encoded in a light-like Wilson line, which for a quark reads

$$V_{ij}(\overrightarrow{x}_T) = \mathscr{P}\left(ig \int_{-\infty}^{\infty} A^{+,c}(z^-, \overrightarrow{x}_T)\, t^c_{ij}\, dz^- \right)$$

path ordering
(for the lattice formulation we actually use anti-path ordering)

SU(3) generator (fundamental rep.)

Wilson lines

For a gluon interacting with the target, we have

$$U_{ab}(\overrightarrow{x}_T) = \mathscr{P}\left(ig \int_{-\infty}^{\infty} A^{+,c}(z^-, \overrightarrow{x}_T)\, T^c_{ab}\, dz^- \right)$$

SU(3) generator (adjoint rep.)

Wilson lines and correlators

$$U_{ab}(\overrightarrow{x}_T) = \mathscr{P}\left(ig \int_{-\infty}^{\infty} A^{+,c}(z^-, \overrightarrow{x}_T)\, T^c_{ab}\, dz^- \right)$$ gluon scattering

$$V_{ij}(\overrightarrow{x}_T) = \mathscr{P}\left(ig \int_{-\infty}^{\infty} A^{+,c}(z^-, \overrightarrow{x}_T)\, t^c_{ij}\, dz^- \right)$$ quark scattering

These Wilson lines are the building blocks of the CGC. At the EIC for example, cross sections will be calculated as convolutions of Wilson line correlators with perturbatively calculable and process-dependent impact factors

In heavy ion collisions, one can compute particle production by determining Wilson lines after the collision from the Wilson lines of the colliding nuclei. We will get to that next time.

Everything is Wilson lines + some perturbative, process dependent stuff

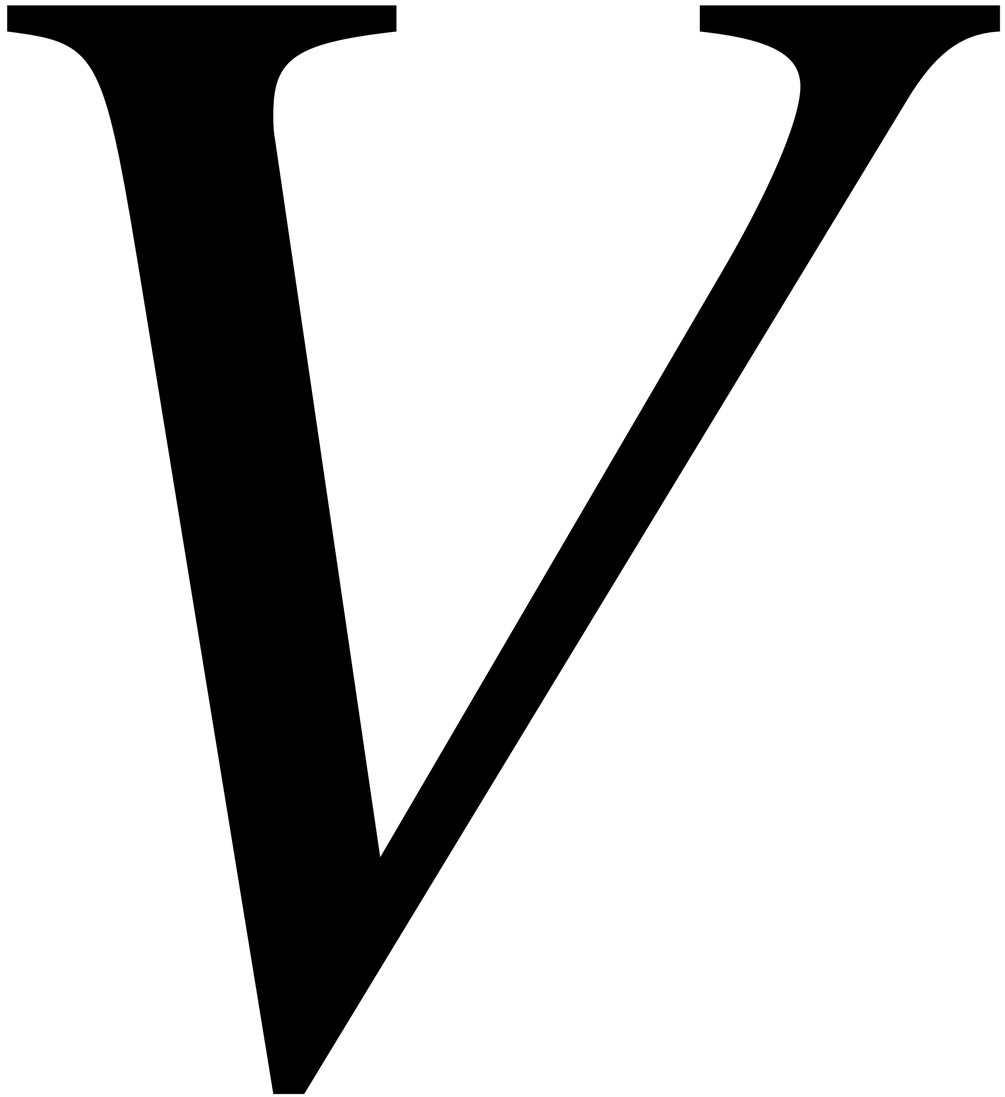

Dipole correlator

$$S^{(2)}_{x_0}(\vec{x}_T, \vec{y}_T) = \frac{1}{N_c}\left\langle \mathrm{Tr}\left[V(\vec{x}_T)V^\dagger(\vec{y}_T)\right]\right\rangle_{x_0}$$

Dipole correlator is the simplest and most important

It appears for example in the deep inelastic scattering (DIS) cross section at small x …

$eA \to e + X$

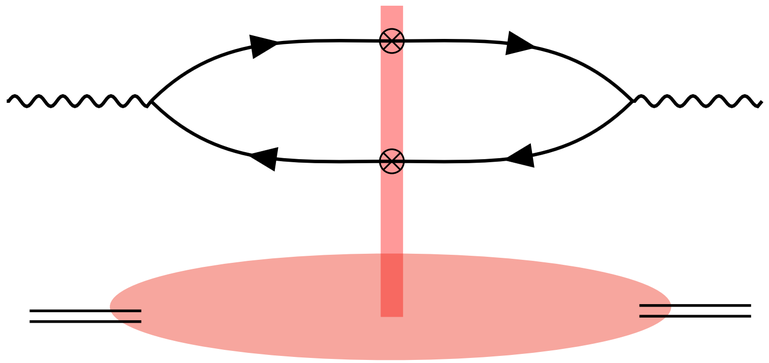

$pA \to h + X$

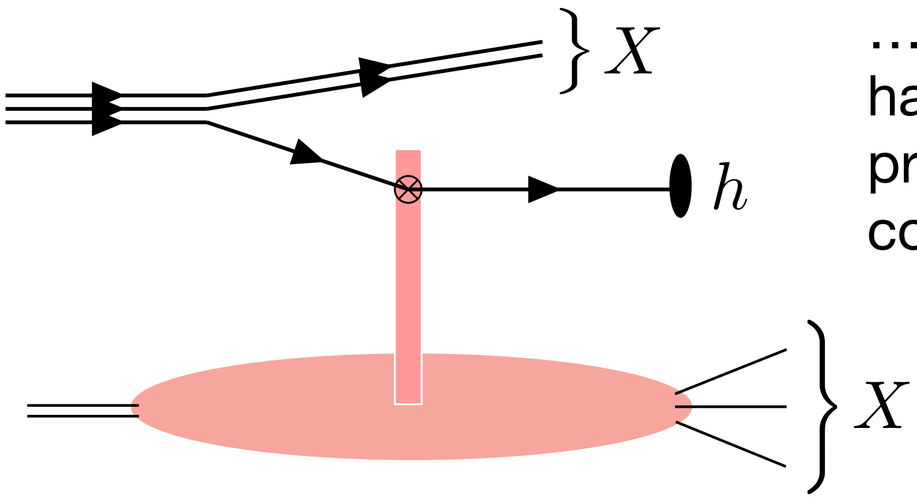

… and also in hadron production in p+A collisions

Dipole correlator in the MV model

$$S_{x_0}^{(2)}(r_T) = \exp\left[-\frac{1}{4}\alpha_s C_F \mu^2 r_T^2 \ln\left(\frac{1}{\Lambda r_T} + e\right)\right]$$

depends only on the dipole size $r_T = |\vec{x}_T - \vec{y}_T|$

Λ is an infrared cutoff

Small r_T: scattering matrix is close to unity, i.e. there is no scattering

Makes sense: an infinitesimally small dipole is a color neutral object

Mathematically this follows from the unitarity of the Wilson lines $V(\vec{x})V^\dagger(\vec{x}) = 1$

Large r_T: Wilson lines decorrelate, correlator goes to zero as it should in the black disk limit

Dipole amplitude and saturation scale

$$D_{x_0}(r_T) = 1 - S^{(2)}_{x_0}(r_T) = 1 - \exp\left[-\frac{1}{4}\alpha_s C_F \mu^2 r_T^2 \ln\left(\frac{1}{\Lambda r_T} + e\right)\right]$$

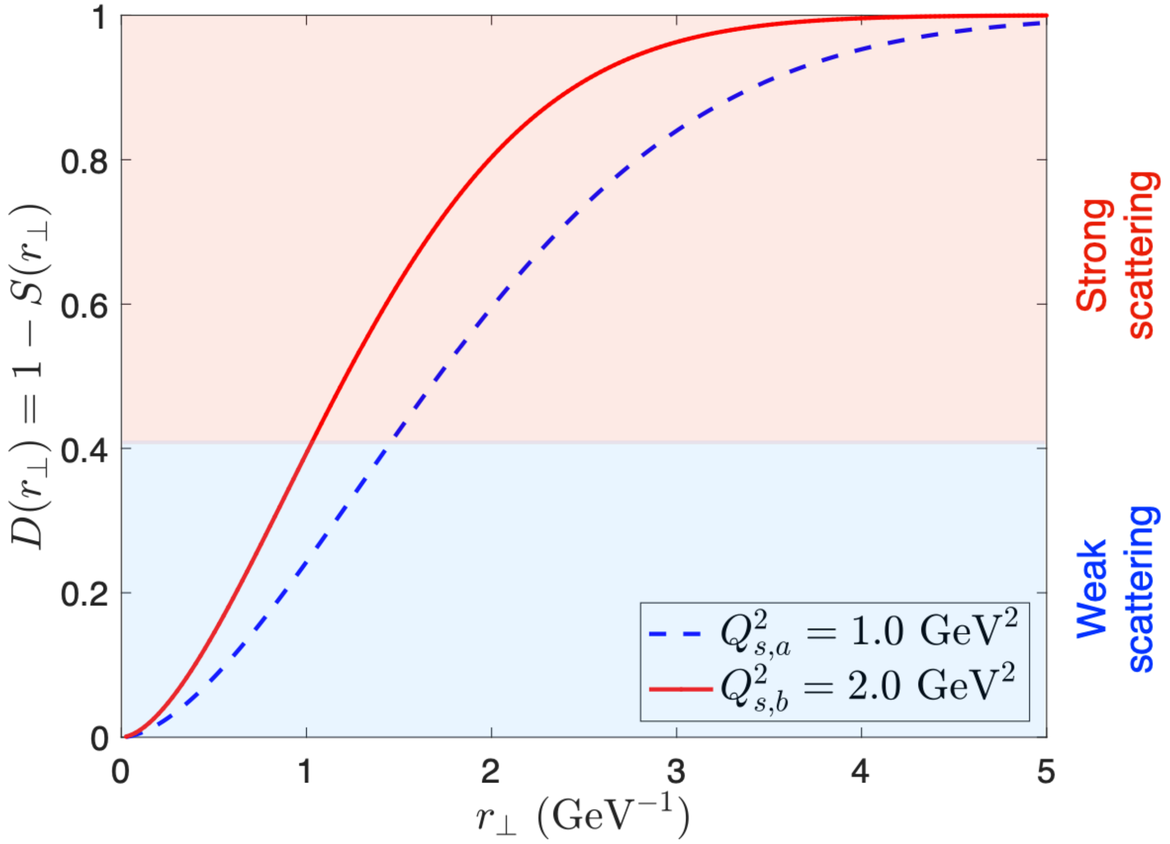

The transition between the weak and strong scattering regimes defines the saturation scale

$$Q_s^2 = \frac{2}{r_{T,s}^2}$$

where

$$S^{(2)}_{x_0}(r_{T,s}) = \exp(-c)$$

with c a constant usually chosen to be $1/2$

Dipole amplitude and saturation scale

$$D_{x_0}(r_T) = 1 - S^{(2)}_{x_0}(r_T) = 1 - \exp\left[-\frac{1}{4}\alpha_s C_F \mu^2 r_T^2 \ln\left(\frac{1}{\Lambda r_T} + e\right)\right]$$

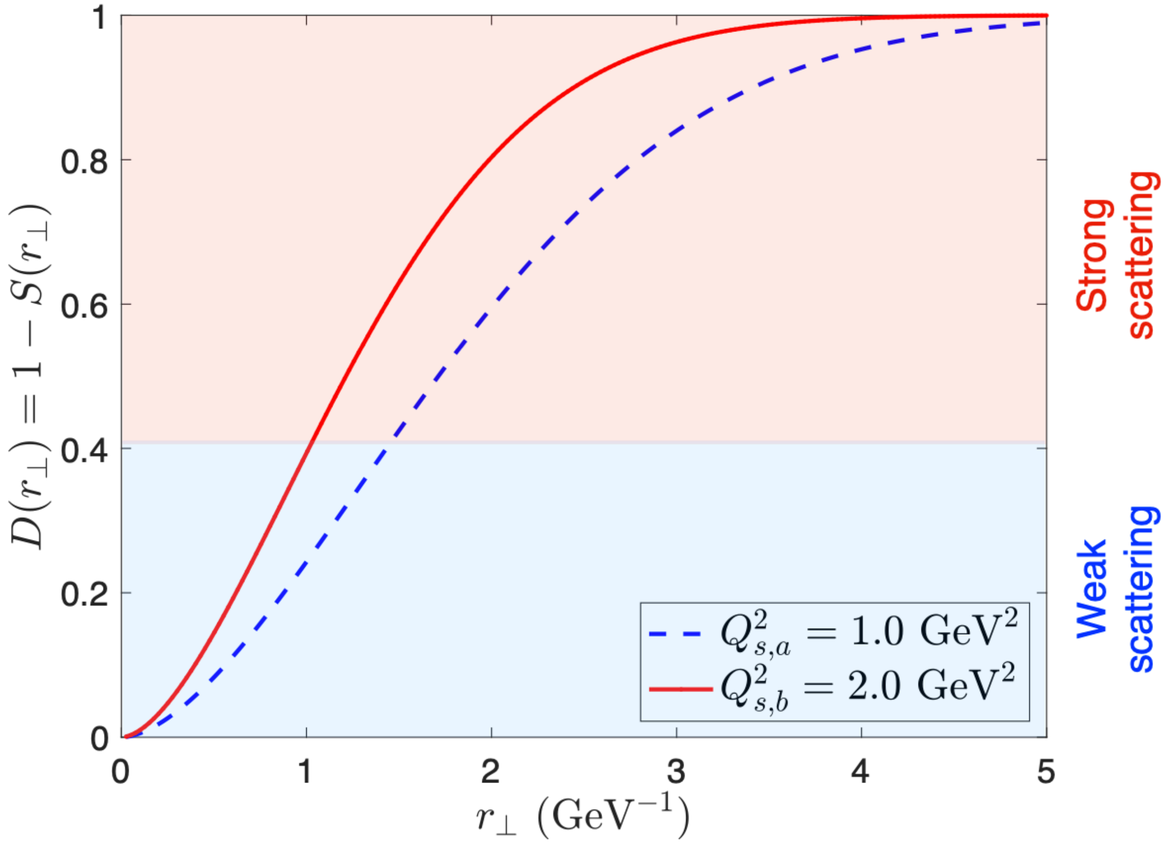

The form above shows $Q_s^2 \sim \mu^2 \sim A^{1/3}$

So Q_s gains a nuclear *oomph* factor when scattering off large nuclei compared to protons

Total DIS cross section

The dipole amplitude appears e.g. in the total DIS cross section

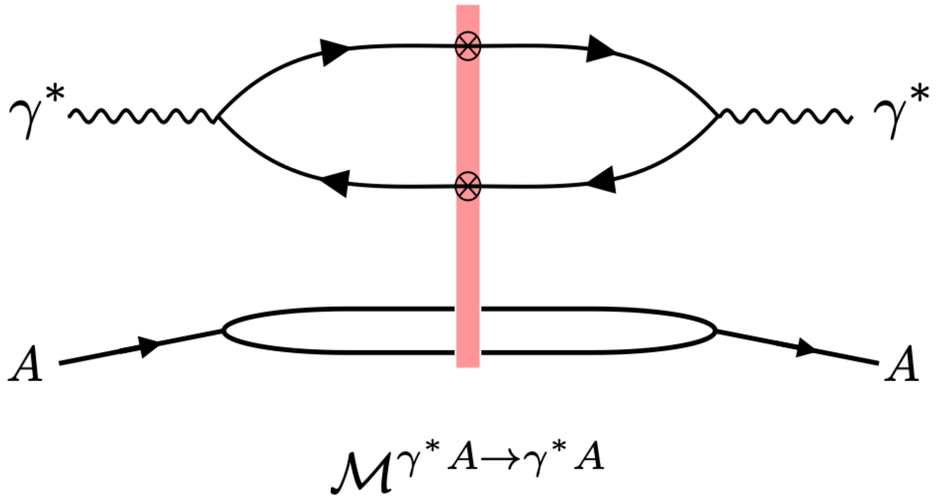

$$\sigma_\lambda^{\gamma^* A} = 2\,\mathrm{Im}(\mathscr{M}_\lambda^{\gamma^* A \to \gamma^* A})$$

$$= 2\int d^2\vec{r}_T\, d^2\overrightarrow{b}_T \int_0^1 dz \left|\psi_\lambda^{\gamma^*}(\vec{r}_T, Q^2, z)\right|^2 \left[1 - S_x^{(2)}\left(\overrightarrow{b}_T + \frac{\vec{r}_T}{2}, \overrightarrow{b}_T - \frac{\vec{r}_T}{2}\right)\right]$$

Q^2 is the virtuality of the photon, λ its polarization
$\psi_\lambda^{\gamma^*}(\vec{r}_T, Q^2, z)$ is the light-cone wave-function that describes the splitting of the virtual photon into the q-$\bar{q}$ pair. Quark has longitudinal momentum fraction z, anti-quark $1 - z$

$\overrightarrow{b}_T$ dependence needs to be modeled...

Total DIS cross section - sensitive to saturation?

x is the longitudinal momentum fraction at which the nucleus is probed

$x = Q^2/W^2$ with W the center of mass energy per nucleon of the photon-nucleus system

$$\sigma_\lambda^{\gamma^* A} = 2\,\mathrm{Im}(\mathscr{M}_\lambda^{\gamma^* A \to \gamma^* A})$$

$$= 2\int d^2\vec{r}_T\, d^2\overrightarrow{b}_T \int_0^1 dz \left|\psi_\lambda^{\gamma^*}(\vec{r}_T, Q^2, z)\right|^2 \left[1 - S_x^{(2)}\left(\overrightarrow{b}_T + \frac{\vec{r}_T}{2}, \overrightarrow{b}_T - \frac{\vec{r}_T}{2}\right)\right]$$

Accessing the saturated regime requires dipole sizes $r_T \sim 1/Q_s$

Now, the lightcone wave function $\psi_\lambda^{\gamma^*}$ suppresses dipole sizes with $r_T^2 \gtrsim 1/Q^2$

So we are limited to virtualities in the range $\Lambda_{QCD}^2 \ll Q^2 \lesssim Q_s^2$ to access saturation in DIS

Forward quark production in p+A collisions

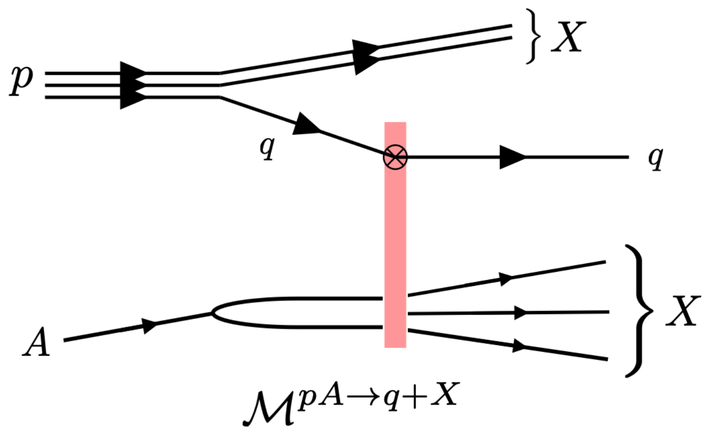

The dipole correlator also appears in the cross section for forward quark production: $V(\overrightarrow{x}_T)$ from the amplitude, $V^\dagger(\overrightarrow{y}_T)$ from the conjugate amplitude.

The cross section reads $$\frac{d\sigma^{pA\to qX}}{dyd^2k_T} = \frac{1}{(2\pi)^2} x_p\, q(x_p)\, C_{x_A}(\overrightarrow{k}_T)$$

where $\overrightarrow{k}_T$ and y are the transverse momentum and rapidity of produced quark

$x_p\, q(x_p)$ is the quark distribution in the proton for a collinear quark with momentum fraction x_p

x_A is the longitudinal momentum fraction of gluons probed in the nucleus

Forward quark production

The cross section reads $$\frac{d\sigma^{pA\to qX}}{dyd^2k_T} = \frac{1}{(2\pi)^2} x_p\, q(x_p)\, C_{x_A}(\vec{k}_T)$$

$$C_{x_A}(\vec{k}_T) = \int d^2x_T d^2y_T e^{-i\vec{k}_T\cdot(\vec{x}_T-\vec{y}_T)} S^{(2)}_{x_A}(\vec{x}_T, \vec{y}_T)$$

determining the transverse momentum kick $\vec{k}_T$ acquired by the quark as it traverses the nucleus

The function has two limits:

Perturbative regime: $C_x(\vec{k}_T) \sim \frac{Q_s^2(x)}{k_T^4}$

Saturation regime: $C_x(\vec{k}_T) \sim \frac{1}{Q_s^2(x)}$

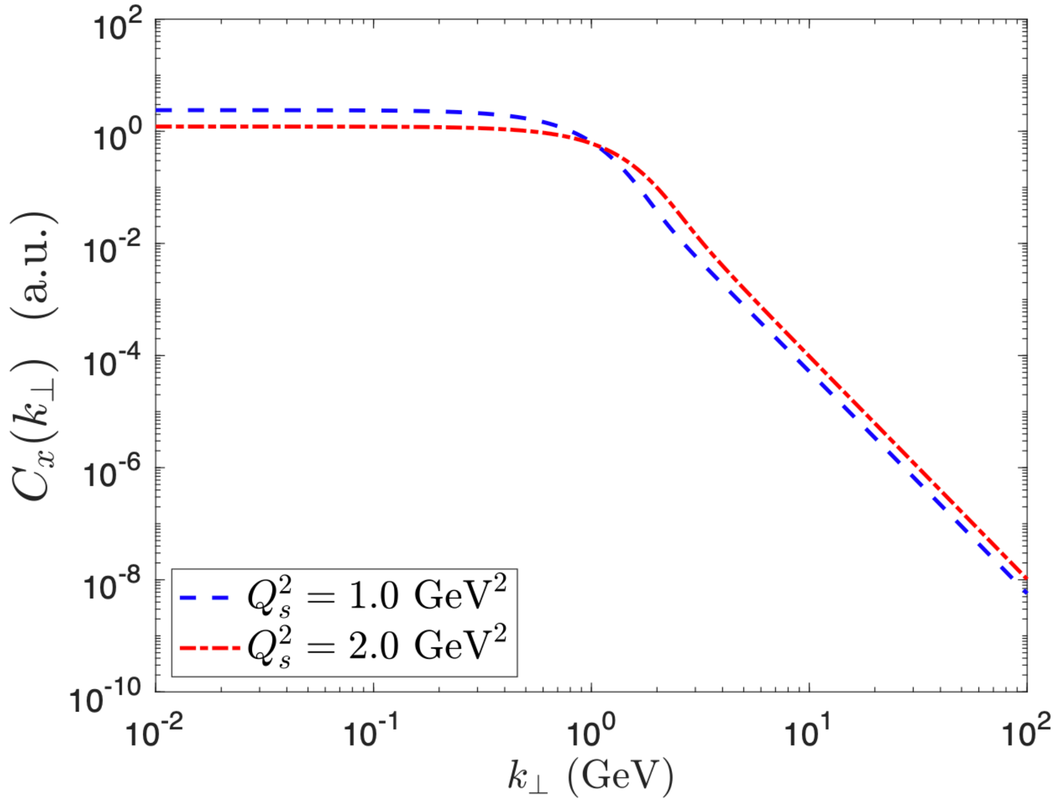

Multi-gluon correlators

Besides the dipole correlator, more complicated correlators of Wilson lines appear for example in cross sections of less exclusive processes or in the small-x evolution equations (which we will get to)

For example:

$$S_{x_0}^{(2,2)} = \frac{1}{N_c^2} \left\langle \mathrm{Tr}[V(\overrightarrow{x}_T)V^\dagger(\overrightarrow{y}_T)]\mathrm{Tr}[V(\overrightarrow{y}'_T)V^\dagger(\overrightarrow{x}'_T)] \right\rangle_{x_0}$$

double dipole

$$S_{x_0}^{(4)} = \frac{1}{N_c} \left\langle \mathrm{Tr}[V(\overrightarrow{x}_T)V^\dagger(\overrightarrow{y}_T)V(\overrightarrow{y}'_T)V^\dagger(\overrightarrow{x}'_T)] \right\rangle_{x_0}$$

quadrupole

quadrupole appears for example in inclusive dijet production in DIS

double dipole appears in diffractive dijet production

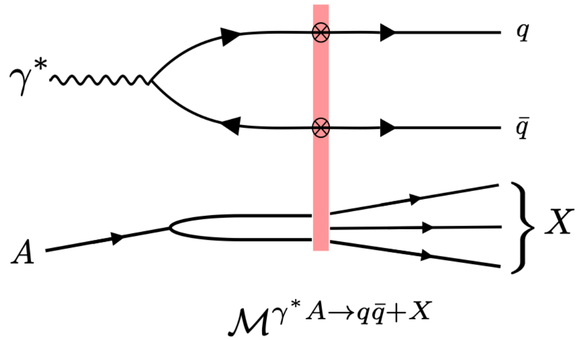

TMD factorization

https://arxiv.org/abs/1101.0715

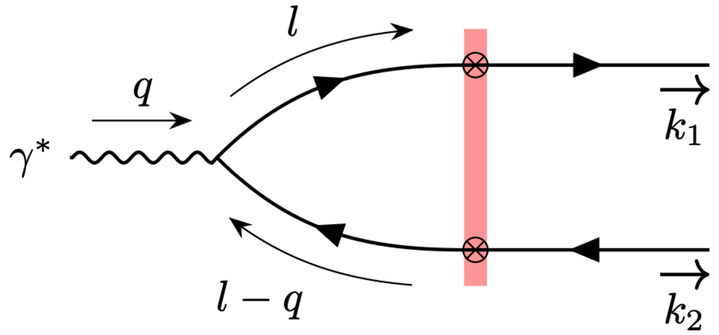

Define $\boldsymbol{k}_\perp = \boldsymbol{k}_{1\perp} + \boldsymbol{k}_{2\perp}\,,$

$\boldsymbol{P}_\perp = z_2\boldsymbol{k}_{1\perp} - z_1\boldsymbol{k}_{2\perp}\,,$

In the back-to-back limit for the dijet (produced q-$\bar{q}$ pair), where $k_T \ll P_T$

one can establish TMD factorization (TMD: Transverse momentum dependent parton distribution function)

That is assuming that the back to back limit is equivalent to the limit $r_T \ll b_T$ *

Then, one expands $\left[\mathbb{1} - V\left(\boldsymbol{x}_\perp\right) V^\dagger\left(\boldsymbol{y}_\perp\right)\right] = -\boldsymbol{r}_\perp^j \left[V\left(\boldsymbol{b}_\perp\right) \partial^j V^\dagger\left(\boldsymbol{b}_\perp\right)\right] + \mathcal{O}\left(\boldsymbol{r}_\perp^2\right)$ in the amplitude

What appears is the gluon field $A^i(\overrightarrow{b}_T) = \frac{i}{g} V(\overrightarrow{b}_T)\partial^i V^\dagger(\overrightarrow{b}_T)$

* : that is not quite true and there are corrections to this:

R. Boussarie, H. Mäntysaari, F. Salazar, B. Schenke, JHEP 09 (2021) 178

TMD factorization

https://arxiv.org/abs/1101.0715

Differential cross section:

$$\frac{d\sigma_{\lambda}^{\gamma^*+A\to q\bar{q}+X}}{dz_1 dz_2 d^2k_T d^2P_T} = \delta(1-z_1-z_2)\, H^{ij,\lambda}_{\gamma^* g\to q\bar{q}}(Q^2, \overrightarrow{P}_T, z)\, xG^{ij}_{\mathrm{WW}}(x, \overrightarrow{k}_T)$$

where $H^{ij,\lambda}_{\gamma^* g\to q\bar{q}}(Q^2, \overrightarrow{P}_T, z)$ is the hard factor, calculable perturbatively,

with $\overrightarrow{P}_T$ the mean transverse momentum of the jets

and $xG^{ij}_{\mathrm{WW}}(x, \overrightarrow{k}_T)$ is the Weizsäcker-Williams gluon TMD with $\overrightarrow{k}_T$ the momentum imbalance

$$xG^{ij}_{\mathrm{WW}}(x, \overrightarrow{k}_T) = \frac{4}{(2\pi)^3}\int d^2b_T d^2b'_T\, e^{-i\overrightarrow{k}_T\cdot(\overrightarrow{b}_T-\overrightarrow{b}'_T)} \left\langle \mathrm{Tr}[A^i(\overrightarrow{b}_T)A^j(\overrightarrow{b}'_T)] \right\rangle_x$$

WW gluon TMD

https://arxiv.org/abs/1101.0715

This distribution

$$xG^{ij}_{\mathrm{WW}}(x,\vec{k}_T) = \frac{4}{(2\pi)^3}\int d^2b_T d^2b'_T\, e^{-i\vec{k}_T\cdot(\vec{b}_T-\vec{b}'_T)}\left\langle \mathrm{Tr}[A^i(\vec{b}_T)A^j(\vec{b}'_T)]\right\rangle_x$$

has a probability density interpretation

(unlike the FT of the dipole correlator)

Perturbative regime: $xG^{ii}(x,\vec{k}_T) \sim \dfrac{Q_s^2(x)}{\vec{k}_T^{\,2}}$

Saturation regime: $xG^{ii}(x,\vec{k}_T) \sim \ln\left(\dfrac{Q_s^2(x)}{\vec{k}_T^{\,2}}\right)$

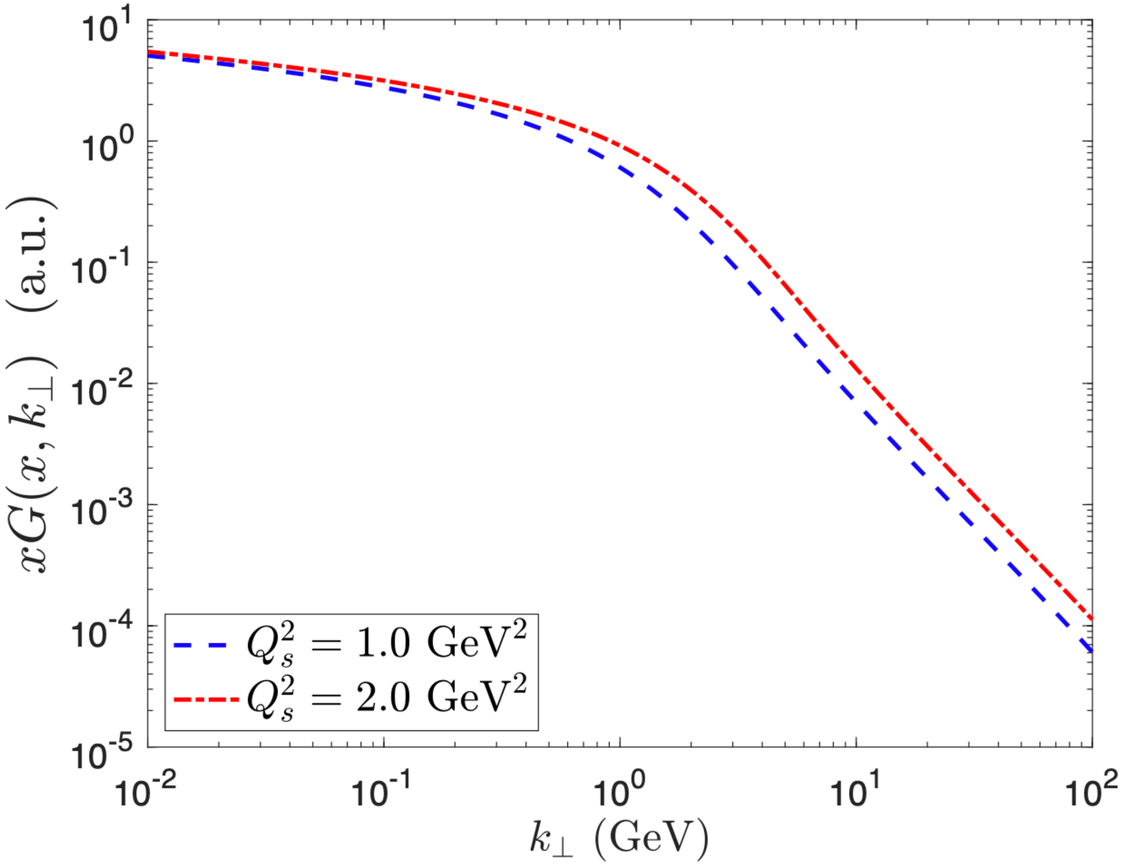

WW gluon TMD

https://arxiv.org/abs/1101.0715

The WW gluon TMD contains a correlator of light-like Wilson lines and their derivatives:

$$xG^{ij}_{\mathrm{WW}}(x, \vec{k}_T) = \frac{4}{(2\pi)^3} \int d^2b_T d^2b'_T \, e^{-i\vec{k}_T\cdot(\vec{b}_T - \vec{b}'_T)} \left\langle \mathrm{Tr}[A^i(\vec{b}_T) A^j(\vec{b}'_T)] \right\rangle_x$$

Transverse momentum imbalance of a dijet
is dictated by WW gluon transverse momentum distribution!

Azimuthal distribution of dijets/dihadrons near back-to-back limit provides access to WW gluon TMD and saturation effects

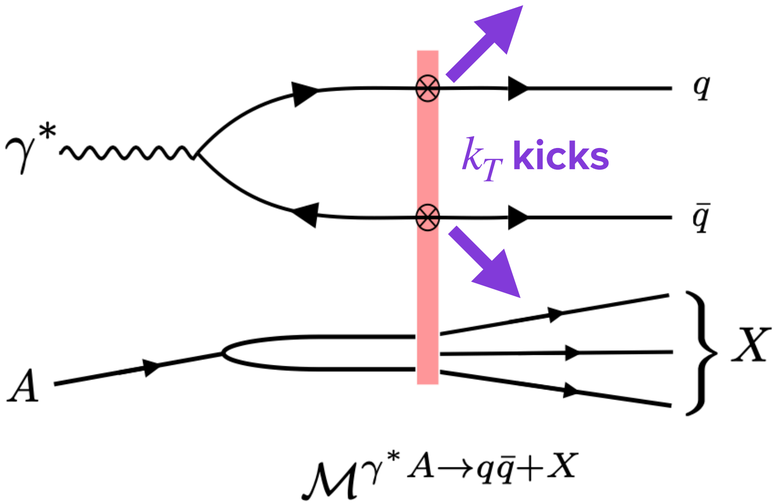

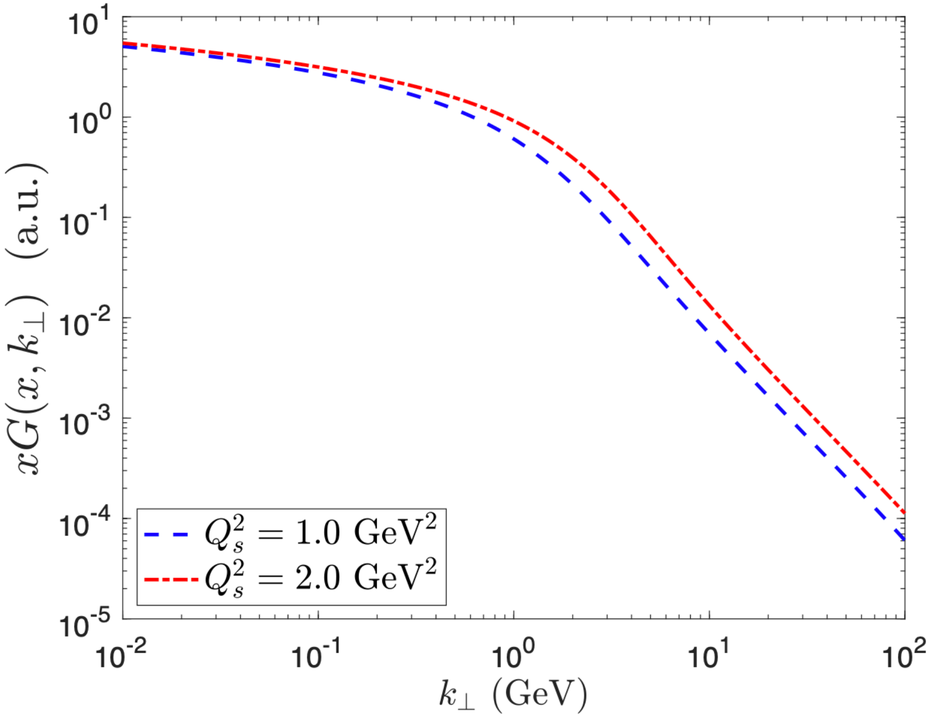

Quantum evolution

Quantum fluctuations around the classical solution are enhanced by terms $\sim \alpha_s \ln(x_0/x)$

Can be understood as gluon emissions in the interval $[x, x_0]$

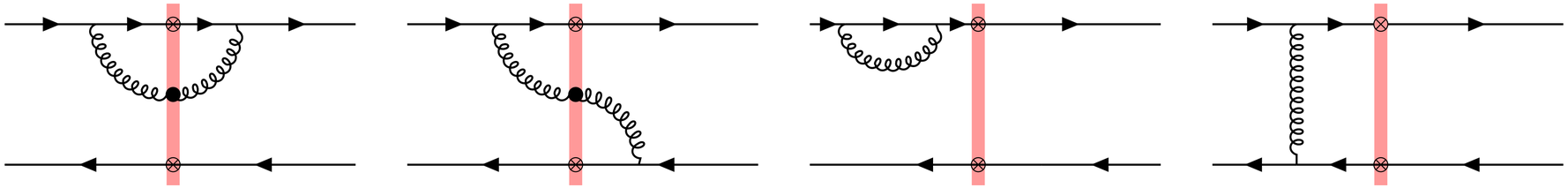

At large N_c, resumming terms enhanced by $\sim \alpha_s \ln(x_0/x)$ results in the Balitsky-Kovchegov (BK) equations

Balitsky, Nucl. Phys. B 1996, 463, 99–160, [hep-ph/9509348]
Kovchegov, Phys. Rev. D 1999, 60, 034008, [hep-ph/9901281]

$$\frac{dS_{x_0}^{(2)}(\vec{r}_T)}{d\ln(1/x)} = \frac{\alpha_s N_c}{2\pi^2}\int d^2 r'_T \frac{\vec{r}_T^{\,2}}{\vec{r}_T'^{\,2}(\vec{r}_T - \vec{r}'_T)^2}\left[S_x^{(2)}(r'_T)S_x^{(2)}(|\vec{r}_T - \vec{r}'_T|) - S_x^{(2)}(r_T)\right]$$

Terms non-linear in $S_x^{(2)}$ arise from real diagrams above where gluon crosses the shockwave

The linear term comes from the virtual contributions

Weak scattering limit, $D_x(r_T) = 1 - S_x^{(2)}(r_T) \ll 1$: BK equations reduce to BFKL equations

JIMWLK equation

Jalilian-Marian, J.; Kovner, A.; McLerran, L.D.; Weigert, H., Phys. Rev. D 1997, 55, 5414–5428, [hep-ph/9606337]
Jalilian-Marian, J.; Kovner, A.; Weigert, H., Phys. Rev. D 1998, 59, 014015, [hep-ph/9709432]
Kovner, A.; Milhano, J.G.; Weigert, H., Phys. Rev. D 2000, 62, 114005, [hep-ph/0004014]
Iancu, E.; Leonidov, A.; McLerran, L.D., Nucl. Phys. A 2001, 692, 583–645,[hep-ph/0011241]
Iancu, E.; Leonidov, A.; McLerran, L.D., Phys. Lett. B 2001, 510, 133–144, [hep-ph/0102009]
Ferreiro, E.; Iancu, E.; Leonidov, A.; McLerran, L., Nucl. Phys. A 2002, 703, 489–538, [hep-ph/0109115]

Alternatively, resum the large logarithmic corrections by evolving the weight functional:

$$\frac{dW_x[\rho]}{d\ln(1/x)} = -\mathscr{H}_{\text{JIMWLK}}\, W_x[\rho]$$

Physically, one absorbs the quantum fluctuations in the interval $[x_0 - dx, x_0]$ into stochastic fluctuations of the color sources by redefining the color sources ρ:

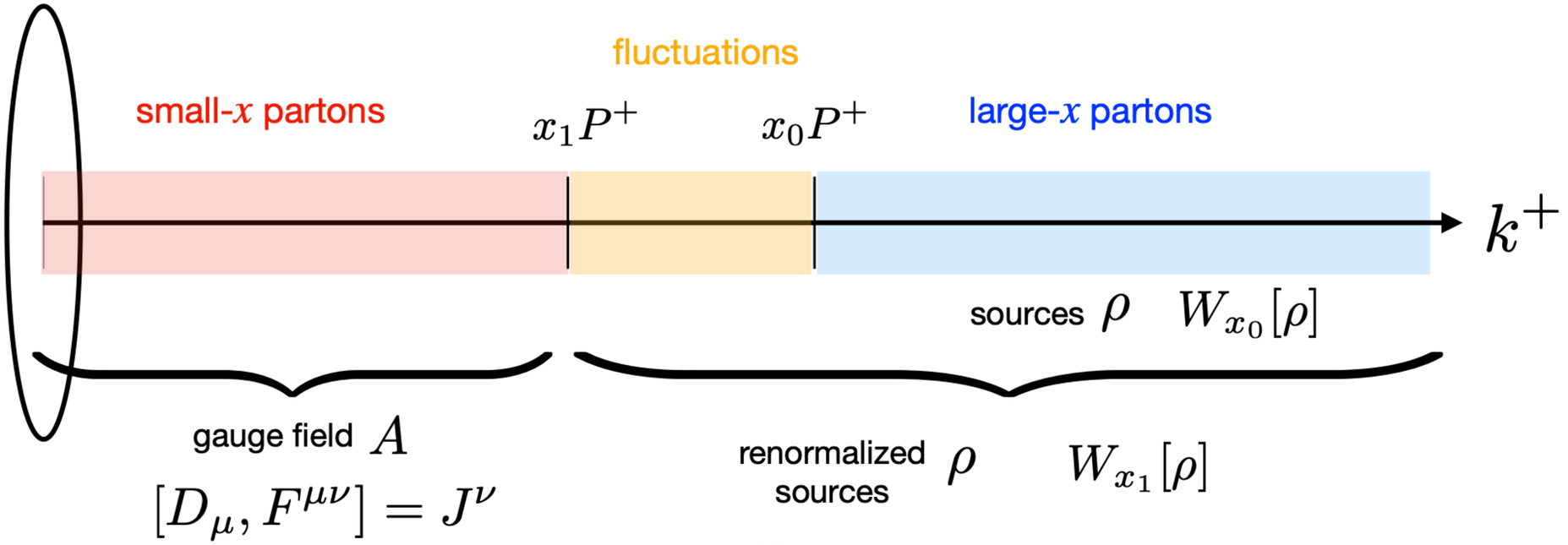

JIMWLK equation

Jalilian-Marian, J.; Kovner, A.; McLerran, L.D.; Weigert, H., Phys. Rev. D 1997, 55, 5414–5428, [hep-ph/9606337]
Jalilian-Marian, J.; Kovner, A.; Weigert, H., Phys. Rev. D 1998, 59, 014015, [hep-ph/9709432]
Kovner, A.; Milhano, J.G.; Weigert, H., Phys. Rev. D 2000, 62, 114005, [hep-ph/0004014]
Iancu, E.; Leonidov, A.; McLerran, L.D., Nucl. Phys. A 2001, 692, 583–645,[hep-ph/0011241]
Iancu, E.; Leonidov, A.; McLerran, L.D., Phys. Lett. B 2001, 510, 133–144, [hep-ph/0102009]
Ferreiro, E.; Iancu, E.; Leonidov, A.; McLerran, L., Nucl. Phys. A 2002, 703, 489–538, [hep-ph/0109115]

The quantum evolution effectively increases the color charge density, and hence Q_s

Effect on the dipole amplitude

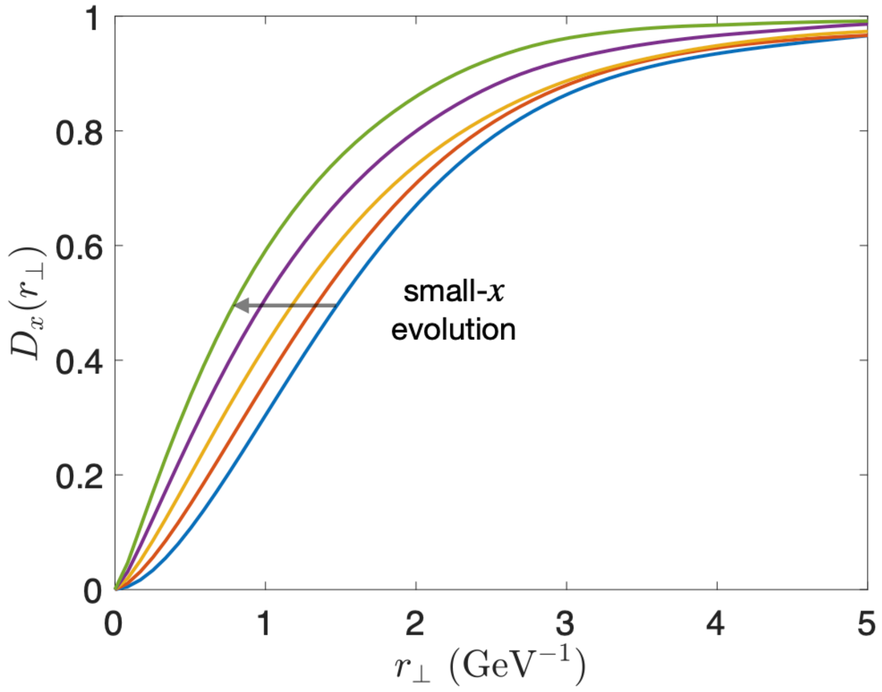

Increasing Q_s with decreasing x

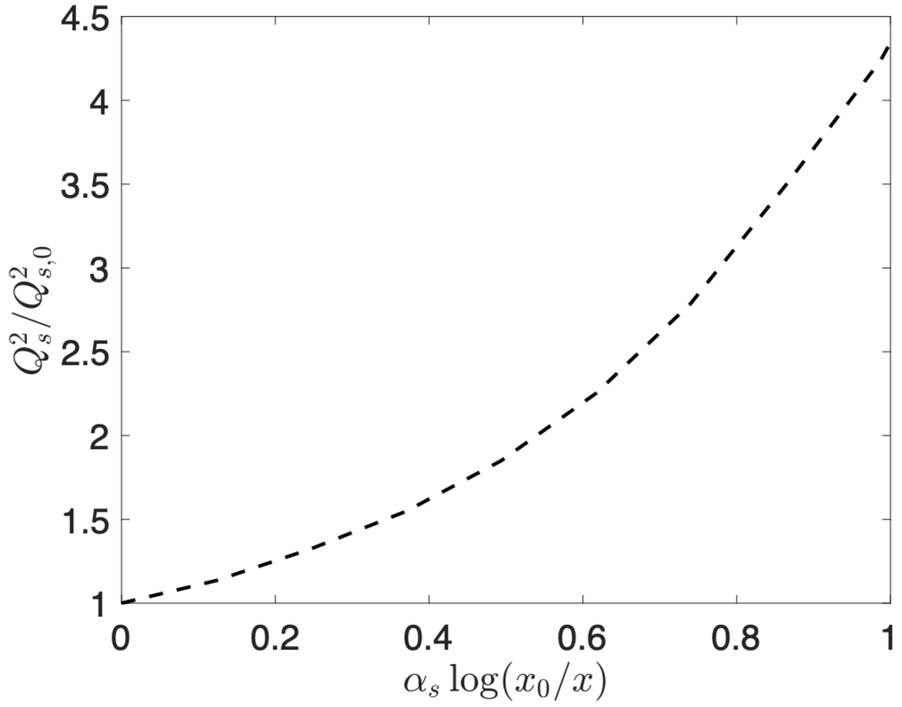

We will return to the effect of the small-x evolution on observables in HICs and at the EIC later

Recap: Saturation scale's A and x dependence

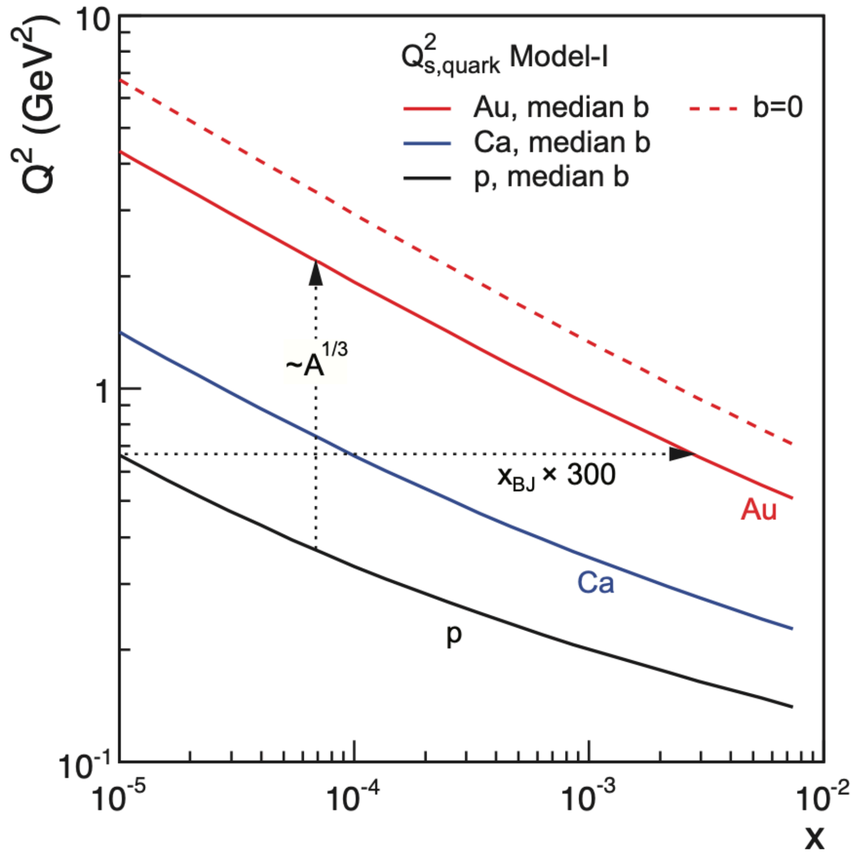

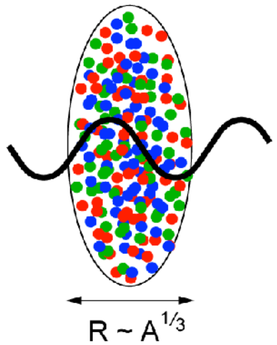

$$(Q_s^A)^2 \approx cQ_0^2\left(\frac{A}{x}\right)^{1/3}$$

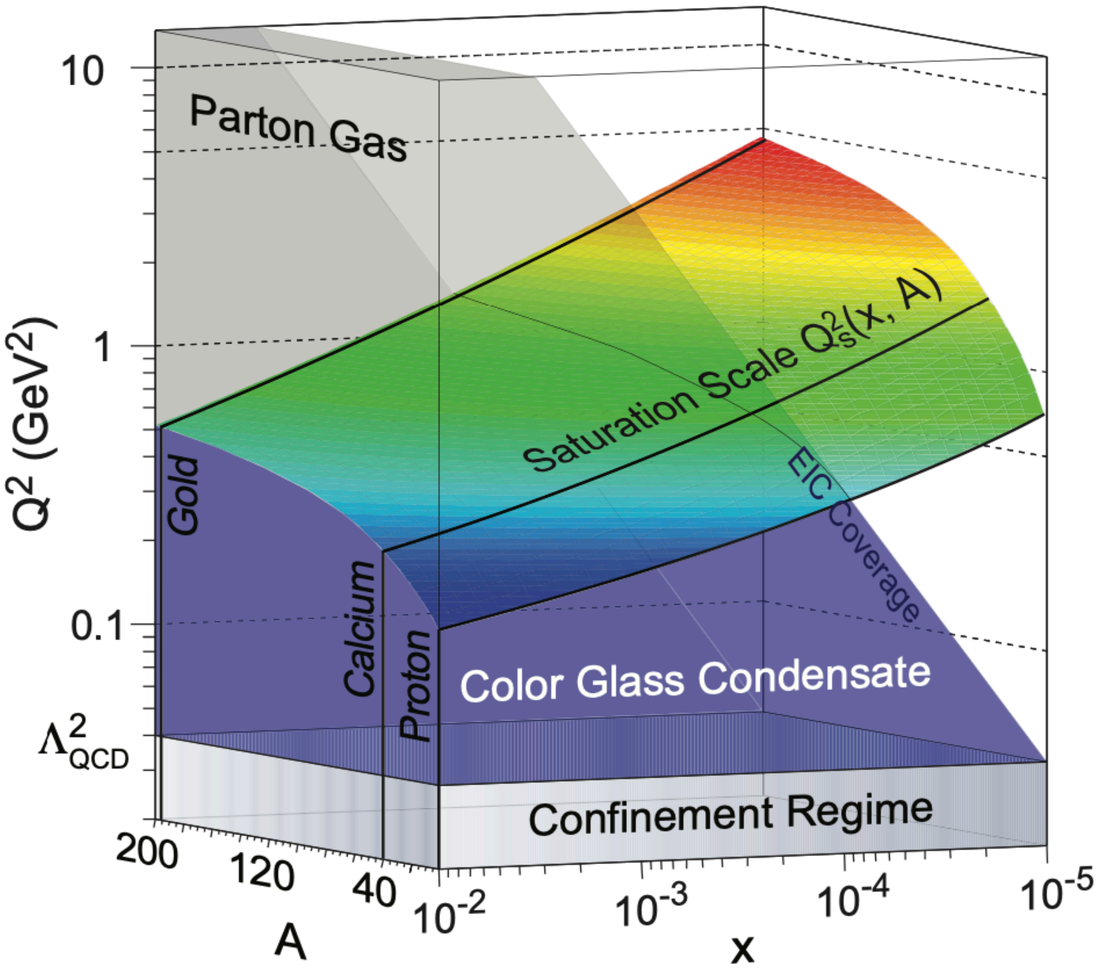

A. Accardi et al., EIC White Paper, Eur.Phys.J.A 52 (2016) 9, 268

Brookhaven National Laboratory

From Heavy Ion Physics to the Electron Ion Collider

The 2022 CFNS Summer School on the Physics of the Electron-Ion Collider

Björn Schenke, Brookhaven National Laboratory

07/15/2022

U.S. DEPARTMENT OF ENERGY | Office of Science

Recap: Saturation scale's A and x dependence

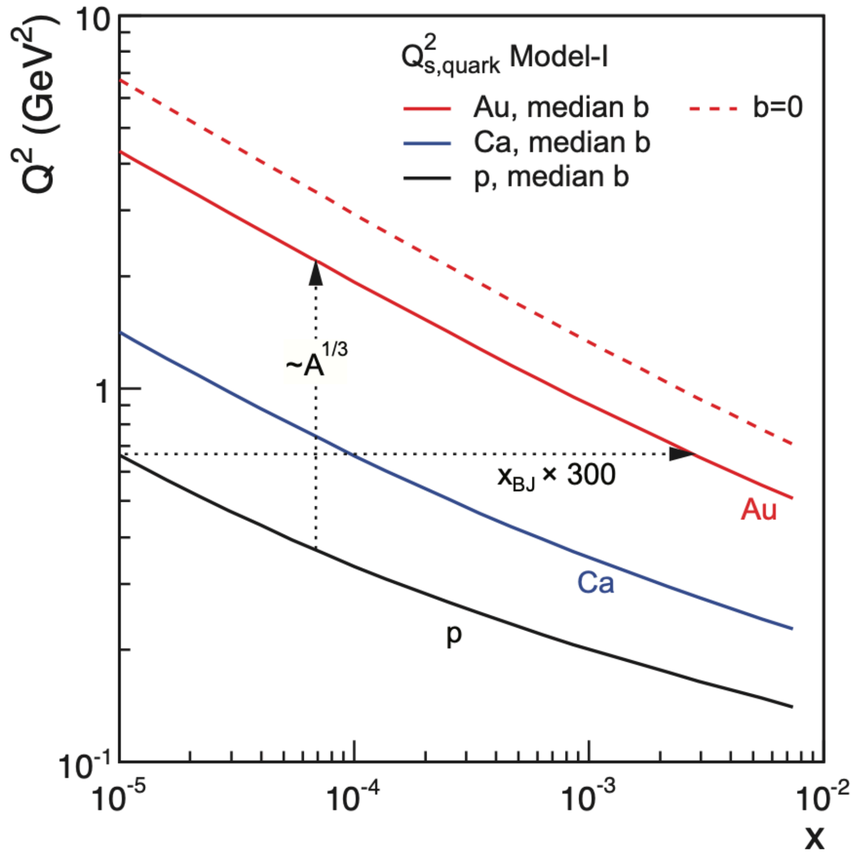

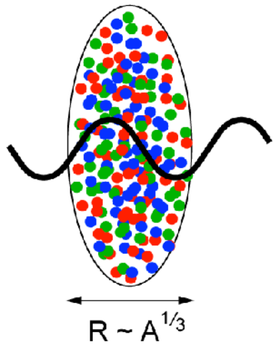

$$(Q_s^A)^2 \approx cQ_0^2\left(\frac{A}{x}\right)^{1/3}$$

Q_s is a transverse momentum scale:

Gluons with $k_T < Q_s(x, A)$ are saturated

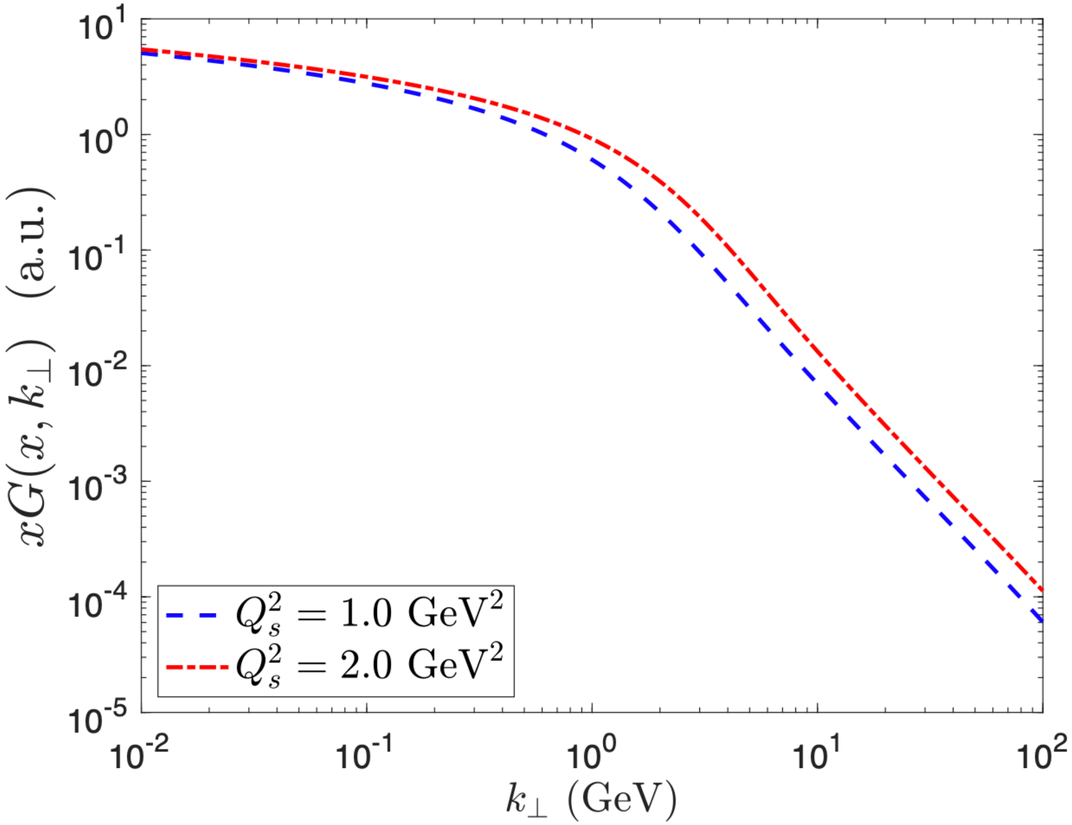

A. Accardi et al., EIC White Paper, Eur.Phys.J.A 52 (2016) 9, 268

Some observables sensitive to saturation

- Inclusive: Structure functions
- Semi-inclusive: dihadron, dijet correlations
- Diffractive processes: e.g. ratio of diffractive and total cross-section, vector meson production, diffractive dijet production, …

for the most recent review: A. Morreale, F. Salazar, Universe 7 (2021) 8, 312 • e-Print: 2108.08254

Saturation effects on structure functions

Structure functions can be determined from the total DIS cross section

$$F_2 = \frac{Q^2}{4\pi^2\alpha_{\rm em}}(\sigma_L^{\gamma^* p} + \sigma_T^{\gamma^* p}),$$

$$F_L = \frac{Q^2}{4\pi^2\alpha_{\rm em}}\sigma_L^{\gamma^* p}.$$

From these objects one can extract quark and gluon distribution functions (PDFs)

HERA data can be described using PDFs at a scale Q_0 that are then evolved using DGLAP to different scales Q

There is evidence that BFKL resummation that resums terms $\sim \alpha_s \ln(x_0/x)$ is required at small x to describe the data Ball, R.D.; Bertone, V.; Bonvini, M.; Marzani, S.; Rojo, J.; Rottoli, L. , Eur. Phys. J. C 2018, 78, 321, [arXiv:hep-ph/1710.05935] Hentschinski, M.; Sabio Vera, A.; Salas, C., Phys. Rev. D 2013, 87, 076005, [arXiv:hep-ph/1301.5283]

At high densities, the non-linear effects included in BK or JIMWLK evolution should become important. Calculations are compatible with data but there is no clear evidence that we have reached the density regime where these effects are absolutely important

Dipole model fits

$$\sigma_r(x, y, Q^2) = F_2(x, Q^2) - \frac{y}{1 + (1 - y)^2} F_L(x, Q^2)$$

H. Mäntysaari, P. Zurita, Phys.Rev.D 98 (2018) 036002

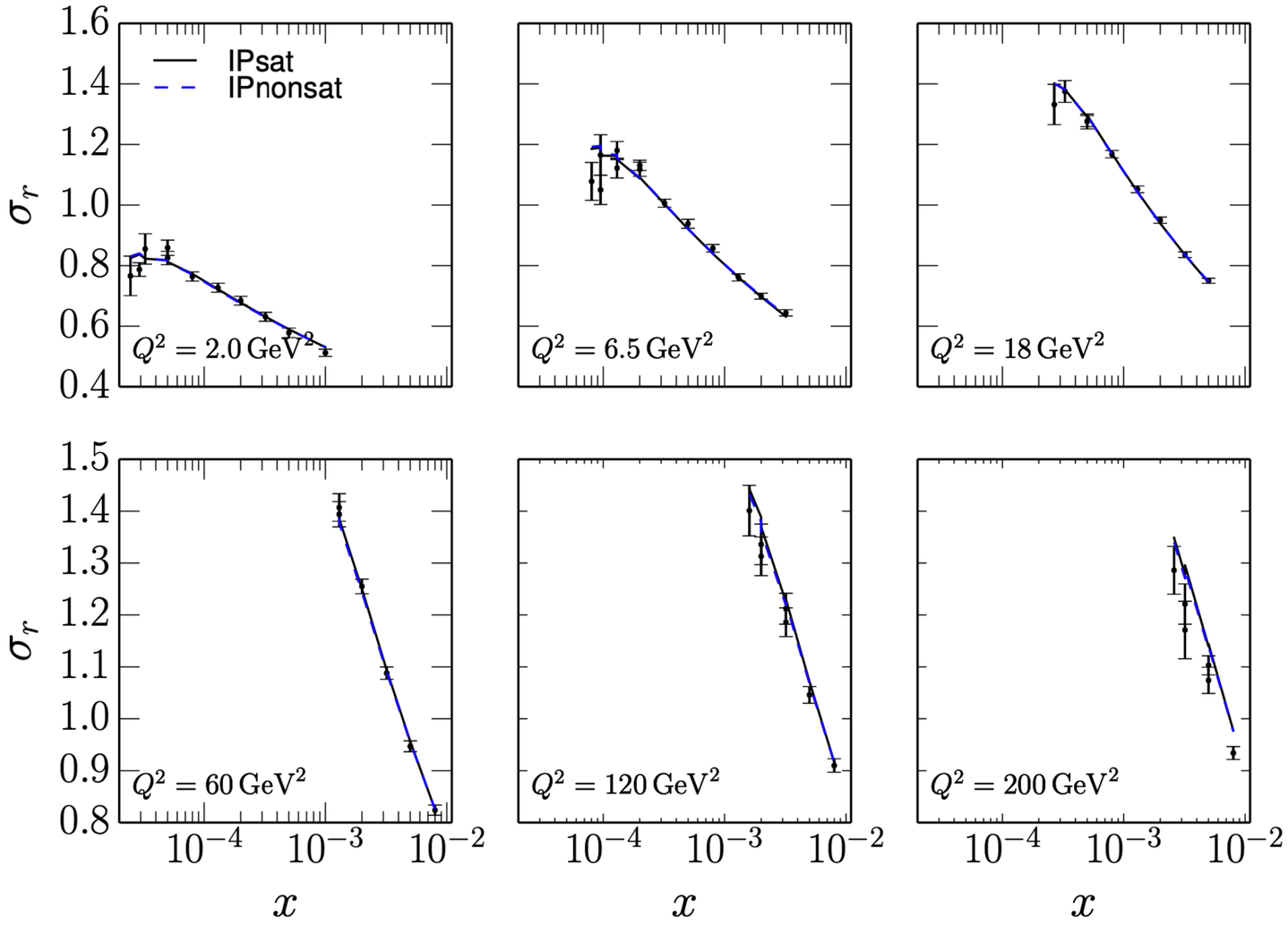

Saturation effects do not seem to show up as the “IPnonSat” model describes the data as well as IPSat (will discuss IPSat in detail later).

IPSat:

$$\frac{\mathrm{d}\sigma_{\mathrm{dip}}}{\mathrm{d}^2\mathbf{b}} = 2\left[1 - \exp\left(-r^2 F(x, r) T_p(\mathbf{b})\right)\right]$$

IPnonSat:

$$\frac{\mathrm{d}\sigma_{\mathrm{dip}}}{\mathrm{d}^2\mathbf{b}} = 2r^2 F(x, r) T_p(\mathbf{b})$$

Problem with structure functions

Dipole picture: at moderate Q^2 non-perturbatively large dipoles contribute to structure function

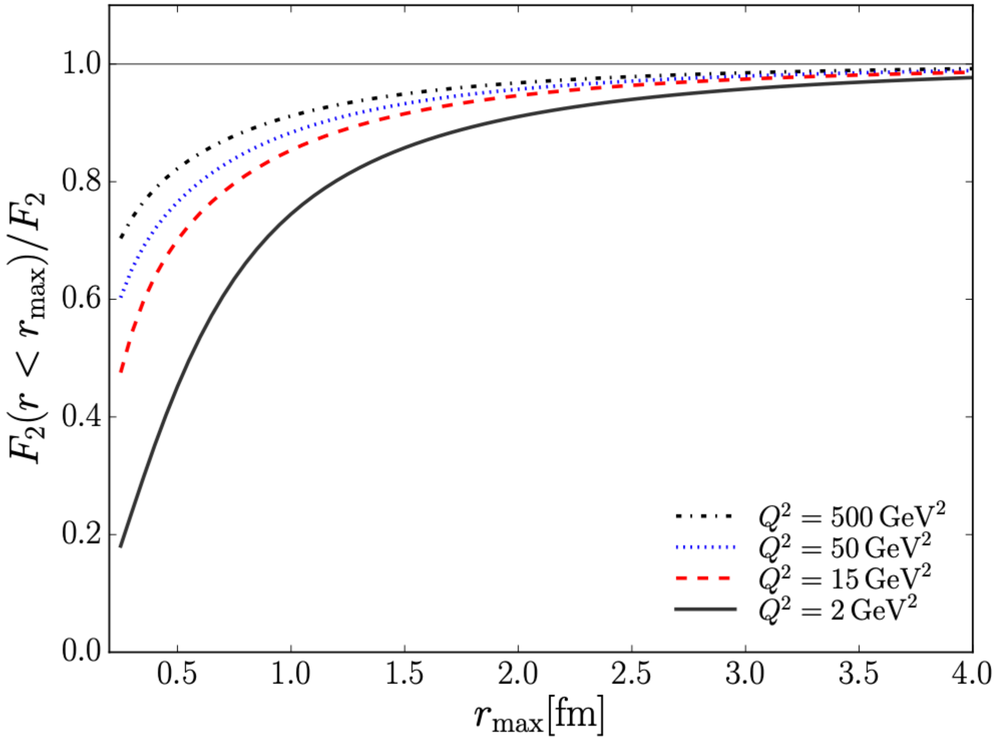

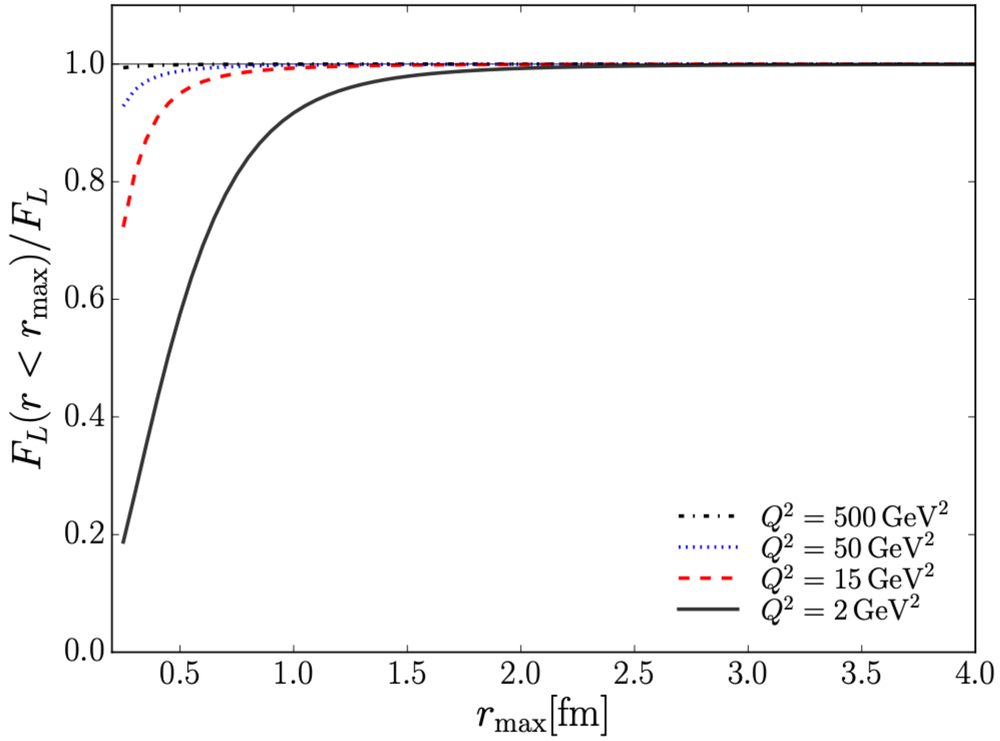

They are suppressed at (very) large Q^2, but then we are also less sensitive to saturation

Charm structure functions are better as the charm mass acts as an infrared cutoff

Freedom in choice of parameters in saturation models used is also a problem for pinning down saturation

Charm reduced cross section with JIMWLK evolution

H. Mäntysaari and B. Schenke, Phys. Rev. D 98, 034013 (2018)

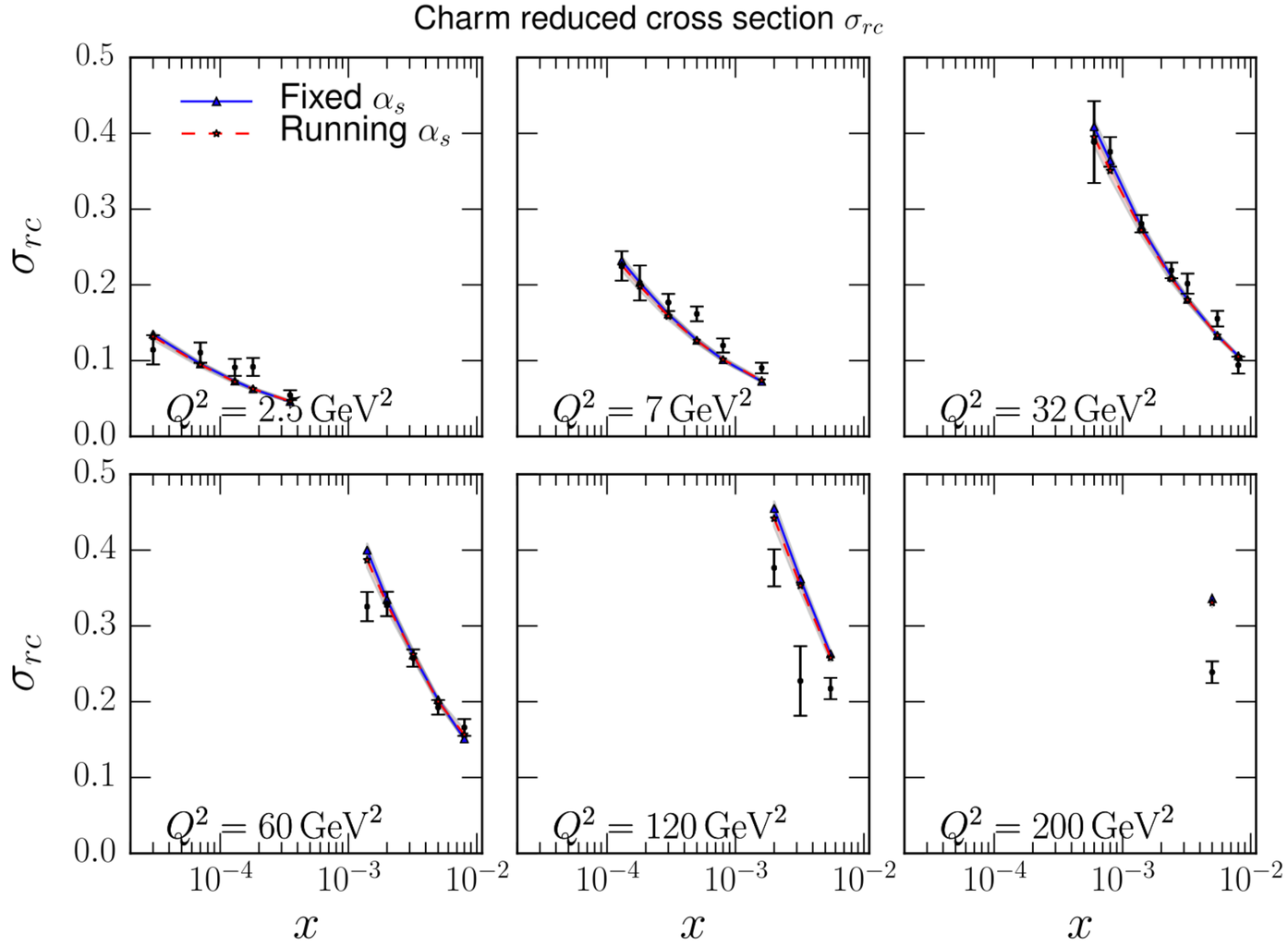

Saturation effects on structure functions

J. Bartels, K. Golec-Biernat, and L. Motyka, Phys. Rev. D81, 054017 (2010)

For nuclei at the EIC, saturation effects on structure functions should become more prominent

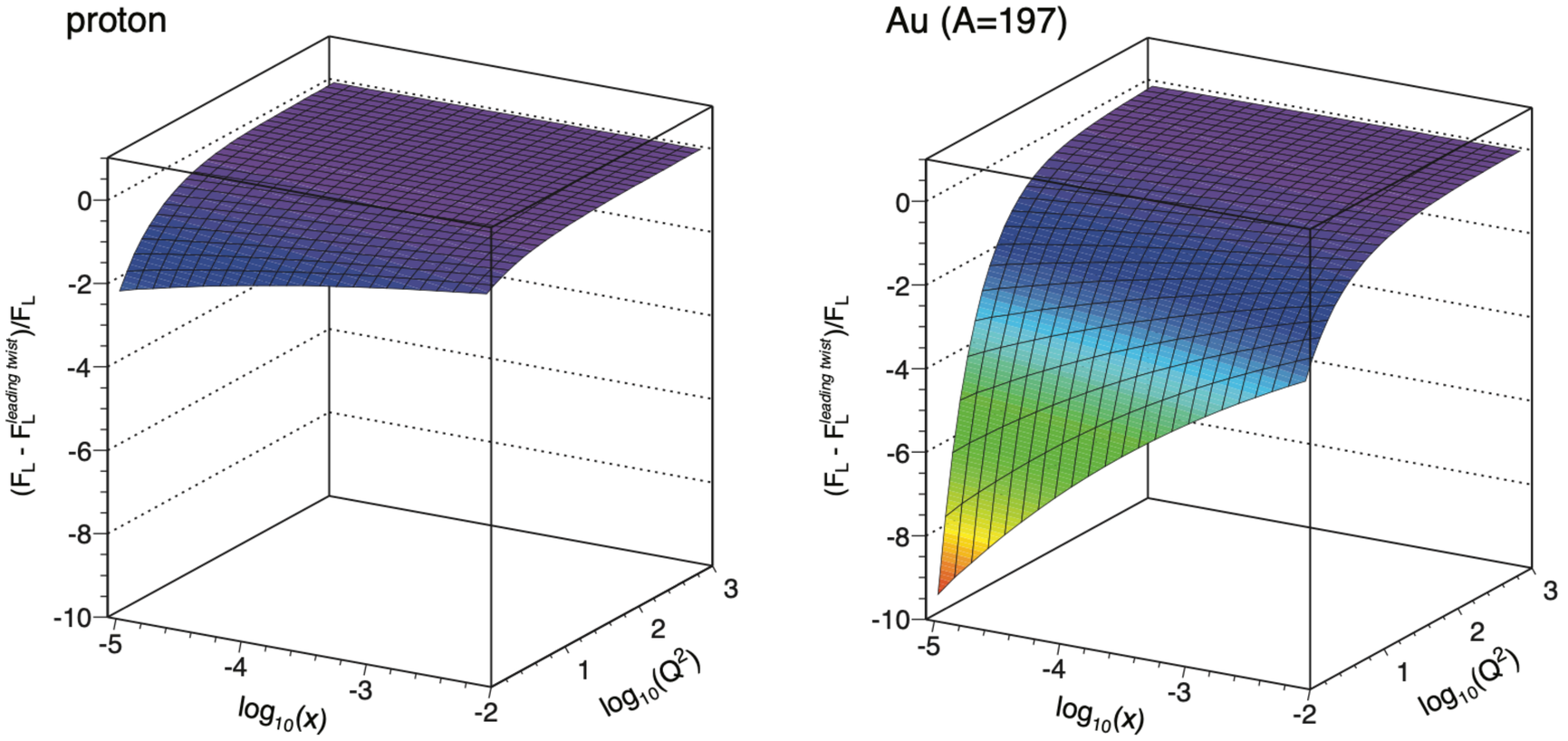

The multiple re-scatterings and gluon mergers contribute at all orders in twists (terms in a $1/Q^2$ expansion).
Their effect increases with increasing A and decreases with increasing x

Single inclusive production

D. Kharzeev, Y.V. Kovchegov, K. Tuchin, Phys. Lett. B 2004, 599, 23–31, [hep-ph/0405045]

Consider light-heavy nucleus collisions: Hybrid framework: incoming partons inside the proton (or deuteron) are treated within the DGLAP collinear approximation and scatter eikonally off the nucleus described by light-like Wilson lines.

Nuclear modification factor $$R_{A_1A_2} = \frac{1}{N_{\mathrm{coll}}} \frac{\mathrm{d}\sigma^{A_1A_2\to hX}}{\mathrm{d}^2\boldsymbol{p}_\perp \mathrm{d}\eta} \Big/ \frac{\mathrm{d}\sigma^{pp\to hX}}{\mathrm{d}^2\boldsymbol{p}_\perp \mathrm{d}\eta}$$

MV model: Saturated gluons with typical momentum $k_T \sim Q_s$ induce a broadening of the transverse momentum distribution of the produced particles

Nuclear modification factor is suppressed for $k_T \lesssim Q_s$ and enhanced for $k_T \gtrsim Q_s$

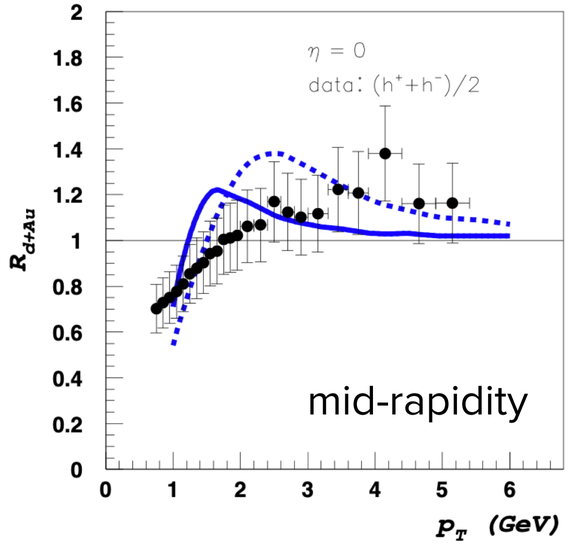

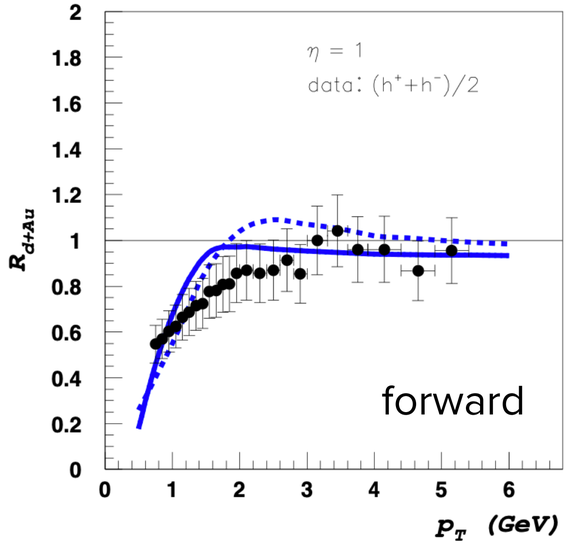

For MV:

$$\int d^2p_T\, \phi^A_{\mathrm{MV}}(p_T) = A \int d^2p_T\, \phi^p_{\mathrm{MV}}(p_T)$$

BK evolution leads to more suppression

dashed curve: $Q_s^2 \to Q_s^2 + \kappa^2 A^{1/3} \quad (\kappa = 1)$

Single inclusive production

Also photon and quarkonium production in p+A collisions can probe saturation

SCANNING SATURATION WITH J/Ψ AND h_c in p+A

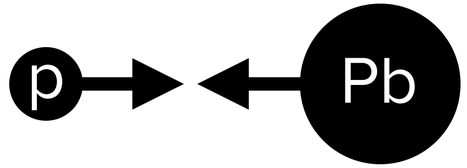

Salazar, Schenke, Soto-Ontoso, Phys.Lett.B 827 (2022)

Study production of J/ψ at different rapidities relative to charged hadrons at midrapidity
Expect varying sensitivity to saturation, depending on probed Q_s and mass:

J/ψ $m_{J/\psi} = 3.1\,\mathrm{GeV}$

h $m_{h_c} \approx 0.5\,\mathrm{GeV}$

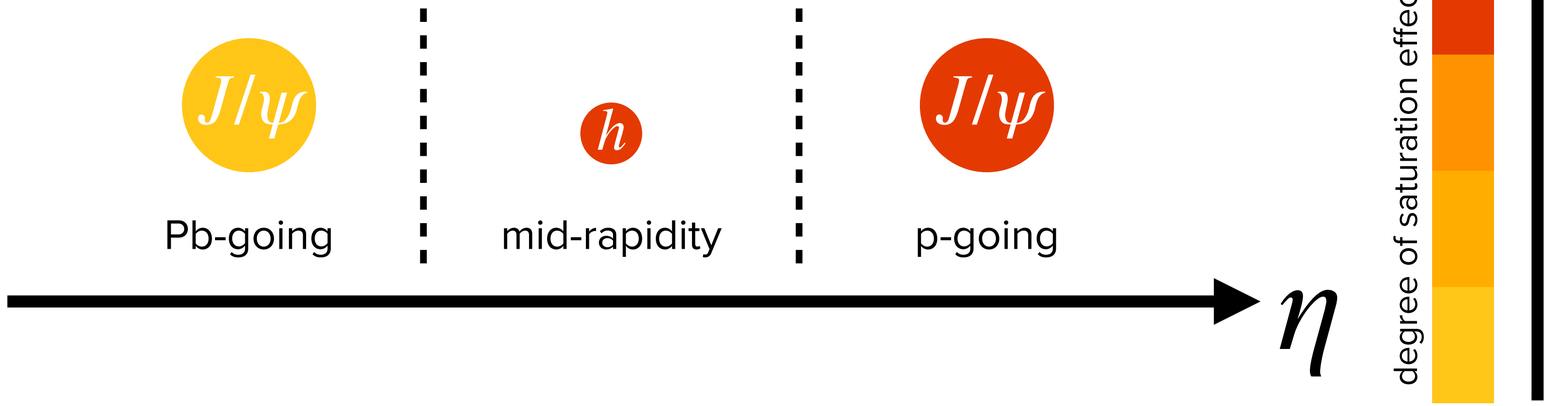

Most important physics in $Q_s^2(x, \boldsymbol{R}_\perp) = T_A(\boldsymbol{R}_\perp) S_\perp Q_s^2(x)$. Depends on rapidity ($x$) and transverse space.

$$x_p = \frac{\sqrt{m^2 + p_T^2}}{\sqrt{s}} \exp(y) \qquad x_{\mathrm{Pb}} = \frac{\sqrt{m^2 + p_T^2}}{\sqrt{s}} \exp(-y)$$

MODEL: CHARGED HADRON PRODUCTION

Salazar, Schenke, Soto-Ontoso, Phys.Lett.B 827 (2022) 136952

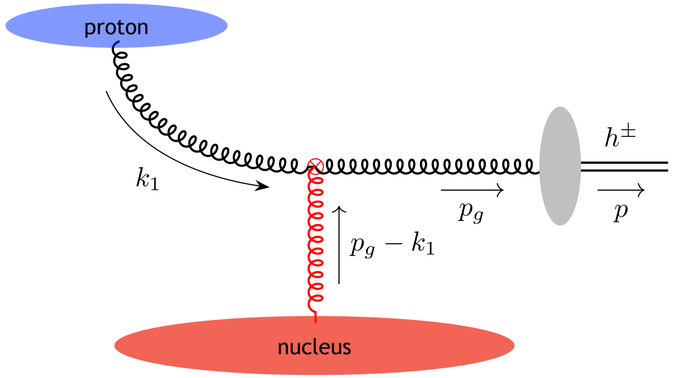

Use k_T-factorization for gluon production Y. V. Kovchegov, K. Tuchin, Phys. Rev. D 65, 074026 (2002); J. P. Blaizot, F. Gelis, R. Venugopalan, Nucl. Phys. A743, 13 (2004)

$$\frac{\mathrm{d}N_g(\boldsymbol{b}_\perp)}{\mathrm{d}^2\boldsymbol{p}_{g\perp}\mathrm{d}y_g} = \frac{\alpha_s}{(\sqrt{2}\pi)^6 C_F}\frac{1}{\boldsymbol{p}_{g\perp}^2}\int_{\boldsymbol{k}_{1\perp},\boldsymbol{R}_\perp} \phi^p(x_p;\boldsymbol{k}_{1\perp};\boldsymbol{R}_\perp)\phi^A(x_A;\boldsymbol{p}_{g\perp}-\boldsymbol{k}_{1\perp};\boldsymbol{R}_\perp-\boldsymbol{b}_\perp)$$

$$\phi(x;\boldsymbol{k}_\perp;\boldsymbol{R}_\perp) = \frac{\boldsymbol{k}_\perp^2 C_F}{2\alpha_s}\widetilde{\mathcal{S}}_{\mathrm{Adj}}(x;\boldsymbol{k}_\perp;\boldsymbol{R}_\perp)$$

Unintegrated gluon distributions ϕ^p and ϕ^A (with $A = p, \mathrm{Pb}$) from Balitsky-Kovchegov evolution with McLerran-Venugopalan initial conditions

$$\widetilde{\mathcal{S}}_{\mathrm{R}}(x;\boldsymbol{k}_\perp;\boldsymbol{R}_\perp) = \int_{\boldsymbol{r}_\perp} e^{-i\boldsymbol{k}_\perp\cdot\boldsymbol{r}_\perp} S_{\mathrm{R}}\left(x;\boldsymbol{R}_\perp+\frac{\boldsymbol{r}_\perp}{2},\boldsymbol{R}_\perp-\frac{\boldsymbol{r}_\perp}{2}\right)$$

Modified to include spatial dependence with nucleon substructure. 3 hot spots locations sampled from

$$P(\boldsymbol{R}_{\perp,i}) = \frac{1}{2\pi B_{\mathrm{qc}}} e^{-\boldsymbol{R}_{\perp,i}^2/(2B_{qc})}$$ and hot spot density distribution $$T_q(\boldsymbol{R}_\perp - \boldsymbol{R}_{\perp,i}) = \xi_{Q_s^2} e^{-(\boldsymbol{R}_\perp-\boldsymbol{R}_{\perp,i})^2/(2(\xi_{B_q})B_q)}$$

fluctuating normalization

fluctuating size

B_q is given an x dependence motivated by JIMWLK evolution of proton size

Hadronize using KKP fragmentation function $$\frac{\mathrm{d}N_{\mathrm{ch}}(\boldsymbol{b}_\perp)}{\mathrm{d}\eta} = \int_{\boldsymbol{p}_\perp}\int_{z_{\mathrm{min}}}^1 \mathrm{d}z \frac{D_h(z)}{z^2}\mathcal{J}_{y\to\eta}\frac{\mathrm{d}N_g(\boldsymbol{b}_\perp)}{\mathrm{d}^2\boldsymbol{p}_{g\perp}\mathrm{d}y_g}\Bigg|_{\boldsymbol{p}_{g\perp}=\boldsymbol{p}_\perp/z}$$

MODEL: J/Ψ PRODUCTION (NRQCD)

Salazar, Schenke, Soto-Ontoso, Phys.Lett.B 827 (2022) 136952

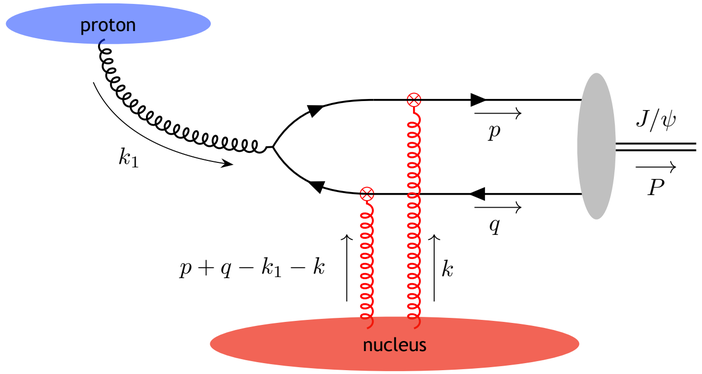

$c\bar{c}$-pair production in NRQCD Z.-B. Kang, Y.-Q. Ma, and R. Venugopalan, JHEP 01, 056 (2014)

$$\frac{\mathrm{d}N^{\kappa}_{c\bar{c}}(\boldsymbol{b}_\perp)}{\mathrm{d}^2\boldsymbol{P}_\perp \mathrm{d}Y} = \frac{\alpha_s}{(2\pi)^9(N_c^2-1)} \int_{\boldsymbol{k}_{1\perp},\boldsymbol{k}_\perp,\boldsymbol{k}'_\perp,\boldsymbol{R}_\perp} \mathscr{H}^{\kappa}(\boldsymbol{P}_\perp - \boldsymbol{k}_{1\perp}, \boldsymbol{k}_\perp, \boldsymbol{k}'_\perp) \frac{\phi^p(x_p, \boldsymbol{k}_{1\perp}, \boldsymbol{R}_\perp)}{\boldsymbol{k}_{1\perp}^2} \tilde{\Xi}^{\kappa}(x_A; \boldsymbol{P}_\perp - \boldsymbol{k}_{1\perp}, \boldsymbol{k}_\perp, \boldsymbol{k}'_\perp; \boldsymbol{R}_\perp - \boldsymbol{b}_\perp)$$

for quantum state κ. The pair momentum is $\boldsymbol{P}_\perp = \boldsymbol{p}_\perp + \boldsymbol{q}_\perp$, $\mathscr{H}^{\kappa}$ are the hard factors, and $\tilde{\Xi}^{\kappa}$ the Wilson line correlators:

$$\tilde{\Xi}^{[8]}(x; \boldsymbol{l}_\perp, \boldsymbol{k}_\perp, \boldsymbol{k}'_\perp; \boldsymbol{R}_\perp) = (2\pi)^2 \delta^{(2)}(\boldsymbol{k}_\perp - \boldsymbol{k}'_\perp) \tilde{\mathcal{S}}^A_{\mathrm{F}}(x; \boldsymbol{k}_\perp; \boldsymbol{R}_\perp) \tilde{\mathcal{S}}^A_{\mathrm{F}}(x; \boldsymbol{l}_\perp - \boldsymbol{k}_\perp; \boldsymbol{R}_\perp) + \mathcal{O}\left(1/N_c\right) \text{ (octet)}$$

$$\tilde{\Xi}^{[1]}(x; \boldsymbol{l}_\perp, \boldsymbol{k}_\perp, \boldsymbol{k}'_\perp; \boldsymbol{R}_\perp) = \tilde{\mathcal{S}}^A_{\mathrm{F}}(x; \boldsymbol{k}_\perp; \boldsymbol{R}_\perp) \tilde{\mathcal{S}}^A_{\mathrm{F}}(x; \boldsymbol{k}'_\perp; \boldsymbol{R}_\perp) \tilde{\mathcal{S}}^A_{\mathrm{F}}(x; \boldsymbol{l}_\perp - \boldsymbol{k}_\perp - \boldsymbol{k}'_\perp, \boldsymbol{R}_\perp) + \mathcal{O}\left(1/N_c\right) \text{ (singlet)}$$

approximation of full expression that involves quadruple

$$\frac{\mathrm{d}N_{J/\psi}(\boldsymbol{b}_\perp)}{\mathrm{d}^2\boldsymbol{P}_\perp \mathrm{d}Y} = \sum_{\kappa} \frac{\mathrm{d}N^{\kappa}_{c\bar{c}}(\boldsymbol{b}_\perp)}{\mathrm{d}^2\boldsymbol{P}_\perp \mathrm{d}Y} \langle \mathcal{O}^{J/\psi}_{\kappa} \rangle$$ with non-perturbative long distance matrix elements $\langle \mathcal{O}^{J/\psi}_{\kappa} \rangle$

K.-T. Chao, Y.-Q. Ma, H.-S. Shao, K. Wang, Y.-J. Zhang, Phys. Rev. Lett. 108, 242004 (2012)
Y.-Q. Ma, R. Venugopalan, H.-F. Zhang, Phys. Rev. D 92, 071901 (2015)

Again, spatial dependence in ϕ^p and $\tilde{\mathcal{S}}^A_F$

$$\tilde{\mathcal{S}}_{\mathrm{R}}(x; \boldsymbol{k}_\perp; \boldsymbol{R}_\perp) = \int_{\boldsymbol{r}_\perp} e^{-i\boldsymbol{k}_\perp \cdot \boldsymbol{r}_\perp} S_{\mathrm{R}}\left(x; \boldsymbol{R}_\perp + \frac{\boldsymbol{r}_\perp}{2}, \boldsymbol{R}_\perp - \frac{\boldsymbol{r}_\perp}{2}\right)$$

RESULTS: FLUCTUATIONS

Salazar, Schenke, Soto-Ontoso, Phys.Lett.B 827 (2022) 136952

- **Charged hadron multiplicity distribution**

  Experimental data: CMS Collaboration, Phys.Lett. B718, 795 (2013), https://twiki.cern.ch/twiki/bin/view/CMSPublic/ PhysicsResultsHIN12015

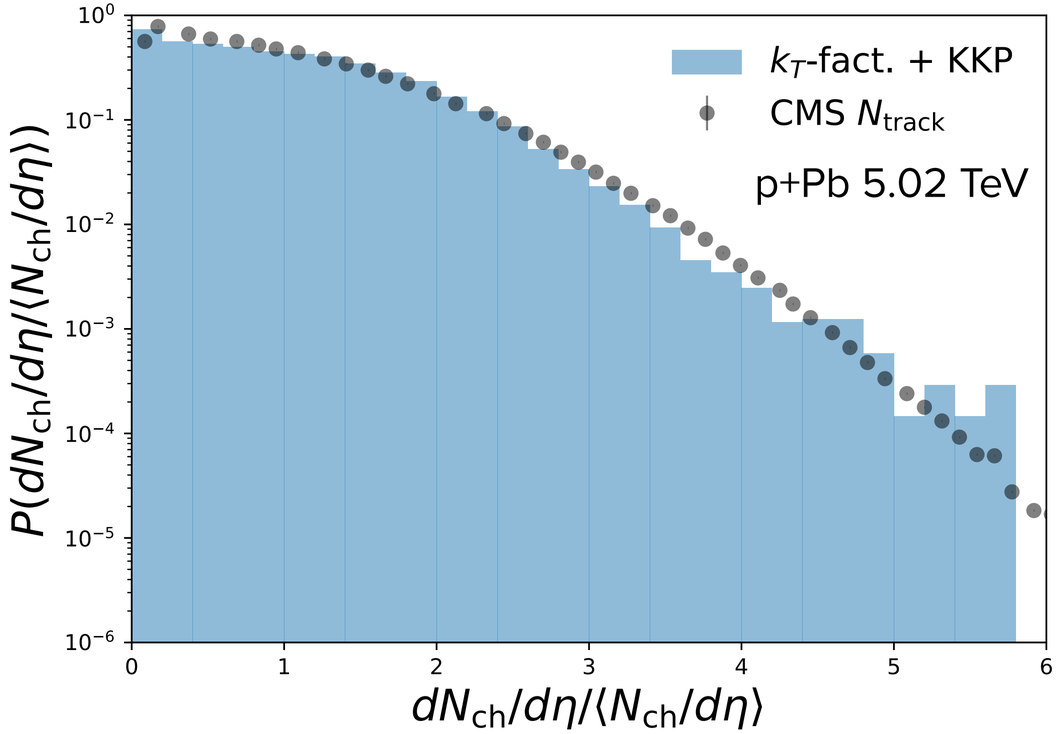

Parameter	Value
N_q	3
B_{qc}	$3\,\text{GeV}^{-2}$
B_q	$1\,\text{GeV}^{-2}$
σ_{B_q}	0.7
$\sigma_{Q_s^2}$	0.1
$S_\perp$	13 mb

Parameter	Value
α_s	0.16
m_{IR}	$0.2\,\text{GeV}$
$m_{J/\psi}$	$3.1\,\text{GeV}$
m_c	$m_{J/\psi}/2$
m_D	$1.87\,\text{GeV}$

σ_{B_q} and σ_{Q_s}: width parameters in log-normal fluctuations ξ

m_{IR}: infrared regulator in the charged hadron calculation

RESULTS: J/Ψ VS. CHARGED HADRON YIELD

Salazar, Schenke, Soto-Ontoso, Phys.Lett.B 827 (2022) 136952

- **Saturation drives the correlation between J/ψ and charged hadrons**

  Experimental data: S. Acharya et al. (ALICE), JHEP 09, 162 (2020), arXiv:2004.12673 [nucl-ex].

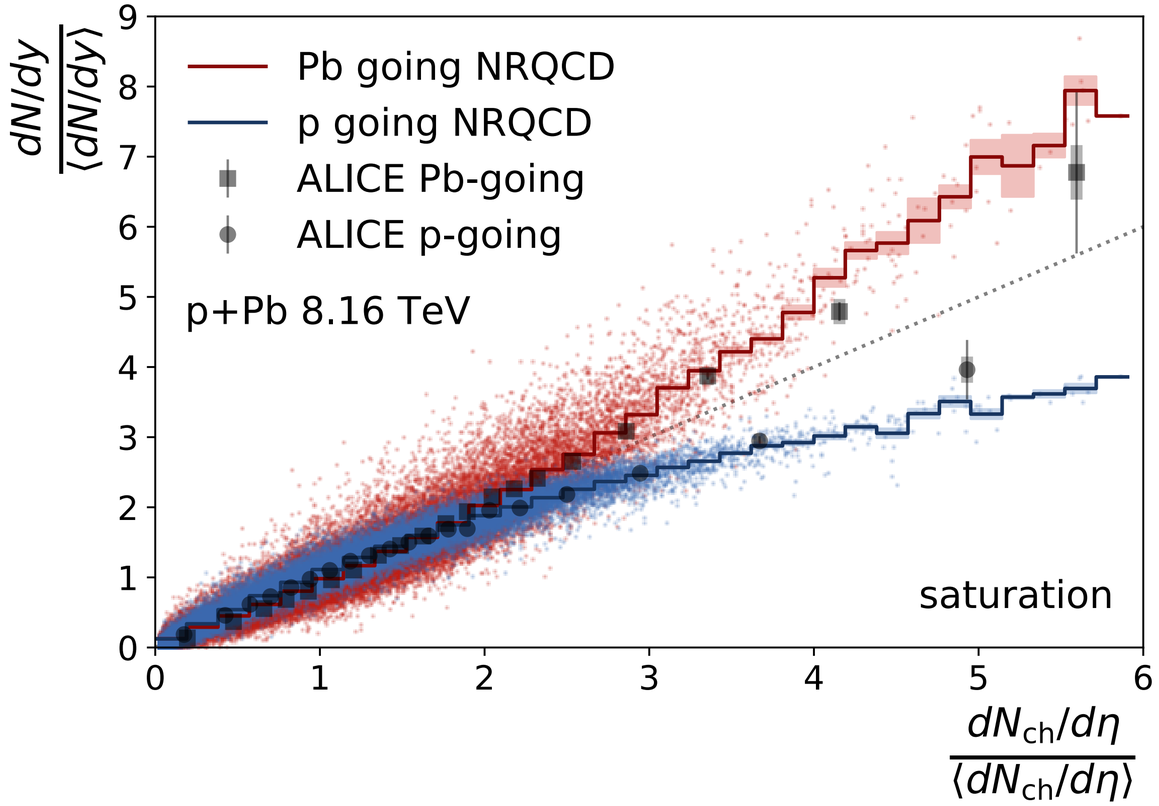

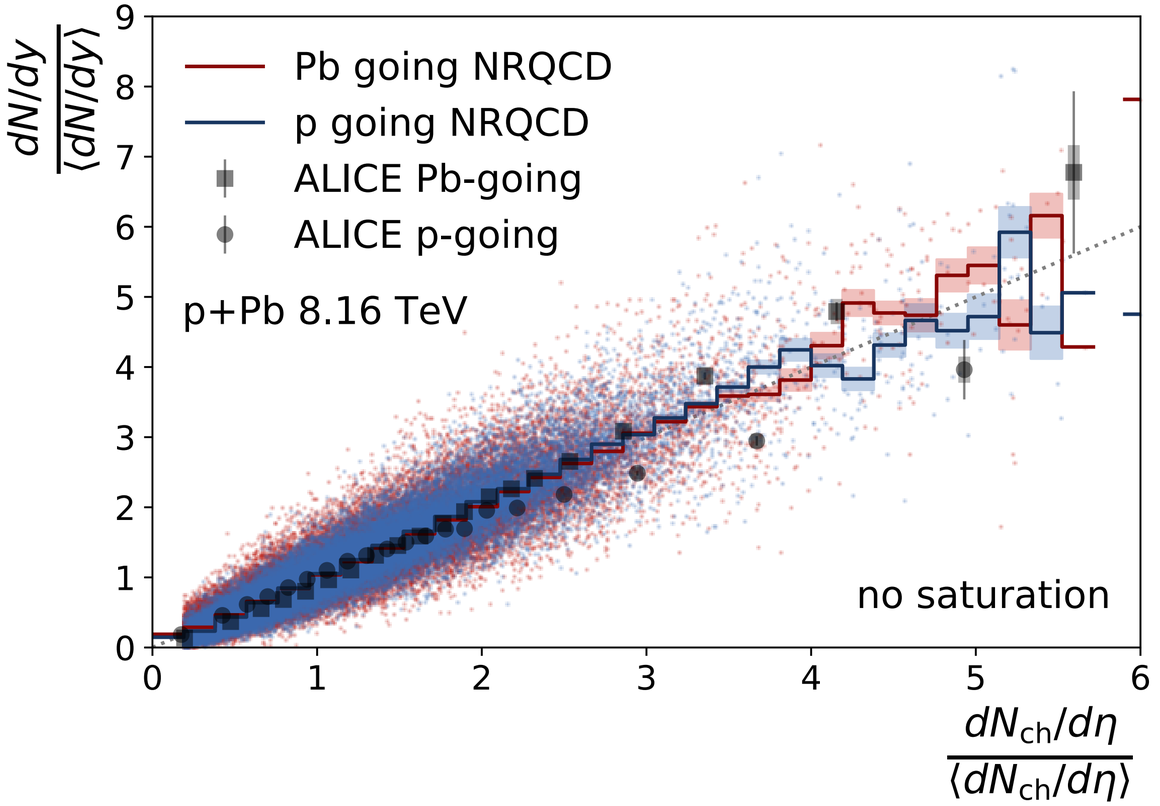

Double-inclusive DIS

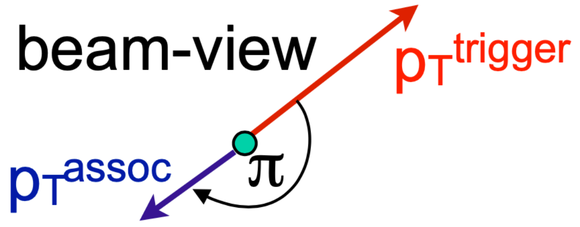

C. Marquet, B. -W. Xiao and F. Yuan, Phys. Lett. B 682 (2009) 207
L. Zheng, E.C. Aschenauer, J.H. Lee, Bo-Wen Xiao, Phys. Rev. D 89, 074037 (2014)

Back-to-back peak suppressed more in larger nuclei as momentum imbalance $\sim Q_s$

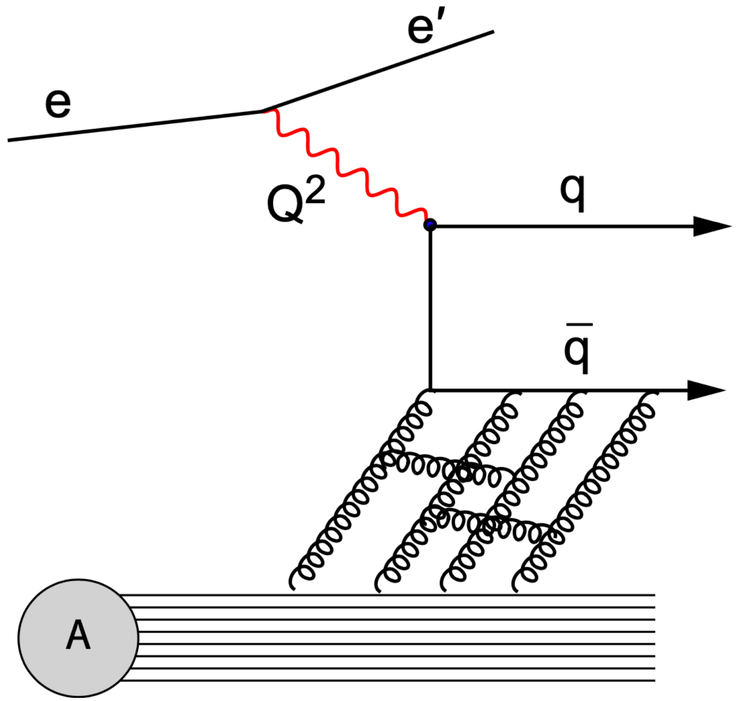

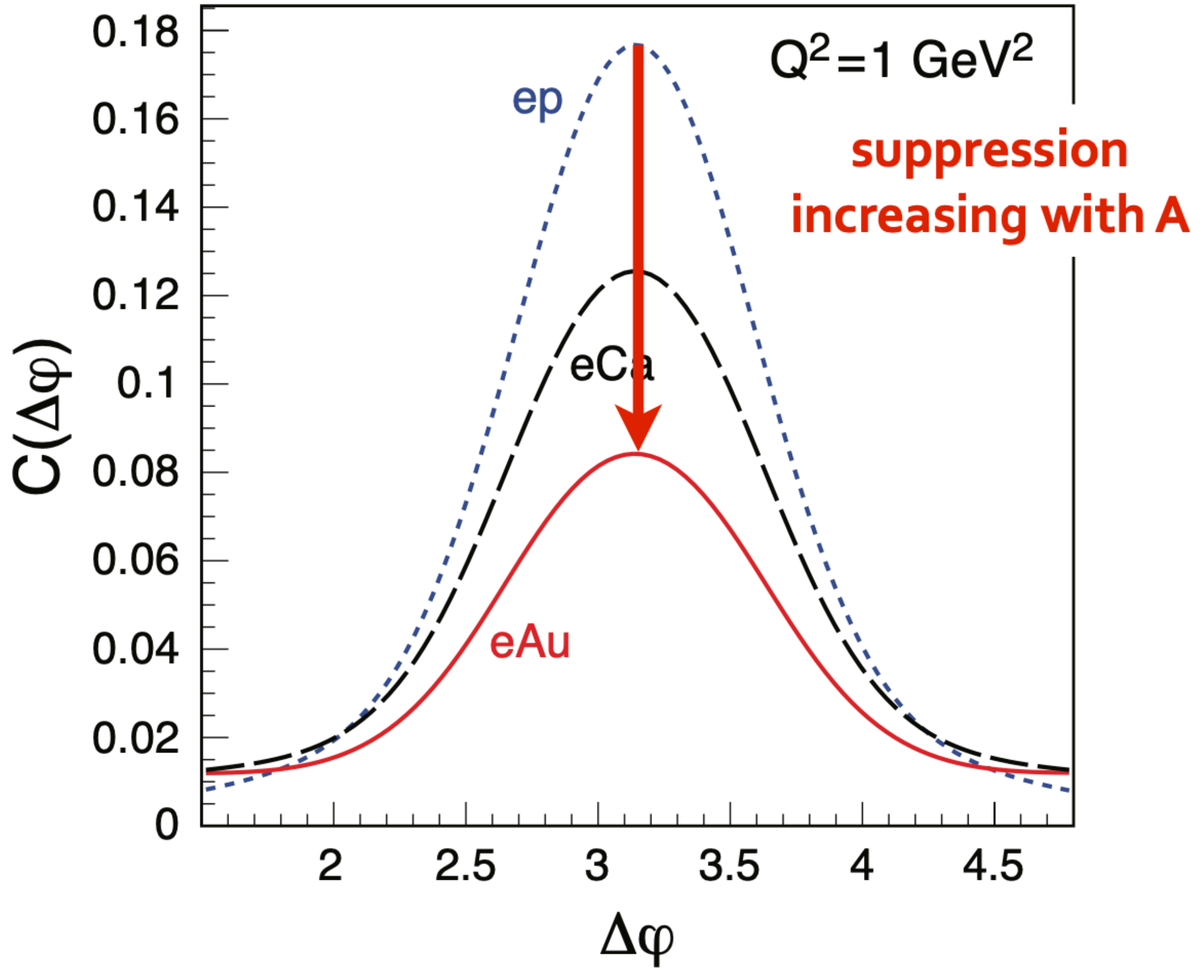

Double-inclusive DIS

C. Marquet, B. -W. Xiao and F. Yuan, Phys. Lett. B 682 (2009) 207
L. Zheng, E.C. Aschenauer, J.H. Lee, Bo-Wen Xiao, Phys. Rev. D 89, 074037 (2014)

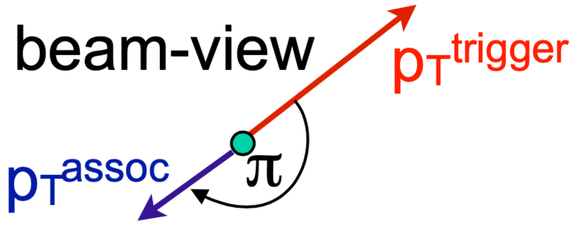

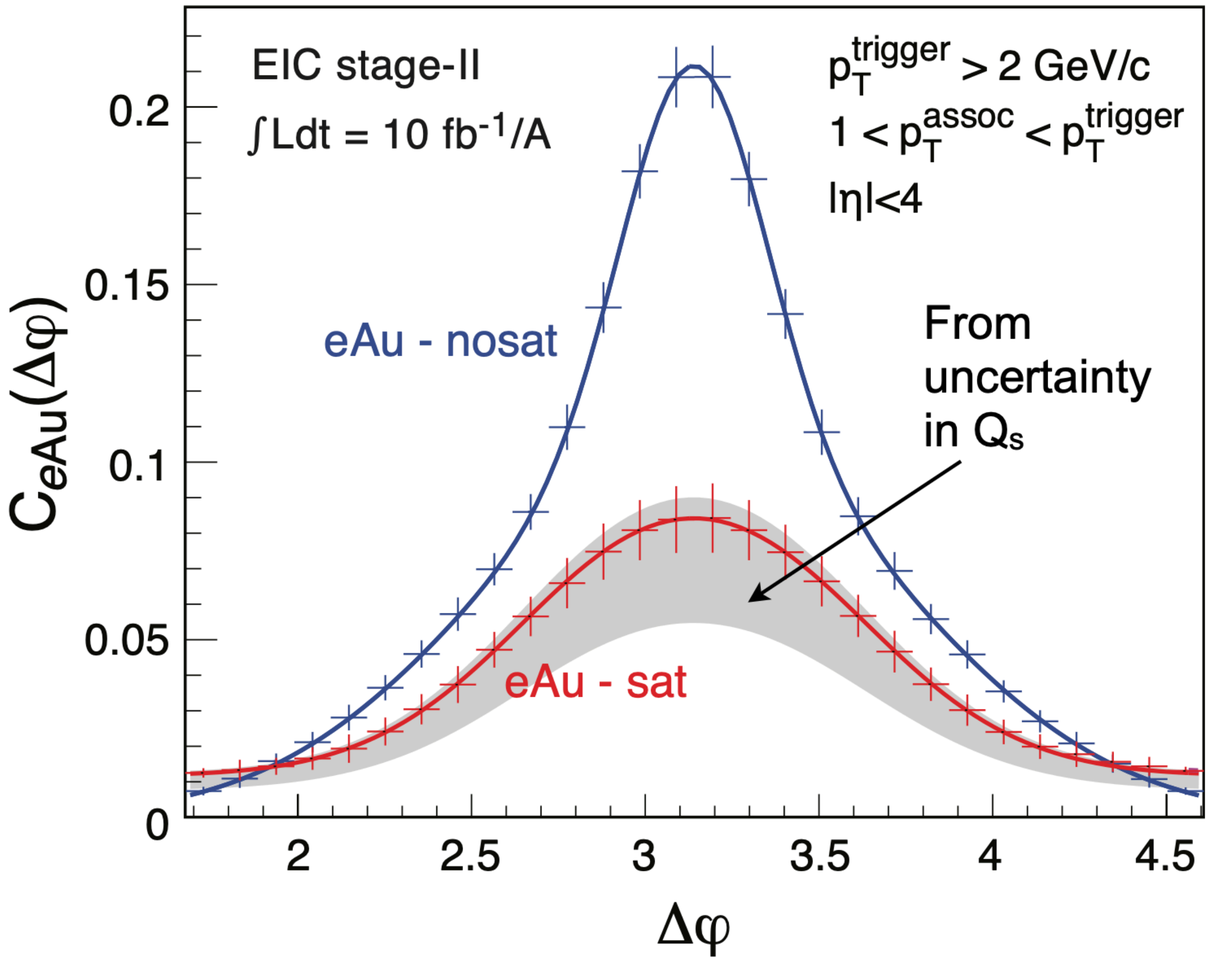

Clear key measurement

- Significant difference between sat and non-sat case
- Has equivalent to pA (e.g. RHIC forward measurements)
- Parton showers can modify predictions

Diffractive processes

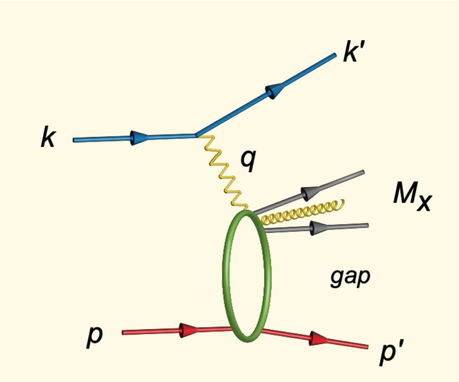

Diffractive events are characterized by rapidity gap

Neutral color exchange requires at least two-gluons → enhanced sensitivity to gluon saturation

Ratio of diffractive and total cross-section in ep and eAu collisions →

Clear difference between saturation models and leading twist shadowing (LTS)

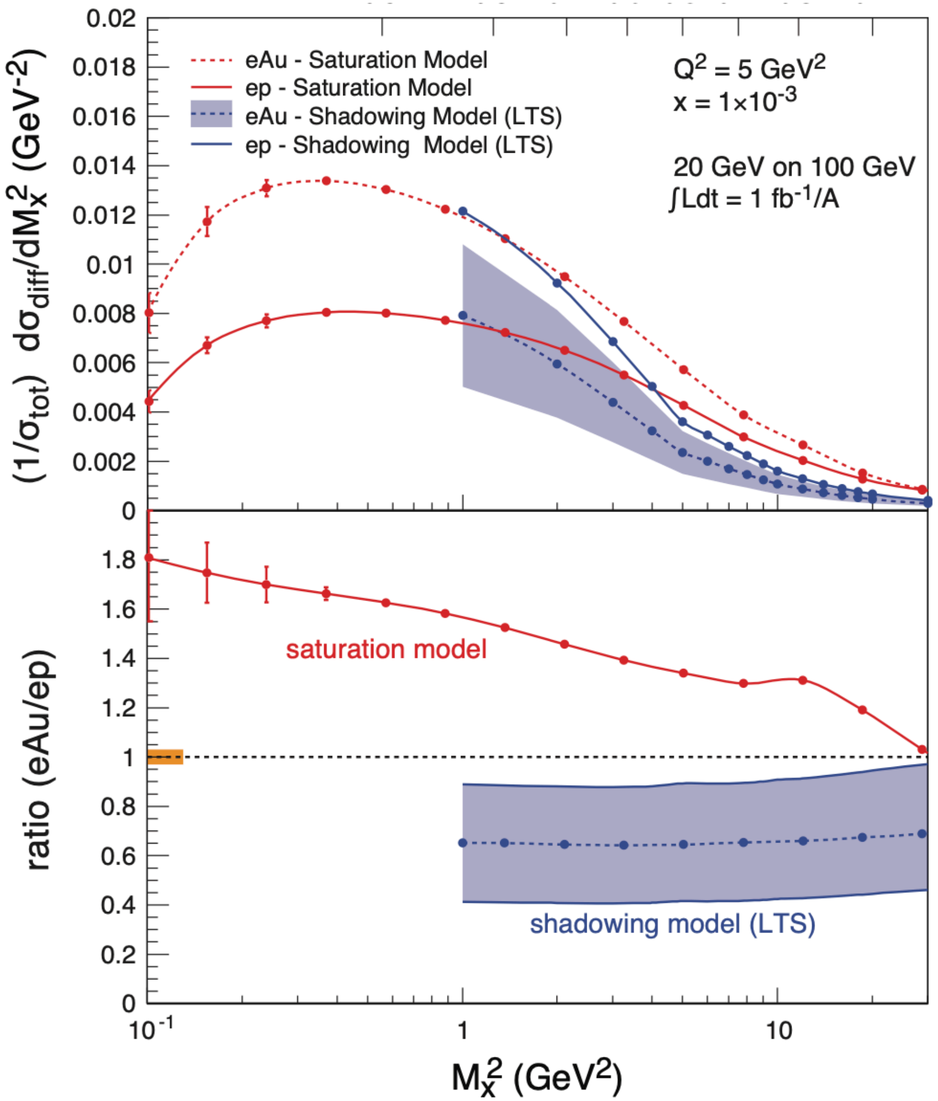

A. Accardi et al., EIC White Paper, Eur.Phys.J.A 52 (2016) 9, 268

Diffractive vector meson production

https://arxiv.org/pdf/1712.02508.pdf

T. Toll, T. Ullrich, Phys.Rev.C 87 (2013) 2, 024913
A. Accardi et al., EIC White Paper, Eur.Phys.J.A 52 (2016) 9, 268

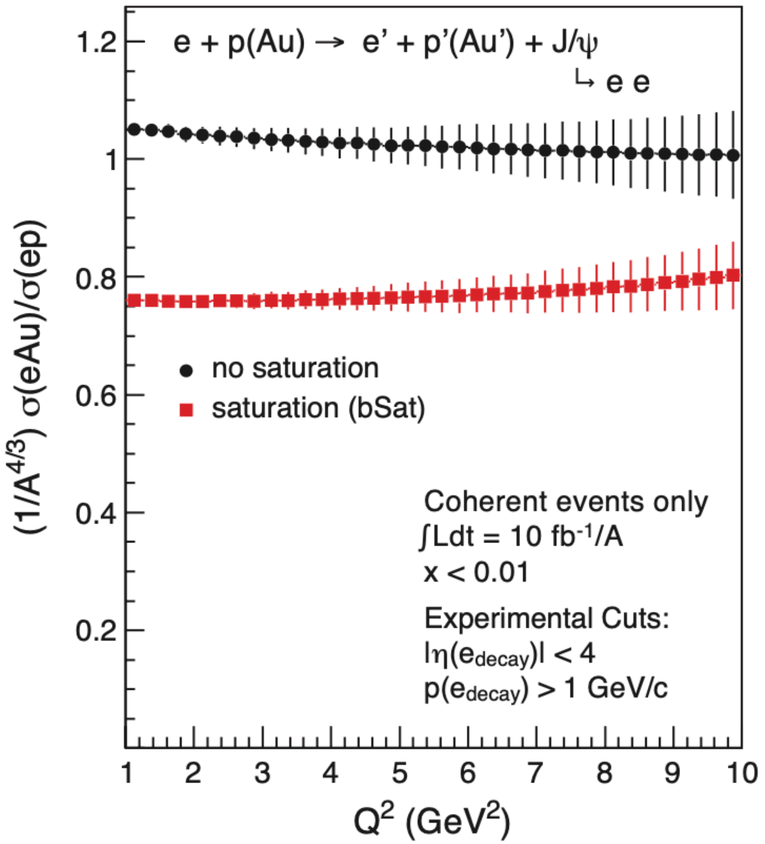

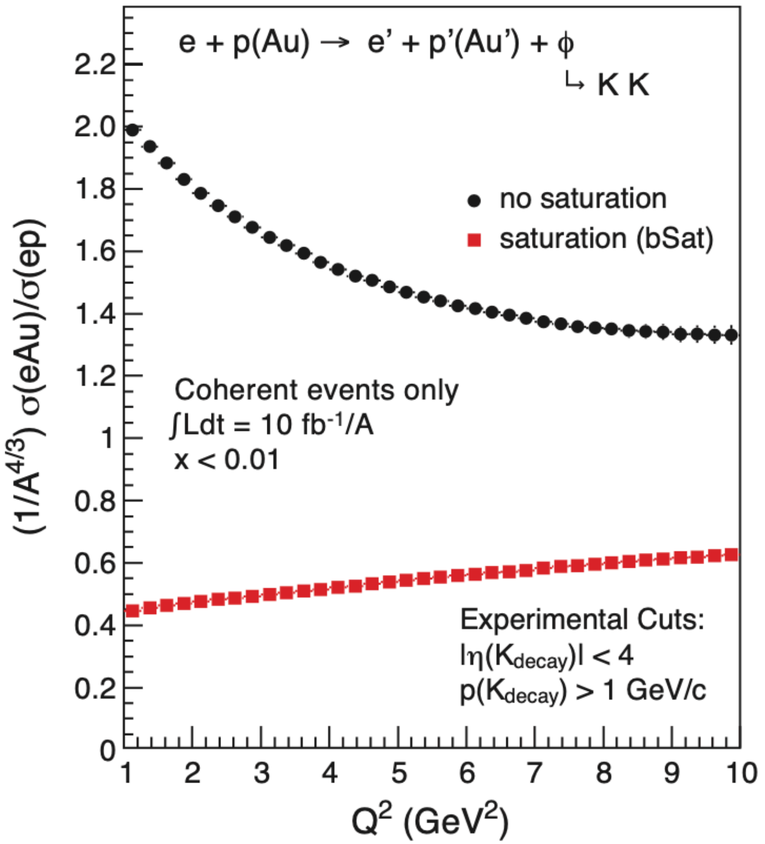

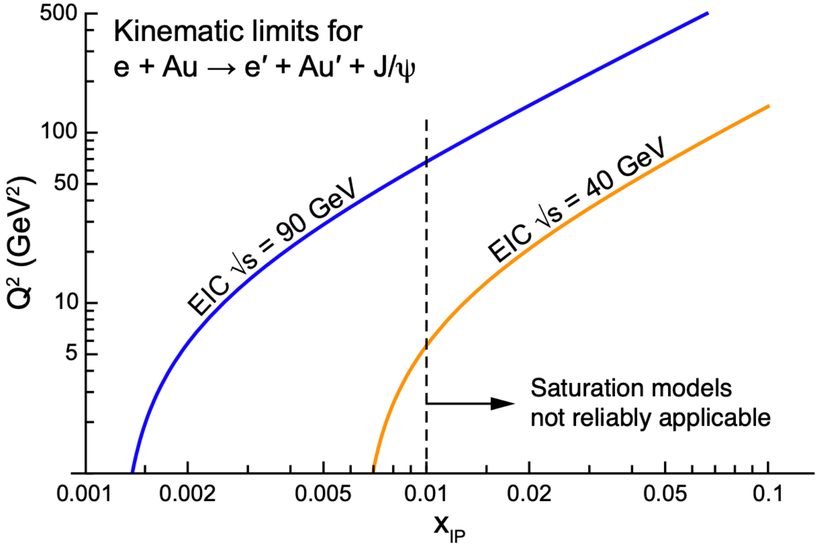

We want high energies to probe saturation

- Sartre event generator (bSat & bNonSat = linearized bSat)
- Big difference for ϕ less so for J/ψ (larger mass cuts off large dipoles)

Diffractive vector meson production

T. Toll, T. Ullrich, Phys.Rev.C 87 (2013) 2, 024913
A. Accardi et al., EIC White Paper, Eur.Phys.J.A 52 (2016) 9, 268

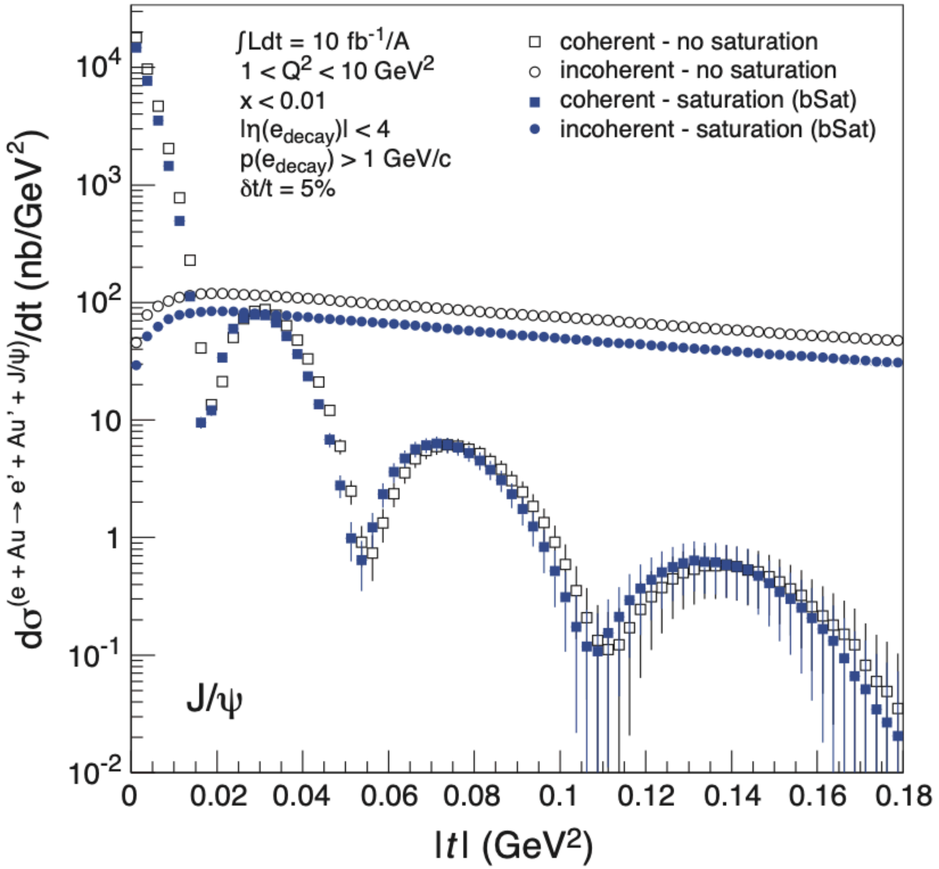

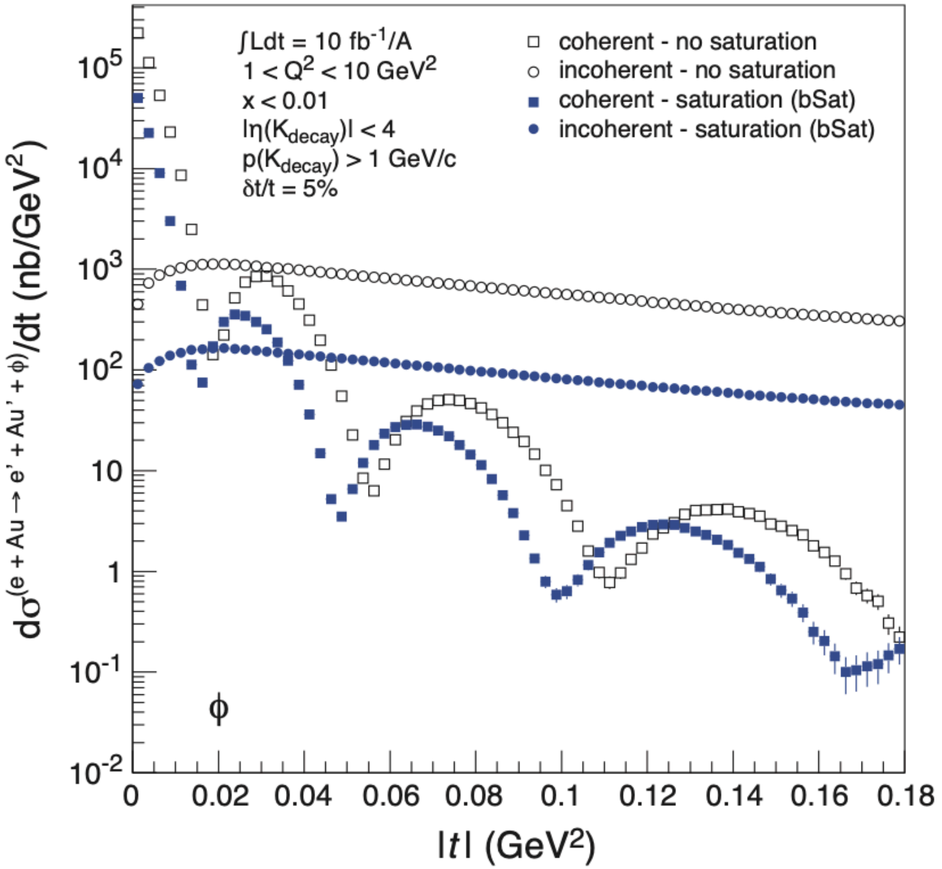

- Sartre event generator (bSat & bNonSat = linearized bSat)
- Big difference for ϕ less so for J/ψ (larger mass cuts off large dipoles)

Diffractive dijet production - saturation effects

F. Salazar, B. Schenke, Phys.Rev. D100 (2019) 034007

Slow-down of growth of
the cross section for heavy nuclei

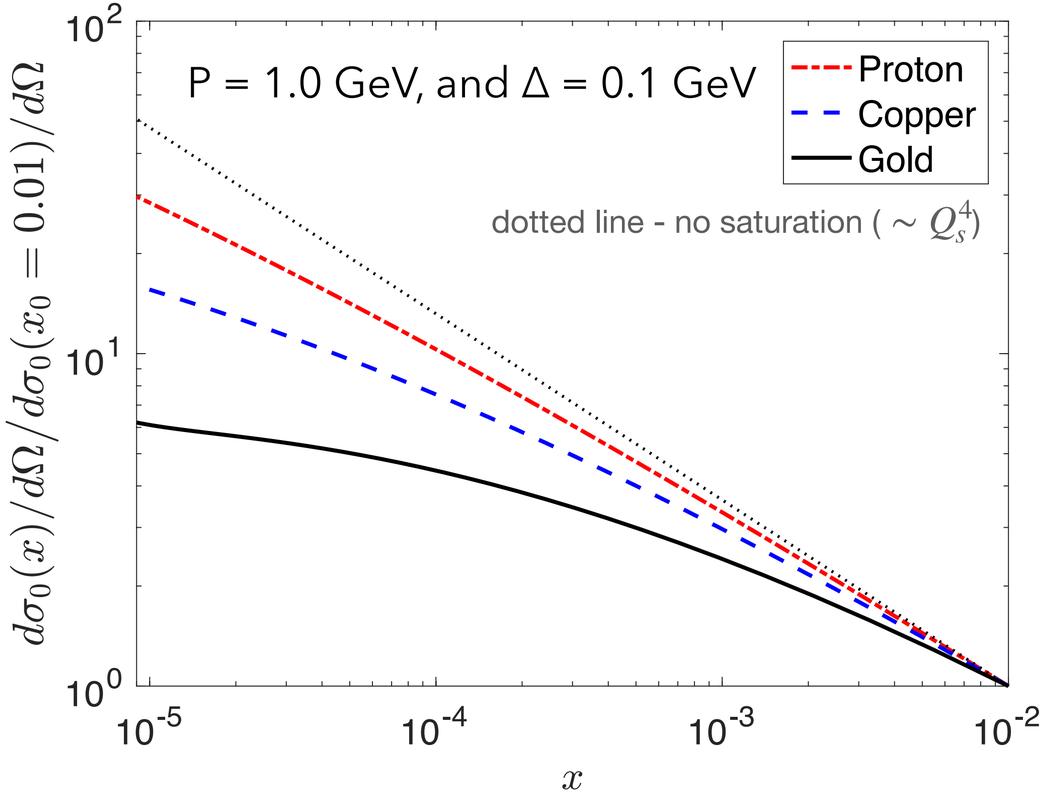

Saturation leads to diffractive dip
even for a Gaussian proton
($T(b)$ appears in the exponential)

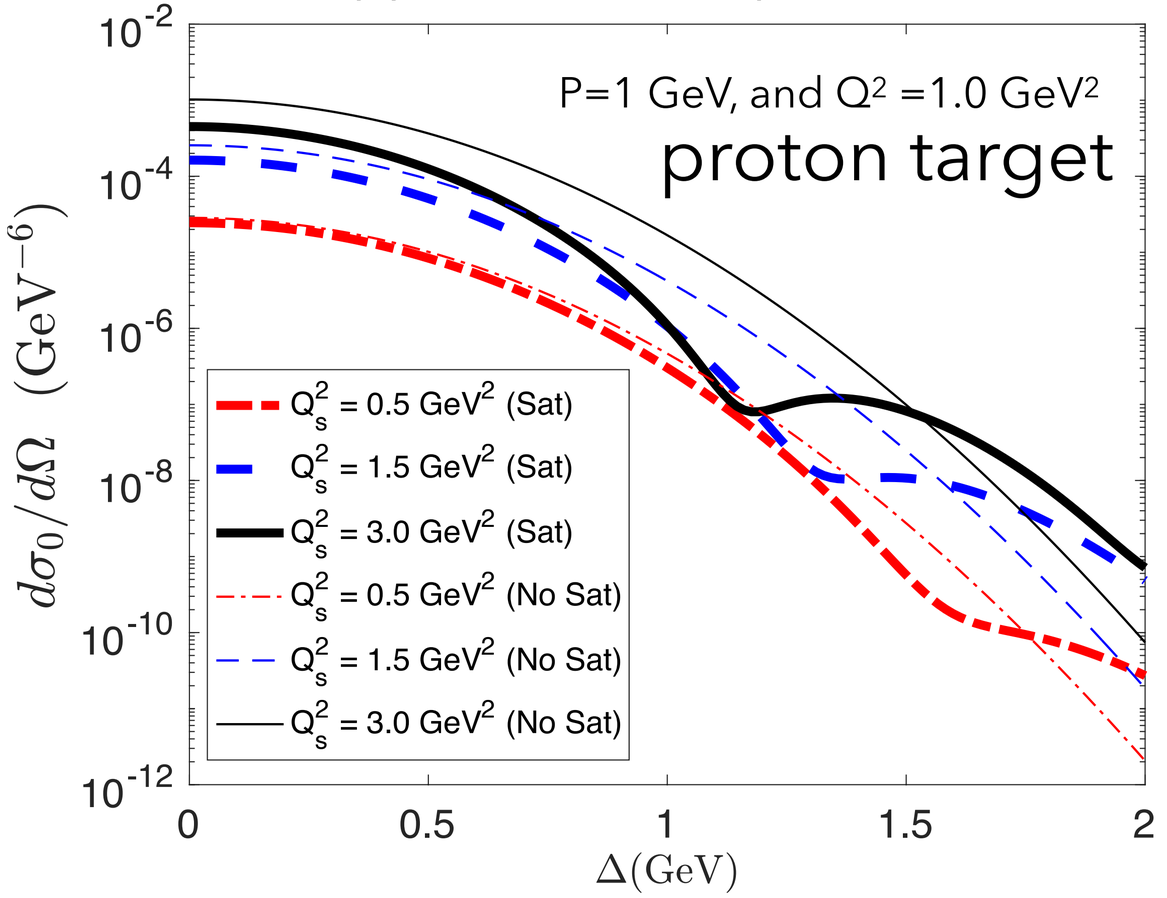

We will return to diffractive processes later

APPLY CGC TO HEAVY ION INITIAL CONDITIONS

- **As discussed, gluon fields follow Yang-Mills equations of motion**

$$[D_\mu, F^{\mu\nu}] = J^\nu$$

with $D_\mu = \partial_\mu + igA_\mu$ **and** $F_{\mu\nu} = \frac{1}{ig}[D_\mu, D_\nu] = \partial_\mu A_\nu - \partial_\nu A_\mu + ig[A_\mu, A_\nu]$

INCOMING CURRENTS AND SOLUTIONS OF YM EQUATIONS

Use light cone coordinates $v^{\pm} = (v^0 \pm v^3)/\sqrt{2}$

Projectile and target currents are then

$$J_P^{\nu} = \delta^{\nu+}\rho_P^a(x^-, \mathbf{x}_\perp)t^a \quad \text{and} \quad J_T^{\nu} = \delta^{\nu-}\rho_T^a(x^+, \mathbf{x}_\perp)t^a$$

assuming color sources ('valence quarks') are static in light cone time

Plug currents into Yang-Mills equations and solve in Lorenz gauge $\partial_\mu A^\mu = 0$

For projectile use ansatz $A^\mu = \delta^{\mu+}A_a^\mu(x^-, \mathbf{x}_\perp)t^a$ **one finds that** A^+ **is independent of** x^+ **because** $\partial_+ A^+ = 0$

Then field strength tensor only has this component $F^{i+} = \partial^i A^+$

INCOMING CURRENTS AND SOLUTIONS OF YM EQUATIONS

Then field strength tensor only has this component $F^{i+} = \partial^i A^+$

plugged into YM equations yields $\partial_i \partial^i A^+ = J^+$, the Poisson equation in the transverse plane:

$$-\Delta_\perp A^+(x^-, \mathbf{x}_\perp) = \rho^a(x^-, \mathbf{x}_\perp) t^a$$

where $\Delta_\perp = \sum_i \partial_i^2$.

Formal solutions to this are

$$A_P^+(x^-, \mathbf{x}_\perp) = -\frac{\rho_P^a(x^-, \mathbf{x}_\perp) t^a}{\Delta_\perp}, \text{ and } A_T^-(x^+, \mathbf{x}_\perp) = -\frac{\rho_T^a(x^+, \mathbf{x}_\perp) t^a}{\Delta_\perp}$$

INCOMING CURRENTS AND SOLUTIONS OF YM EQUATIONS

An infrared regulator m gets rid of Coulomb tails:

$$A^{\pm}_{P/T}(x^{\mp}, \mathbf{x}_\perp) = -\frac{\rho^a_{P/T}(x^{\mp}, \mathbf{x}_\perp) t^a}{\Delta_\perp - m^2}$$

The same could be achieved by enforcing color neutrality on length scales $\sim 1/\Lambda_{\rm QCD}$

This concludes the calculation of the incoming gluon fields.

But, note that $\rho^a_{P/T}(x^{\mp}, \mathbf{x}_\perp)$ has not been specified yet.

BEYOND CLASSICAL FIELDS (NOT OFTEN USED IN HICS)

The gluon fields are defined at a certain momentum fraction x.

The x-dependence can be computed using the JIMWLK equations

Example on the right:

Wilson line

$$V^\dagger(x^-, \mathbf{x}_\perp) = \mathscr{P} \exp\left(-ig \int_{-\infty}^{x^-} dz^- A^+(z^-, \mathbf{x}_\perp)\right)$$

correlator for constant color charge density and Gaussian distributed ρ^a

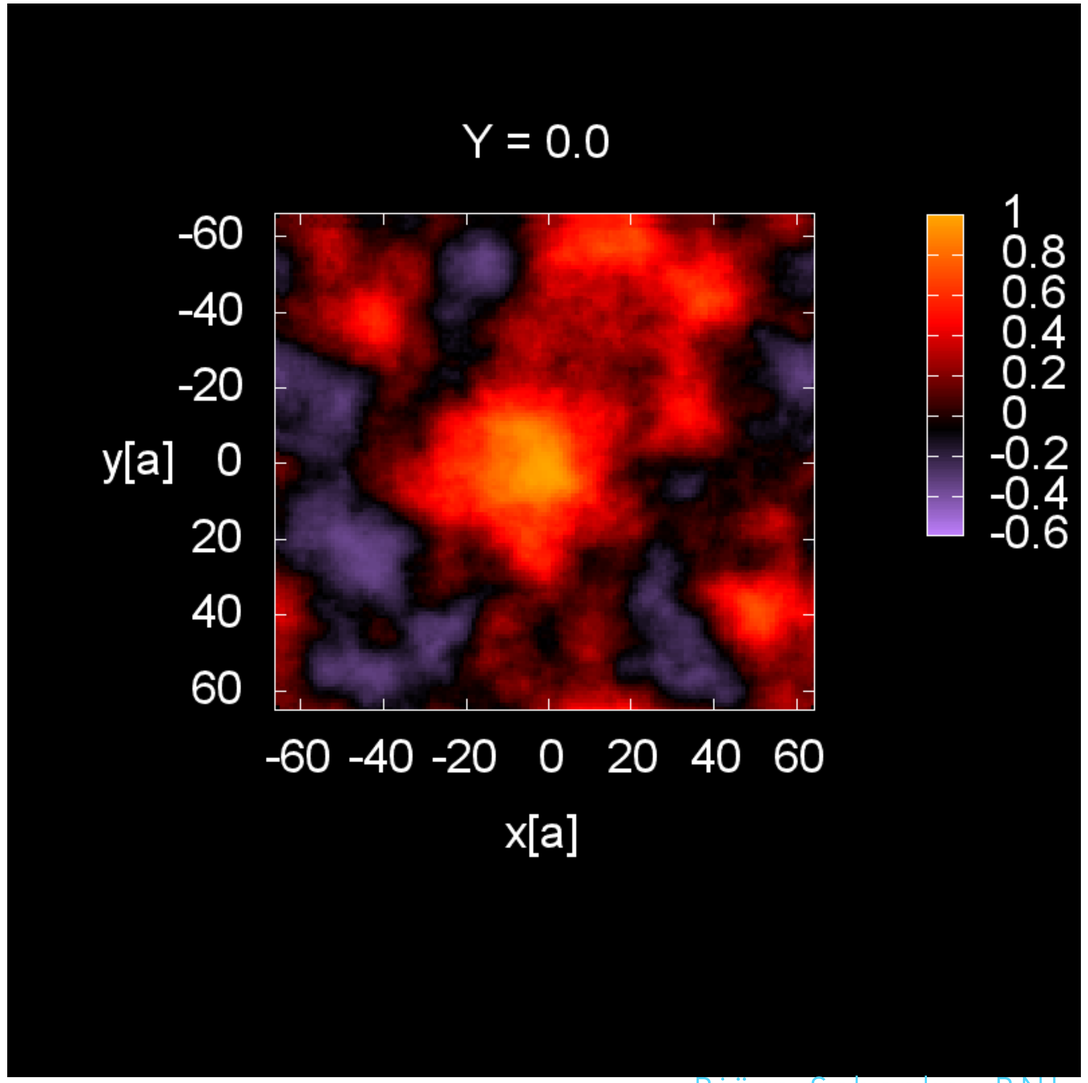

THE COLLISION - LIGHT CONE GAUGE

- **Computing gluon fields after the collision is more conveniently done in light cone gauge $A^+ = 0$ for a right moving nucleus, $A^- = 0$ for a left moving nucleus**

gauge transformation: $$A_\mu(x) \to V(x)\left(A_\mu(x) - \frac{i}{g}\partial_\mu\right)V^\dagger(x)$$

To achieve $A^+ = 0$ the Wilson line must fulfill

$$\partial_- V^\dagger(x^-, \mathbf{x}_\perp) = -igA^+(x^-, \mathbf{x}_\perp)V^\dagger(x^-, \mathbf{x}_\perp)$$

which is solved by $$V^\dagger(x^-, \mathbf{x}_\perp) = \mathscr{P}\exp\left(-ig\int_{-\infty}^{x^-} dz^- A^+(z^-, \mathbf{x}_\perp)\right)$$

Also $\partial_+ V^\dagger = 0$, so $A^- = 0$ as well.

These are the Wilson lines we have been using all along (note $\mathscr{P}$ is path ordering here)

THE COLLISION - LIGHT CONE GAUGE

- **The transverse components are not zero but pure gauge fields:**

$$A^i(x^-, \mathbf{x}_\perp) = \frac{1}{ig} V(x^-, \mathbf{x}_\perp) \partial^i V^\dagger(x^-, \mathbf{x}_\perp)$$

- **Color current in light cone gauge is**

$$J^+_{\mathrm{LC}}(x^-, \mathbf{x}_\perp) = \rho_{\mathrm{LC}}(x^-, \mathbf{x}_\perp) = V(x^-, \mathbf{x}_\perp) \rho(x^-, \mathbf{x}_\perp) V^\dagger(x^-, \mathbf{x}_\perp)$$

- **Again, REALLY high energy approximation:** $\rho(x^-, \mathbf{x}_\perp) = \delta(x^-)\rho(\mathbf{x}_\perp)$ **(thin sheet)**

  A^+ **has the same support and Wilson line is only nontrivial if** x^- **integration limit is >0.**

- **So** $A^i(x^-, \mathbf{x}_\perp) = \theta(x^-)\alpha^i(\mathbf{x}_\perp)$ **with** $\alpha^i(\mathbf{x}_\perp) = \frac{1}{ig} V(\mathbf{x}_\perp)\partial^i V^\dagger(\mathbf{x}_\perp)$ **and** $V^\dagger(\mathbf{x}_\perp) = V^\dagger(x^- \to \infty, \mathbf{x}_\perp)$

THE COLLISION - LIGHT CONE GAUGE

- Doing the same for the left moving nucleus and choosing the gauge field to be zero for the quadrant where $x^- < 0$ and $x^+ < 0$ one finds

$$A^i(\mathbf{x}_\perp) = \theta(x^-)\theta(-x^+)\alpha_P^i(\mathbf{x}_\perp) + \theta(x^+)\theta(-x^-)\alpha_T^i(\mathbf{x}_\perp)$$

$$= \theta(x^-)\theta(-x^+)\frac{1}{ig}V_P(\mathbf{x}_\perp)\partial^i V_P^\dagger(\mathbf{x}_\perp) + \theta(x^+)\theta(-x^-)\frac{1}{ig}V_T(\mathbf{x}_\perp)\partial^i V_T^\dagger(\mathbf{x}_\perp)$$

for the fields before the collision (all transverse)

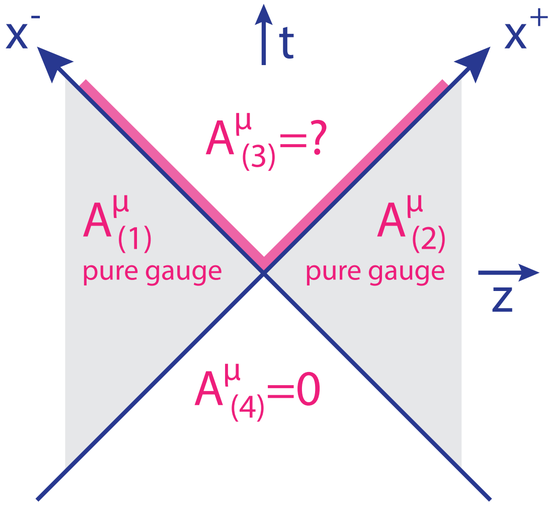

- Now for the forward light cone. We choose Fock-Schwinger gauge: $x^+A^- + x^-A^+ = 0$

BOOST INVARIANCE

- At super high energy, currents are proportional to delta functions

$$J^\nu = \delta^{\nu+}\rho_P(\mathbf{x}_\perp)\delta(x^-) + \delta^{\nu-}\rho_T(\mathbf{x}_\perp)\delta(x^+)$$

In this case, the current, and the solutions for the gluon fields are invariant under longitudinal boosts ("boost invariant"), meaning invariant under

$$x^\pm \to x'^\pm = e^{\pm\beta}x^\pm$$
$$J^\pm(x) \to J'^\pm(x') = e^{\pm\beta}J^\pm(x)$$

with β the longitudinal boost parameter (no mixing, just rescaling!).

- Current does not change its form: $J^\pm_{P/T}(x^\mp, \mathbf{x}_\perp) \to e^{\pm\beta}\delta(e^{\pm\beta}x'^\mp)\rho_{P/T}(\mathbf{x}_\perp) = \delta(x'^\mp)\rho_{P/T}(\mathbf{x}_\perp)$

BOOST INVARIANCE

In the future light cone define $x^+ = \frac{\tau}{\sqrt{2}} e^{+\eta}$, and $x^- = \frac{\tau}{\sqrt{2}} e^{-\eta}$

or inverted $\tau = \sqrt{2x^+x^-}$, and $\eta = \frac{1}{2} \ln\left(\frac{x^+}{x^-}\right)$

The gauge field transforms as $A'^{\mu}(x') = \frac{\partial x'^{\mu}}{\partial x^{\nu}} A^{\nu}(x)$**, leading to**

$$A^{\tau} = \frac{1}{\tau}(x^- A^+ + x^+ A^-) = A_{\tau} \quad \textbf{and} \quad A^{\eta} = \frac{1}{\tau^2}(x^- A^+ - x^+ A^-) = -\frac{1}{\tau^2} A_{\eta}$$

Choose the gauge fields to be η**-independent**

SOLUTION IN THE FORWARD LIGHT CONE

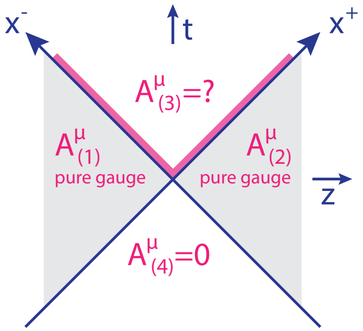

To find the solution in the forward light cone, write general expression

$$A^i(x) = \theta(x^+)\theta(x^-)\alpha^i(\tau, \mathbf{x}_\perp) + \theta(x^-)\theta(-x^+)\alpha_P^i(\mathbf{x}_\perp) + \theta(x^+)\theta(-x^-)\alpha_T^i(\mathbf{x}_\perp)$$

$$A^\eta(x) = \theta(x^+)\theta(x^-)\alpha^\eta(\tau, \mathbf{x}_\perp)$$

$A^\tau = 0$, **because we chose Fock-Schwinger gauge** $x^+A^- + x^-A^+ = 0$

Plugging above ansatz into YM equations leads to singular terms on the boundary $\tau \to 0$ **from derivatives of** θ**-functions.**

Requiring that the singularities vanish leads to the solutions

$$\alpha^i = \alpha_P^i + \alpha_T^i \qquad \alpha^\eta = -\frac{ig}{2}\left[\alpha_{Pj}, \alpha_T^j\right] \qquad \partial_\tau \alpha^i = 0 \qquad \partial_\tau \alpha^\eta = 0$$

INITIAL CONDITIONS FOR HEAVY ION COLLISIONS

From the gluon fields in the forward light cone compute the energy momentum tensor

$$T^{\mu\nu} = -g^{\mu\alpha} g^{\nu\beta} g^{\gamma\delta} F_{\alpha\gamma} F_{\beta\delta} + \frac{1}{4} g^{\mu\nu} g^{\alpha\gamma} g^{\beta\delta} F_{\alpha\beta} F_{\gamma\delta}$$

$$T^{\tau\tau} = \frac{1}{2}(E^{\eta})^2 + \frac{1}{2\tau^2}[(E^{x})^2 + (E^{y})^2] + \frac{1}{2} F_{xy} F_{xy} + \frac{1}{2\tau^2}(F_{x\eta}^2 + F_{y\eta}^2)$$

longitudinal electric field

transverse electric field

longitudinal magnetic field

transverse magnetic field

COLOR CHARGE DISTRIBUTION

In the heavy ion discussion, we have not defined $\rho^a_{P/T}(x^{\mp}, \mathbf{x}_\perp)$ yet.

As before, we assume a really large nucleus, where the color charges are locally Gaussian correlated: $\langle \rho^a(\mathbf{b}_\perp)\rho^b(\mathbf{x}_\perp)\rangle = g^2\mu^2(x, \mathbf{b}_\perp)\delta^{ab}\delta^{(2)}(\mathbf{b}_\perp - \mathbf{x}_\perp)$ and have zero mean.

Again, that's the McLerran-Venugopalan model (originally with homogeneous μ).

Here, $g^2\mu(x, \mathbf{b}_\perp)$ depends on the longitudinal momentum fraction x and the transverse position $\mathbf{b}_\perp$, both functional dependencies that need to be modeled.

In the IP-Glasma model, that modeling is done in part by using the IPSat model and in part by a Monte Carlo model for the fluctuating geometry of a nucleus or proton projectile

IPSAT

Kowalski, Teaney, Phys.Rev. D68 (2003) 114005

- The total cross section for a small dipole passing through a dilute gluon cloud is proportional to the dipole area, the strong coupling constant, and the number of gluons in the cloud: L. Frankfurt, A. Radyushkin, and M. Strikman, Phys. Rev. D55, 98 (1997)

$$\sigma_{q\bar{q}} = \frac{\pi^2}{N_c} r_T^2 \alpha_s(\mu^2) x g(x, \mu^2)$$

  where $xg(x, \mu^2)$ is the gluon density at some scale μ^2

- From that we get the Glauber-Mueller dipole cross section in a dense gluon system

$$\frac{d\sigma_{q\bar{q}}}{d^2 b_T} = 2(1 - \mathrm{Re}S(b_T)) = 2\left[1 - \exp\left(-\frac{\pi^2}{2N_c} r_T^2 \alpha_s(\mu^2) x g(x, \mu^2) T(b_T)\right)\right]$$

- $T(\mathbf{b})$ and $xg(x, \mu^2)$ are determined from fits to HERA DIS data (b, x, and initial scale μ_0^2 dependence) and DGLAP evolution in μ^2

IPSAT MODEL

Kowalski, Teaney, Phys.Rev. D68 (2003) 114005

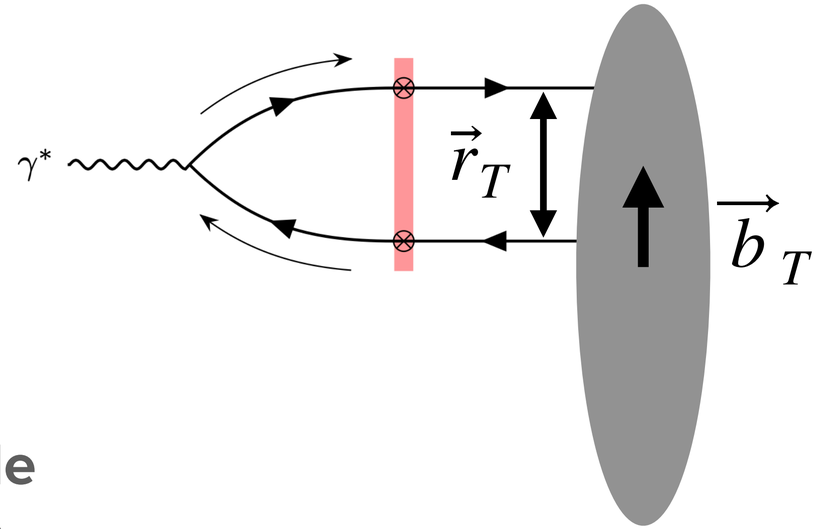

- Deeply inelastic scattering off a proton
- Factorized processes: electron emits γ*, γ* splits into quark-antiquark pair of spatial size $r_\perp$, this dipole interacts elastically with the target (eikonal process)
- The splitting is determined by the photon light-cone wave function computed in light-cone perturbation theory J.D. Bjorken, J.B. Kogut and D.E. Soper, Phys. Rev. D3, 1382 (1970)
- The elastic scattering of the dipole with transverse momentum transfer $\Delta^2=-t$ described by the scattering amplitude $A_{\rm el}^{q\bar{q}}(x, \vec{r}_T, \vec{\Delta})$
- From the optical theorem, we get the total cross section at a given r_T

$$\sigma_{q\bar{q}}(x, r_T) = \mathrm{Im} iA_{\rm el}^{q\bar{q}}(x, r_T, 0) = 2\int [1 - \mathrm{Re}\, S(r_T, \vec{b}_T)] d^2 b_T$$

IPSAT MODEL

Kowalski, Teaney, Phys.Rev. D68 (2003) 114005

- $\sigma_{q\bar{q}}(x, r_T) = \mathrm{Im} iA_{\mathrm{el}}^{q\bar{q}}(x, r_T, 0) = 2\int [1 - \mathrm{Re}\, S(r_T, \overrightarrow{b}_T)] d^2 b_T$
- Here $S(b_T)$ is the S-matrix at distance b_T from the center
- The total cross section for a small dipole to pass through a dilute gluon cloud is proportional to the dipole area, the strong coupling constant, and the number of gluons in the cloud L. Frankfurt, A. Radyushkin, and M. Strikman, Phys. Rev. D55, 98 (1997)

$$\sigma_{q\bar{q}} = \frac{\pi^2}{N_c} r_T^2 \, \alpha_s(\mu^2) \, xg(x, \mu^2)$$

where $xg(x, \mu^2)$ is the gluon density at some scale μ^2

- If the target is dense, the probability that the dipole does not scatter inelastically at impact parameter b_T is

$$P(b_T) = 1 - \frac{\pi^2}{N_c} r_T^2 \alpha_s(\mu^2) xg(x, \mu^2) \, \rho(b_T, z) \, dz$$

IPSAT MODEL

Kowalski, Teaney, Phys.Rev. D68 (2003) 114005

total prob. for no inel. interaction

$$
\begin{aligned}
P(-L < z \leq L) &= \lim_{n\to\infty} \Pi_{i=0}^{n-1} P(z_i < z \leq z_{i+1}) \\
&= \lim_{n\to\infty} \Pi_{i=0}^{n-1} (1 - \sigma_{q\bar{q}} \rho(b, z_i < z \leq z_{i+1}) dz) \\
&= \lim_{n\to\infty} \Pi_{i=0}^{n-1} \exp(-\sigma_{q\bar{q}} \rho(b, z_i < z \leq z_{i+1}) dz) \\
&= \exp(- \lim_{n\to\infty} \sum_{i=0}^{n-1} \sigma_{q\bar{q}} \rho(b, z_i < z \leq z_{i+1}) dz) \\
&= \exp\left(- \int_{-L}^{L} \sigma_{q\bar{q}} \rho(b, z) dz\right) \\
&= \exp(-\sigma_{q\bar{q}} T(b)) = P_{\mathrm{tot}}(b) \qquad \text{letting } L \to \infty
\end{aligned}
$$

IPSAT MODEL

Kowalski, Teaney, Phys.Rev. D68 (2003) 114005

- **So the probability for the dipole not to interact inelastically passing through the entire target is:**

$$|S(b_T)|^2 = P_{\text{tot}}(b_T) = \exp\left(-\frac{\pi}{N_c} r_T^2 \alpha_s(\mu^2) x g(x,\mu^2) T(b_T)\right)$$

- **Assuming the S-matrix element is predominantly real, we have**

$$\frac{d\sigma_{q\bar{q}}}{d^2 b_T} = 2(1 - \text{Re}S(b_T)) = 2\left[1 - \exp\left(-\frac{\pi}{2N_c} r_T^2\, \alpha_s(\mu^2)\, x g(x,\mu^2)\, T(b_T)\right)\right]$$

- **This is the Glauber-Mueller dipole cross section** A.H. Mueller, Nucl. Phys. B335, 115 (1990)

- $T(b_T)$ **and** $xg(x,\mu^2)$ **are determined from fits to HERA DIS data (**b_T**,** x**, and initial scale** μ_0^2 **dependence) and DGLAP evolution in** μ^2

GEOMETRY

- The thickness function $T(b)$ is modeled
- For a nucleon use a Gaussian or a collection of smaller Gaussians (substructure)

$$T(b_T) = \frac{1}{2\pi B_G} \exp\left(-\frac{b_T^2}{2B_G}\right)$$

- Usually B_G is assumed to be energy independent and fit yields $\sim 4\mathrm{GeV}^{-2}$
- It is related to the average squared gluonic radius $\langle b_T^2 \rangle = 2B_G$
- This radius is ~0.56 fm
- For a nucleus, do as in MC Glauber and sample nucleon positions from a nuclear density distribution (e.g. a Woods-Saxon distribution)
- Sum all nucleon $T(\vec{b})$ to get the total nuclear $T(\vec{b})$

GEOMETRY

from Schenke, Shen, Tribedy, Phys.Rev.C 102 (2020) 4, 044905

$$\rho(r,\theta) = \frac{\rho_0}{1+\exp[(r-R'(\theta))/a]}\,, \tag{9}$$

with $R'(\theta) = R[1+\beta_2 Y_2^0(\theta)+\beta_4 Y_4^0(\theta)]$, and ρ_0 the nuclear density at the center of the nucleus. R is the radius parameter, a the skin depth.

Nucleus	R [fm]	a [fm]	β_2	β_4
^{238}U	6.81	0.55	0.28	0.093
^{208}Pb	6.62	0.546	0	0
^{197}Au	6.37	0.535	-0.13	-0.03
^{129}Xe	5.42	0.57	0.162	-0.003
^{96}Ru	5.085	0.46	0.158	0
^{96}Zr	5.02	0.46	0	0

Smaller nuclei, such as ^{16}O, and ^{3}He are described using a variational Monte-Carlo method (VMC) using the Argonne v18 (AV18) two-nucleon potential +UIX interactions [63]. In practice we use the ^{3}He and ^{16}O configurations available in the PHOBOS Monte-Carlo Glauber distribution [64, 65].

For the results we will show involving the deuteron, we employ a simple Hulthen wave function of the form [66]

$$\phi(d_{\rm pn}) = \frac{\sqrt{a_H b_H (a_H+b_H)}}{b_H - a_H}\,\frac{e^{-a_H d_{\rm pn}} - e^{-b_H d_{\rm pn}}}{\sqrt{2\pi} d_{\rm pn}}\,, \tag{10}$$

where $d_{\rm pn}$ is the separation between the proton and the neutron, and the parameters are experimentally determined to be $a_H = 0.228\,{\rm fm}^{-1}$ and $b_H = 1.18\,{\rm fm}^{-1}$.

SUMMARY OF THE PROCESS

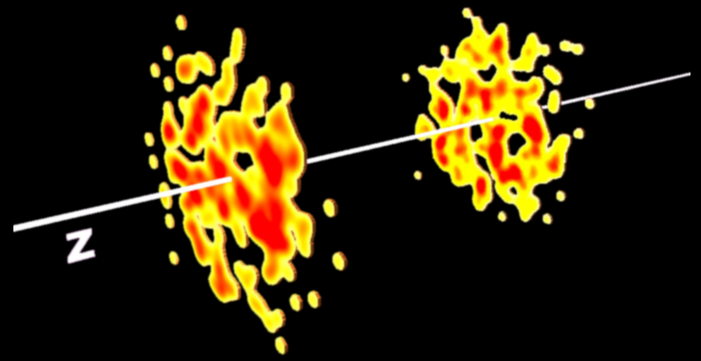

- Incoming nuclei described within color glass condensate: large *x* d.o.f. are color sources, small *x* classical gluon fields
- Incoming currents need to be constructed first:
  - Sample nucleons from nuclear density distributions
  - Add the *T(b)* at every transverse position
  - Extract Q_s from the IPSat dipole amplitude
  - Obtain the color charge density: $g^4\mu^2 \sim (Q_s)^2$
  - Sample color charges ρ^q from local Gaussian distributions
- The color charges generate the eikonal color current that sources the small-x classical gluon fields
- Gluon fields are determined from the Yang-Mills equations
- Solve for the gluon fields in the forward light cone
- Solve source-less YM equations forward in time
- Compute the energy momentum tensor - this is your initial condition for hydrodynamics

INITIAL CONDITIONS FOR HEAVY ION COLLISIONS

$$\frac{1}{2}(E^{\eta})^2 + \frac{1}{2\tau^2}[(E^{x})^2 + (E^{y})^2] + \frac{1}{2}F_{xy}F_{xy} + \frac{1}{2\tau^2}(F_{x\eta}^2 + F_{y\eta}^2)$$

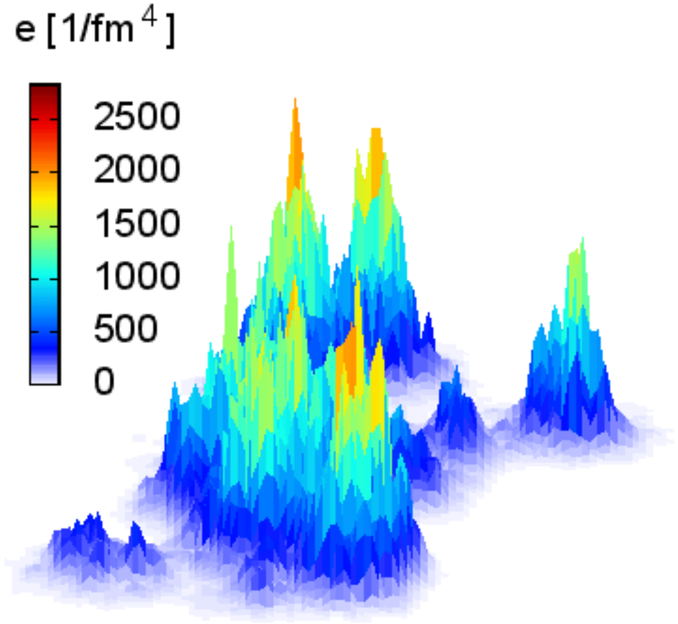

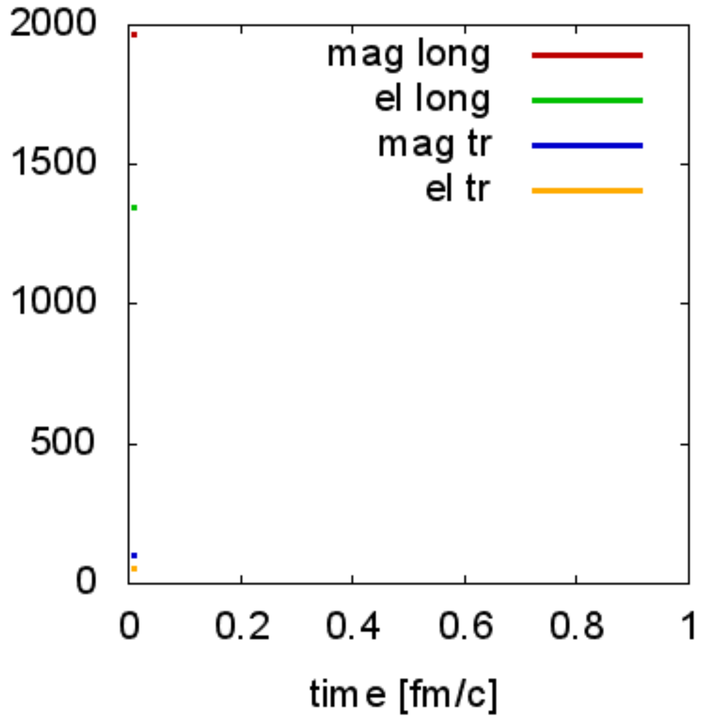

Solve the source free YM equations in time

Any hints of saturation in the typical heavy ion collision?

- The x dependence of the gluon distribution and from that of Q_s determines the multiplicity dependence on the center of mass energy
- Let's take a quick look at a complete model that uses the IP-Glasma initial state together with viscous hydrodynamics and a hadron cascade

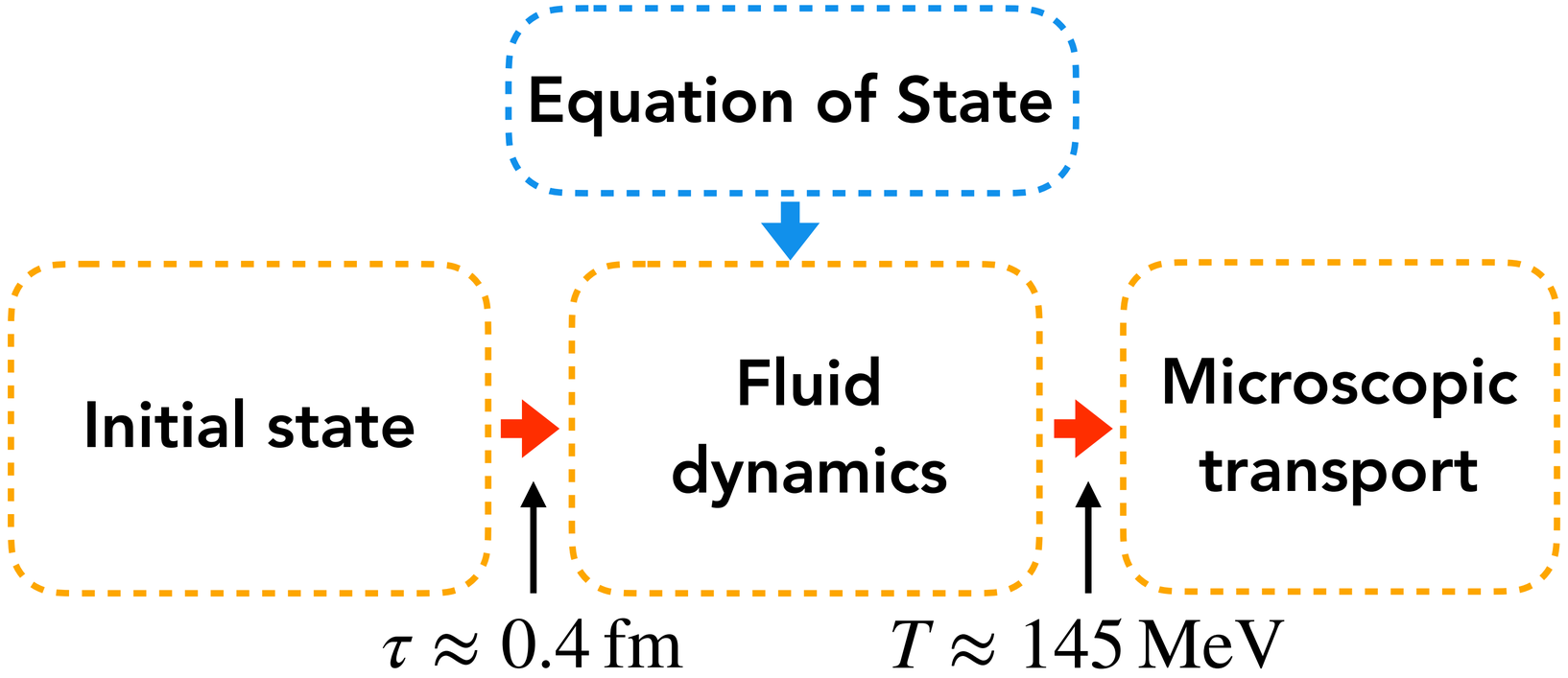

see e.g.
B. Schenke, C. Shen, P. Tribedy, Phys. Rev. C 102 (2020) 4, 044905

Energy dependence in heavy ion collisions well described

B. Schenke, C. Shen, P. Tribedy, Phys. Rev. C 102 (2020) 4, 044905

RHIC energies

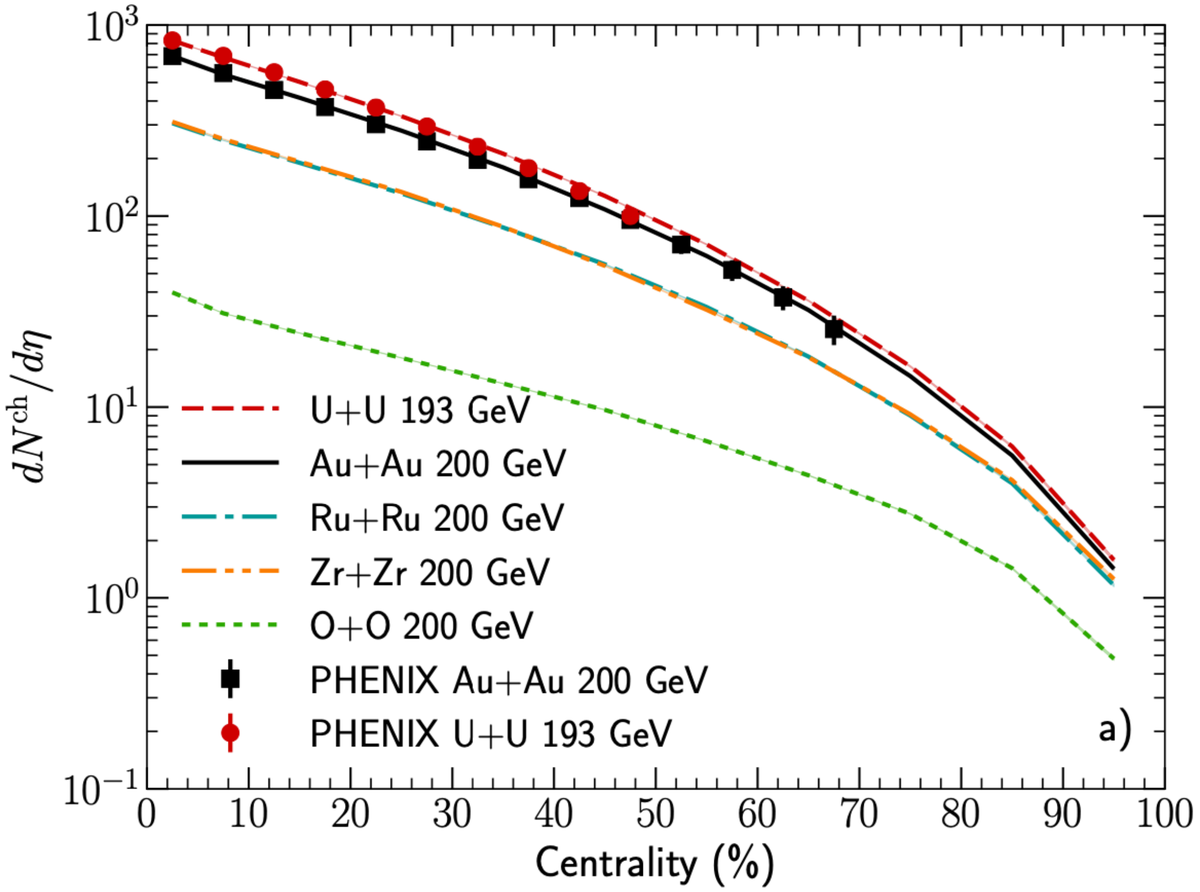

LHC energies

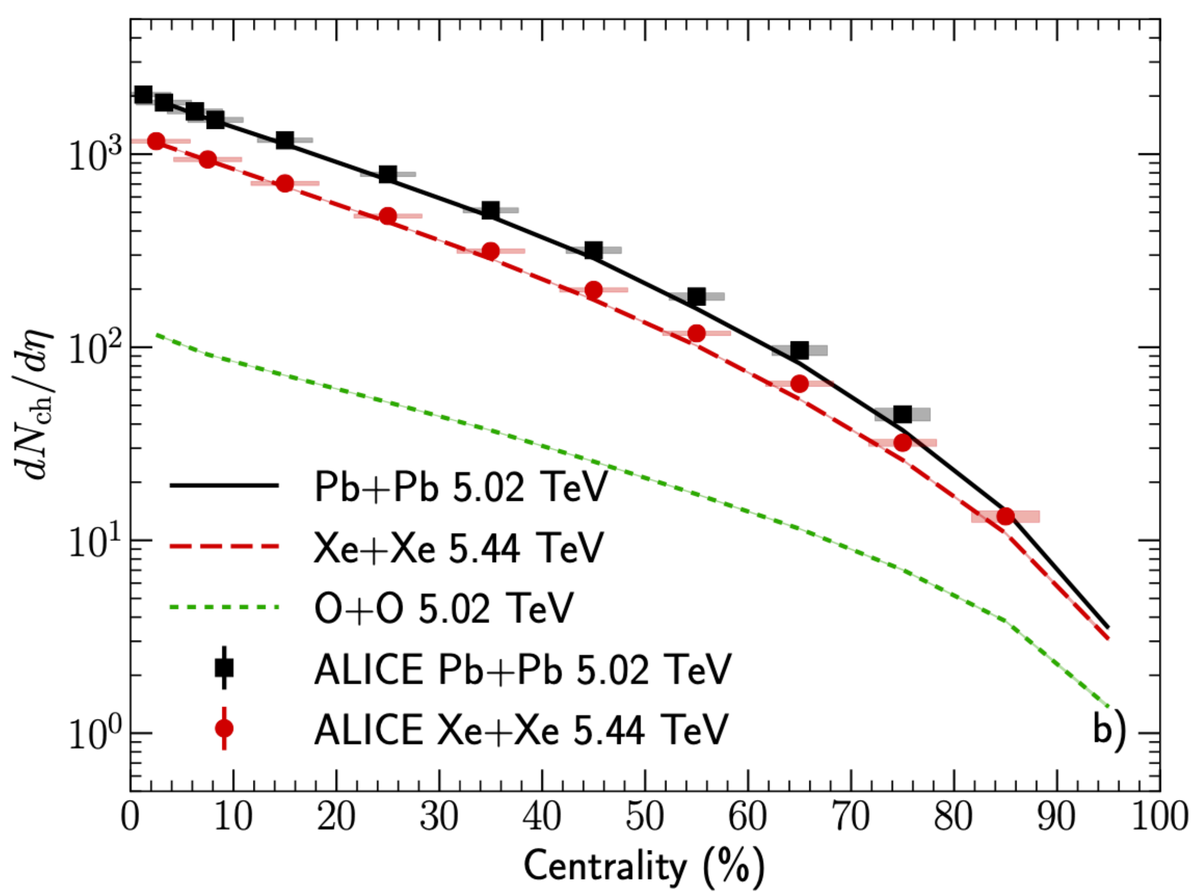

- Note that most other models (like Trento) fit the normalization for each energy separately

Back to diffractive vector-meson production

- Studying diffractive vector meson production can provide input on nucleon size, sub-nucleon fluctuations, saturation effects in nuclei
- These constraints can provide input into heavy ion collision initial state descriptions

Diffractive vector meson production

- Diffractive processes can constrain the average shape of the target and probe event-by-event fluctuations at different distance scales

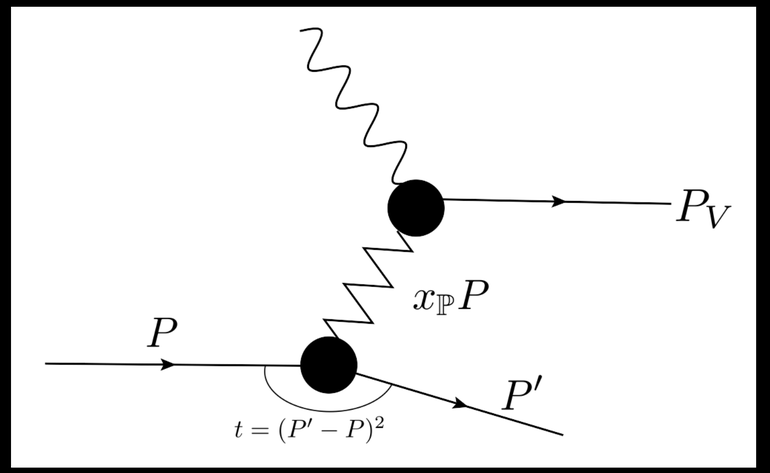

- High energy: Use dipole picture and color glass condensate to describe the target

- Saturation effects show up in e.g. Q^2 dependence and $|t|$ spectra

Coherent diffraction:

Target remains in the same quantum state after the interaction

Apply Good-Walker formalism: Cross section is determined by the average interaction of the states that diagonalize the scattering matrix with the target. M. L. Good and W. D. Walker, Phys. Rev. 120 (1960) 1857

High energy: Fock states of the incoming virtual photon with a fixed number of partons (LO: quark-antiquark pair) at fixed transverse coordinates, probing a fixed configuration of the target.

$$\frac{d\sigma^{\gamma^* A \to VA}}{dt} = \frac{1}{16\pi} \left| \left\langle \mathcal{A}^{\gamma^* A \to VA} \right\rangle \right|^2$$

Incoherent diffraction:

Initial state: $|i\rangle$; Final state: $|f\rangle$; Amplitude for diffractive scattering: $\mathcal{A}$

Squared transition amplitude, which enters in the cross section:

H. I. Miettinen and J. Pumplin, Phys. Rev. D18 (1978) 1696

$$\sum_{f\neq i} |\langle f|\mathcal{A}|i\rangle|^2 = \sum_f \langle i|\mathcal{A}^*|f\rangle\langle f|\mathcal{A}|i\rangle - \langle i|\mathcal{A}|i\rangle\langle i|\mathcal{A}^*|i\rangle$$

$$= \langle i|\mathcal{A}^*\mathcal{A}|i\rangle - |\langle i|\mathcal{A}|i\rangle|^2$$

Sum over final states includes all possible states for the final state target

Average over all possible initial states → cross section

$$\frac{d\sigma^{\gamma^* A\to VA}}{dt} = \frac{1}{16\pi}\left(\left\langle\left|\mathcal{A}^{\gamma^* A\to VA}\right|^2\right\rangle - \left|\left\langle\mathcal{A}^{\gamma^* A\to VA}\right\rangle\right|^2\right)$$

Summary of cross sections

Coherent diffraction: Target stays intact

$$\frac{\mathrm{d}\sigma^{\gamma^* p\to Vp}}{\mathrm{d}t} = \frac{1}{16\pi}\left|\langle\mathcal{A}^{\gamma^* p\to Vp}(x_{\mathbb{P}}, Q^2, \boldsymbol{\Delta})\rangle\right|^2$$

Incoherent diffraction: Target breaks up

$$\frac{\mathrm{d}\sigma^{\gamma^* p\to Vp^*}}{\mathrm{d}t} = \frac{1}{16\pi}\left(\left\langle\left|\mathcal{A}^{\gamma^* p\to Vp}(x_{\mathbb{P}}, Q^2, \boldsymbol{\Delta})\right|^2\right\rangle - \left|\langle\mathcal{A}^{\gamma^* p\to Vp}(x_{\mathbb{P}}, Q^2, \boldsymbol{\Delta})\rangle\right|^2\right)$$

$$-t \approx \boldsymbol{\Delta}^2$$

M. L. Good and W. D. Walker, Phys. Rev. 120 (1960) 1857
H. I. Miettinen and J. Pumplin, Phys. Rev. D18 (1978) 1696
Y. V. Kovchegov and L. D. McLerran, Phys. Rev. D60 (1999) 054025
A. Kovner and U. A. Wiedemann, Phys. Rev. D64 (2001) 114002

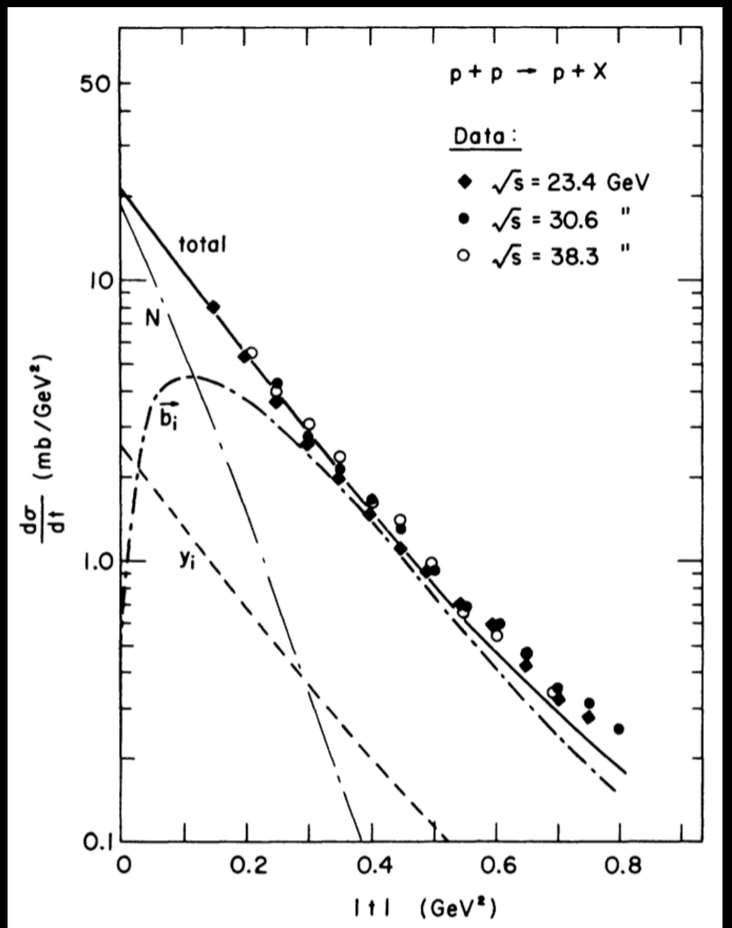

FIG. 5. The momentum-transfer dependence of beam dissociation, $\int(d\sigma/dtdm^2)dm^2$ for $pp \to p^*p$, predicted by our model. The experimental data are from Ref. 4. Also shown is a decomposition of the full cross section into contributions due to fluctuations in the number (N), rapidities (y_i), and relative impact parameters ($\vec{b}_i$) of the wee partons. The N-fluctuation contribution is seen to dominate near $t = 0$, and the $\vec{b}_i$-fluctuation component at large-t values.

Dipole picture: Scattering amplitude

H. Mäntysaari, B. Schenke, Phys. Rev. Lett. 117 (2016) 052301; Phys.Rev. D94 (2016) 034042

High energy factorization:

- $\gamma^* \to q\bar{q} : \psi^{\gamma}(r, Q^2, z)$
- $q\bar{q}$ dipole scatters with amplitude N
- $q\bar{q} \to V : \psi^{V}(r, Q^2, z)$

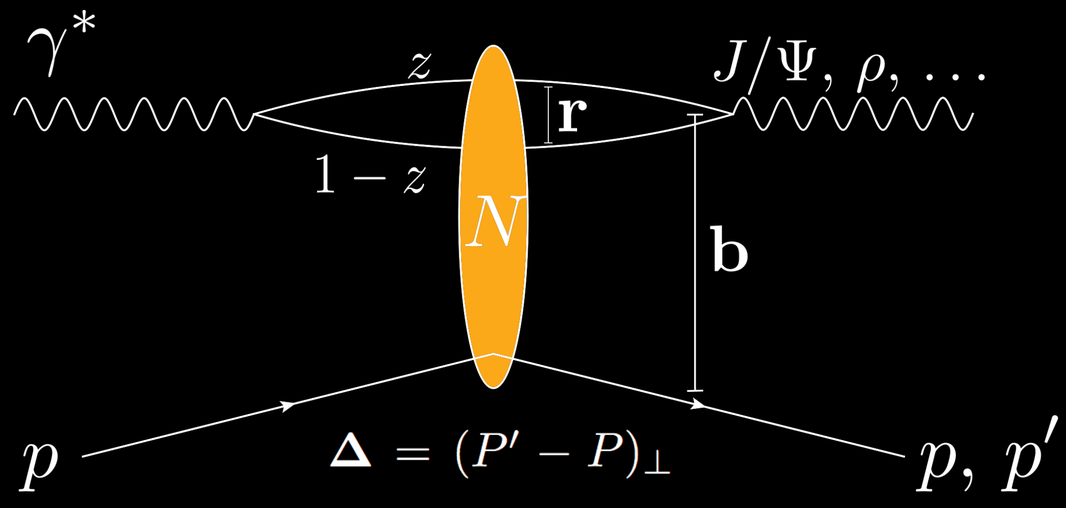

$$\mathcal{A} \sim \int \mathrm{d}^2 b \mathrm{d} z \mathrm{d}^2 r \Psi^* \Psi^V(r, z, Q^2) e^{-ib\cdot\Delta} N(r, x, b)$$

- Impact parameter ***b*** is the Fourier conjugate of transverse momentum transfer ***Δ*** → Access spatial structure ($t = -\Delta^2$)
- Total F_2: forward scattering amplitude (***Δ***=0) for V=γ (same N)

Modeling the dipole amplitude

H. Mäntysaari, B. Schenke, Phys. Rev. Lett. 117 (2016) 052301; Phys.Rev. D94 (2016) 034042

One way: IPSat model:

$$N = 1 - \exp[-r^2 F(x, r^2) T(\vec{b})] \quad \text{with} \quad F(x, \vec{r}^2) = \frac{\pi^2}{2N_c} \alpha_s \left(\mu_0^2 + \frac{C}{r^2}\right) xg\left(x, \mu_0^2 + \frac{C}{r^2}\right)$$

Proton targets: parameters $\mu_0^2, C, xg(x, \mu_0^2), B_{\mathrm{p}}$(in T) constrained by HERA data; Scale dependence of xg obtained from DGLAP evolution

Two models for the proton shape …

Modeling the dipole amplitude

H. Mäntysaari, B. Schenke, Phys. Rev. Lett. 117 (2016) 052301; Phys.Rev. D94 (2016) 034042

1) Assume Gaussian proton shape:

$$T(\vec{b}) = T_{\mathrm{p}}(\vec{b}) = \frac{1}{2\pi B_{\mathrm{p}}} e^{-b^2/(2B_{\mathrm{p}})}$$

2) Assume Gaussian distributed and Gaussian shaped hot spots:

$$P(b_i) = \frac{1}{2\pi B_{\mathrm{qc}}} e^{-b_i^2/(2B_{\mathrm{qc}})}$$ (angles uniformly distributed)

$$T_{\mathrm{p}}(\vec{b}) = \frac{1}{N_{\mathrm{q}}} \sum_{i=1}^{N_{\mathrm{q}}} T_{\mathrm{q}}(\vec{b} - \vec{b}_i)$$ with N_{q}=3 hot spots; $$T_{\mathrm{q}}(\vec{b}) = \frac{1}{2\pi B_{\mathrm{q}}} e^{-b^2/(2B_{\mathrm{q}})}$$

Results compared to HERA data

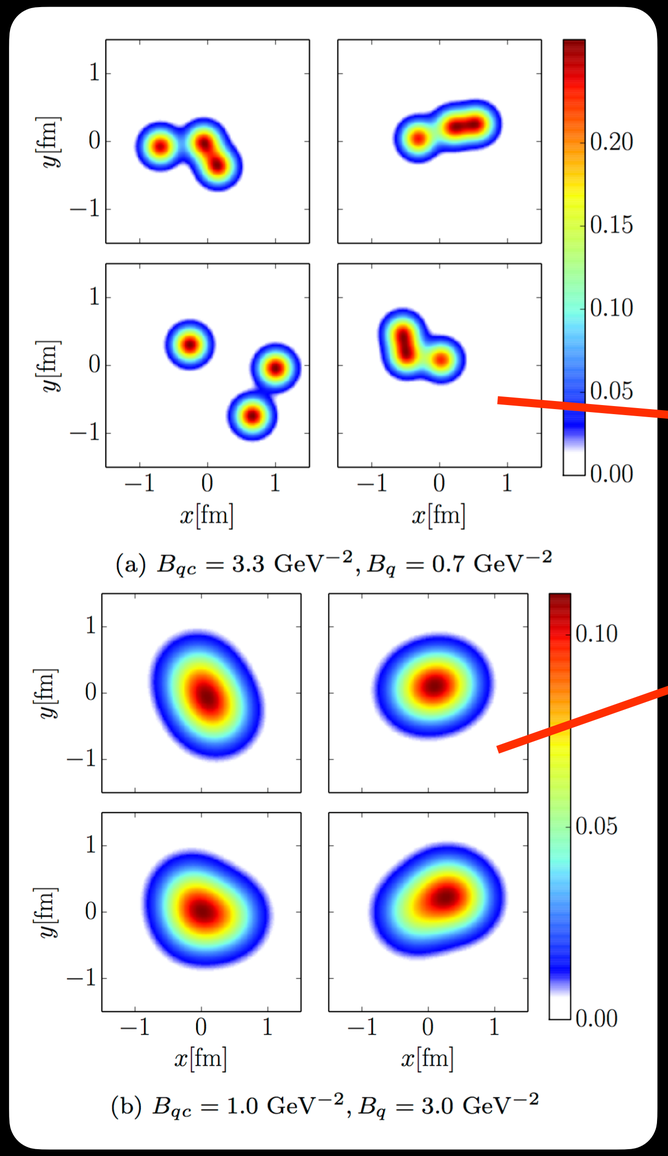

H. Mäntysaari, B. Schenke, Phys. Rev. Lett. 117 (2016) 052301
Phys.Rev. D94 (2016) 034042

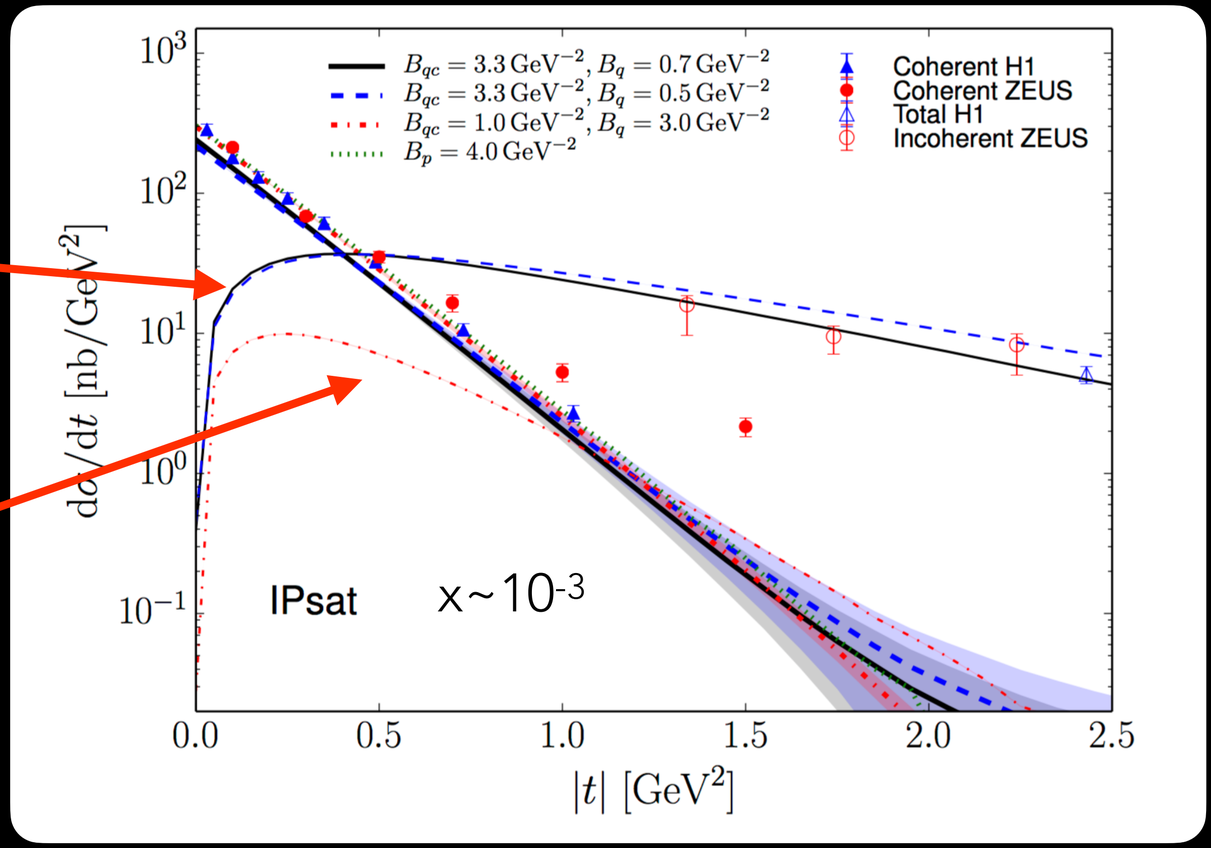

H1 collaboration, Eur. Phys. J. C46 (2006) 585, Phys. Lett. B568 (2003) 205
ZEUS collaboration, Eur. Phys. J. C24 (2002) 345, Eur. Phys. J. C26 (2003) 389

Color Glass Condensate formalism

H. Mäntysaari, B. Schenke, Phys.Rev.D 98 (2018) 3, 034013

Alternatively, compute the dipole amplitude from Wilson lines using the MV model and JIMWLK evolution (with the geometry as in IPSat)

Sample (local Gaussian) color charges with zero mean and

$$\langle \rho^a \rho^b \rangle \sim \delta^{ab} \delta^{(2)}(\vec{x} - \vec{y}) \delta(x^- - y^-) Q_s^2(\vec{x})$$

where Q_s at the initial x_0 is obtained from IPSat

MV model: L. D. McLerran and R. Venugopalan, Phys. Rev. D49 (1994) 2233
JIMWLK: J. Jalilian-Marian, A. Kovner, A. Leonidov, and H. Weigert,
Nucl. Phys. B504, 415 (1997), Phys. Rev. D59, 014014 (1999)
E. Iancu, A. Leonidov, and L. D. McLerran, Nucl. Phys. A692, 583 (2001)
E. Ferreiro, E. Iancu, A. Leonidov, and L. McLerran, Nucl. Phys. A703, 489 (2002)
A. H. Mueller, Phys. Lett. B523, 243 (2001)

Color Glass Condensate formalism

H. Mäntysaari, B. Schenke, Phys.Rev.D 98 (2018) 3, 034013

From color charges we obtain Wilson lines at the initial $x_0 = 0.01$

$$V(\vec{x}) = P \exp\left(-ig \int dx^- \frac{\rho(x^-, \vec{x})}{\vec{\nabla}^2 + \tilde{m}^2} \right)$$

from solution of Yang-Mills equations, with regulator $\tilde{m}$

Dipole amplitude: $N(\vec{r}, x_{\mathbb{P}}, \vec{b}) = N(\vec{x} - \vec{y}, x_{\mathbb{P}}, (\vec{x} + \vec{y})/2) = \mathrm{Tr} V(\vec{x}) V^\dagger(\vec{y})/N_c$

Evolution is done using the Langevin formulation of the JIMWLK equations

K. Rummukainen and H. Weigert Nucl. Phys. A739 (2004) 183; T. Lappi, H. Mäntysaari, Eur. Phys. J. C73 (2013) 2307

Long distance tales are tamed by imposing a regulator in the JIMWLK kernel, *m* S. Schlichting, B. Schenke, Phys.Lett. B739 (2014) 313-319

JIMWK evolution

Rapidity evolution of Wilson lines in Langevin form:

H. WEIGERT, NUCL. PHYS. A 703, 823 (2002).
T. LAPPI AND H. MANTYSAARI, EUR. PHYS. J. C 73, 2307 (2013)

$$V_{\mathbf{x}}(Y+dY) = \exp\left\{-i\frac{\sqrt{\alpha_s dY}}{\pi}\int_{\mathbf{z}} K_{\mathbf{x}-\mathbf{z}}\cdot(V_{\mathbf{z}}\boldsymbol{\xi}_{\mathbf{z}}V_{\mathbf{z}}^{\dagger})\right\}$$
$$\times V_{\mathbf{x}}(Y)\exp\left\{i\frac{\sqrt{\alpha_s dY}}{\pi}\int_{\mathbf{z}} K_{\mathbf{x}-\mathbf{z}}\cdot\boldsymbol{\xi}_{\mathbf{z}}\right\}$$

ξ is Gaussian noise with zero average and

$$\left\langle \xi^a_{\mathbf{x},i}(Y)\xi^b_{\mathbf{y},j}(Y')\right\rangle = \delta^{ab}\delta^{ij}\delta^{(2)}_{\mathbf{xy}}\delta(Y-Y')$$

The JIMWLK Kernel is modified to avoid infrared tails:

$$K^{\mathrm{mod}}_{\mathbf{x}-\mathbf{z}} = m|\mathbf{x}-\mathbf{z}|K_1(m|\mathbf{x}-\mathbf{z}|)\frac{\mathbf{x}-\mathbf{z}}{(\mathbf{x}-\mathbf{z})^2}$$

e+p compared to HERA data

H. Mäntysaari, B. Schenke, Phys.Rev.D 98 (2018) 3, 034013

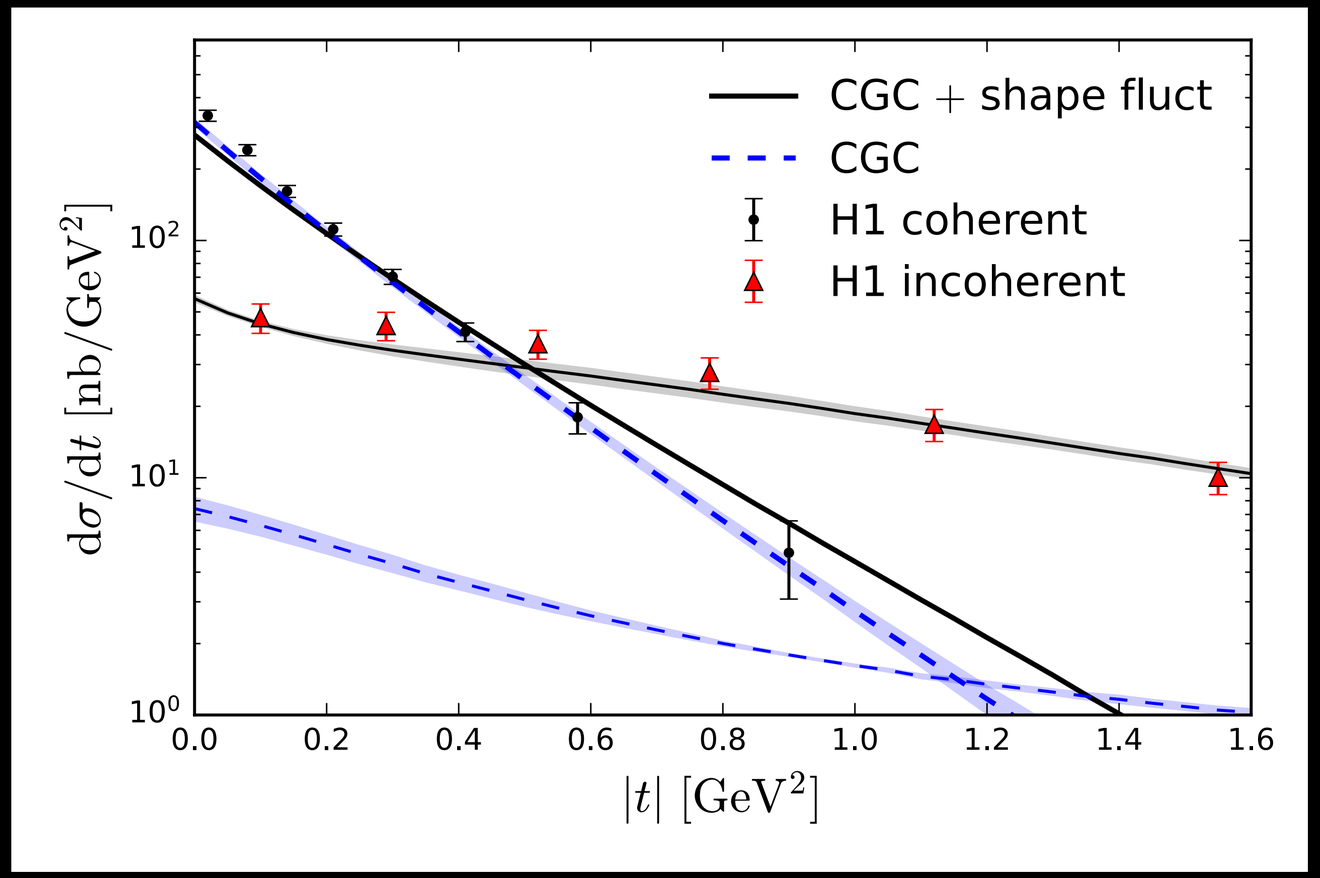

H1 collaboration, Eur. Phys. J. C73 (2013) no. 6 2466

Latest results: Bayesian inference

H. Mäntysaari, B. Schenke, C. Shen, W. Zhao, arXiv:2202.01998 [hep-ph]

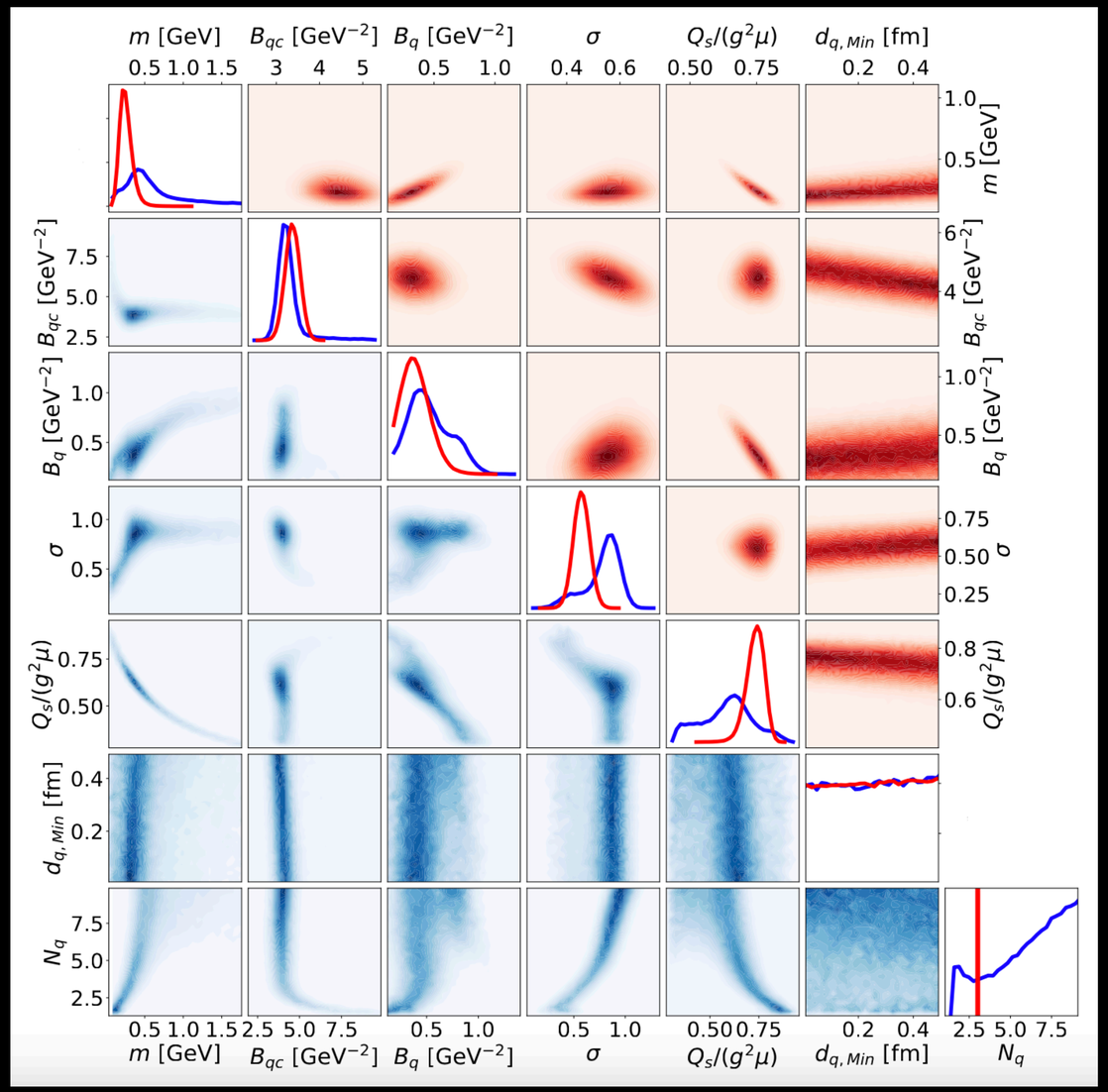

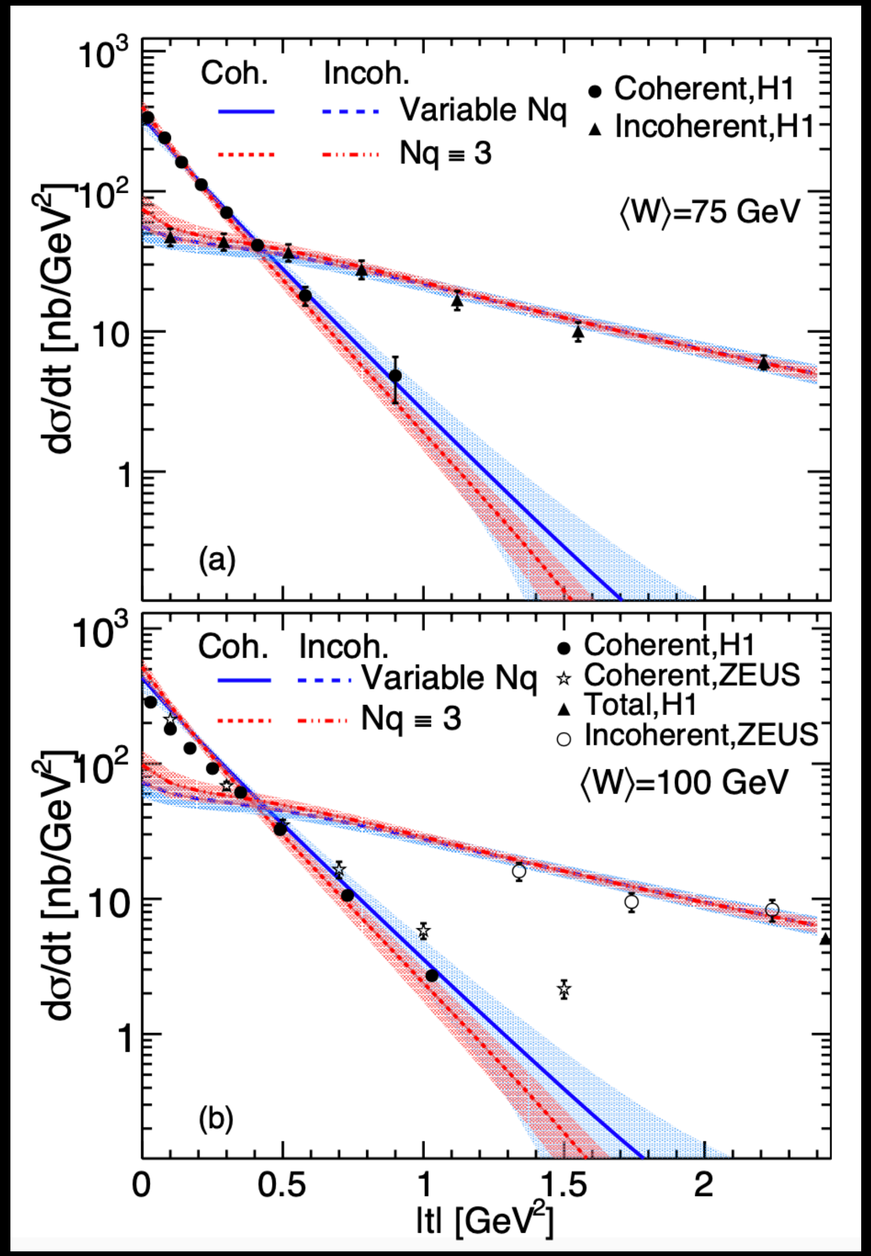

Latest results: Bayesian inference

H. Mäntysaari, B. Schenke, C. Shen, W. Zhao, arXiv:2202.01998 [hep-ph]

See the effect of changing parameters on the cross sections at

https://share.streamlit.io/chunshen1987/ipglasmadiffractionstreamlit/main/IPGlasmaDiffraction_app.py

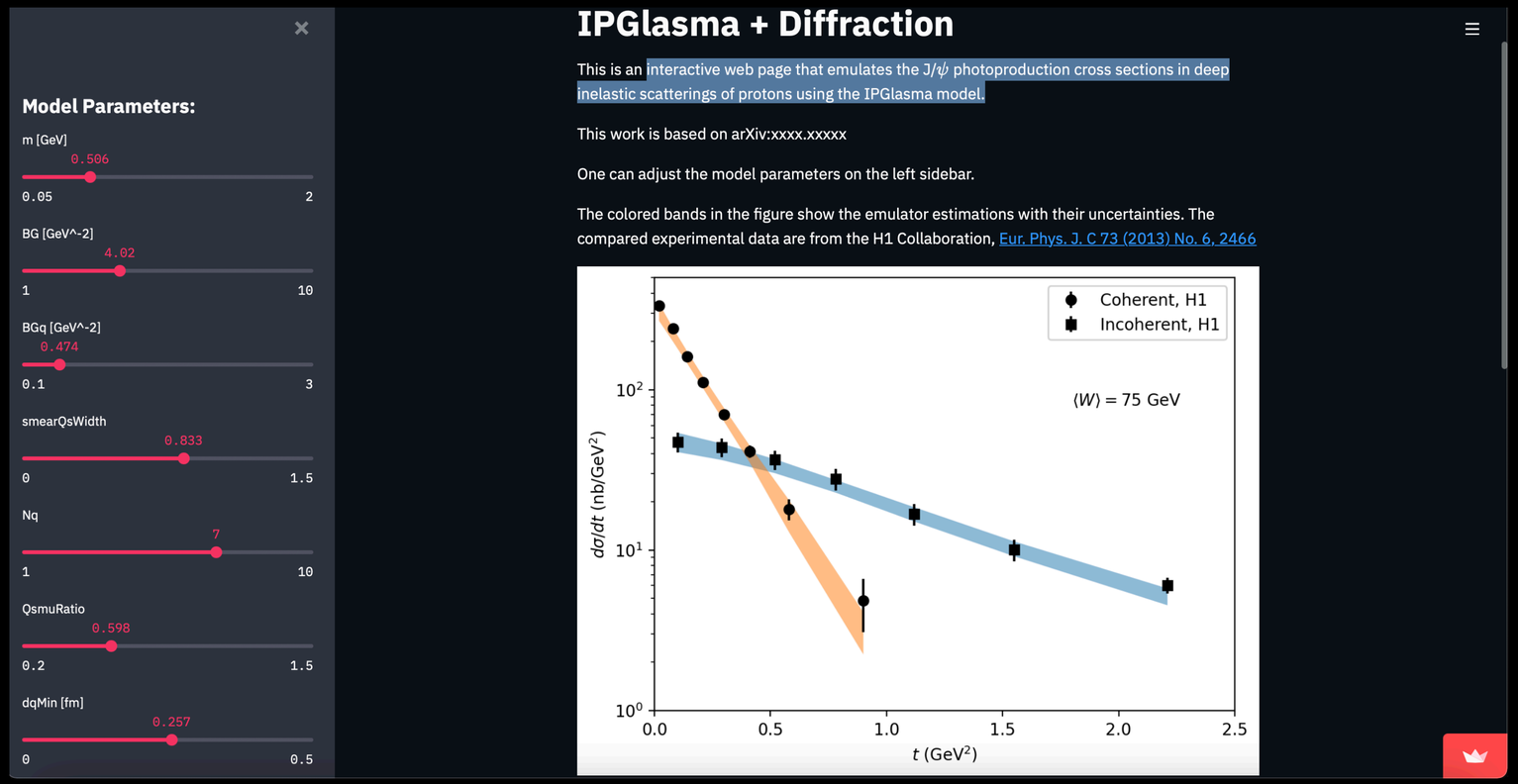

This website also provides posterior samples for your own application

Consistency with p+A collisions

B. Schenke, Rep. Prog. Phys. 84 082301 (2021)

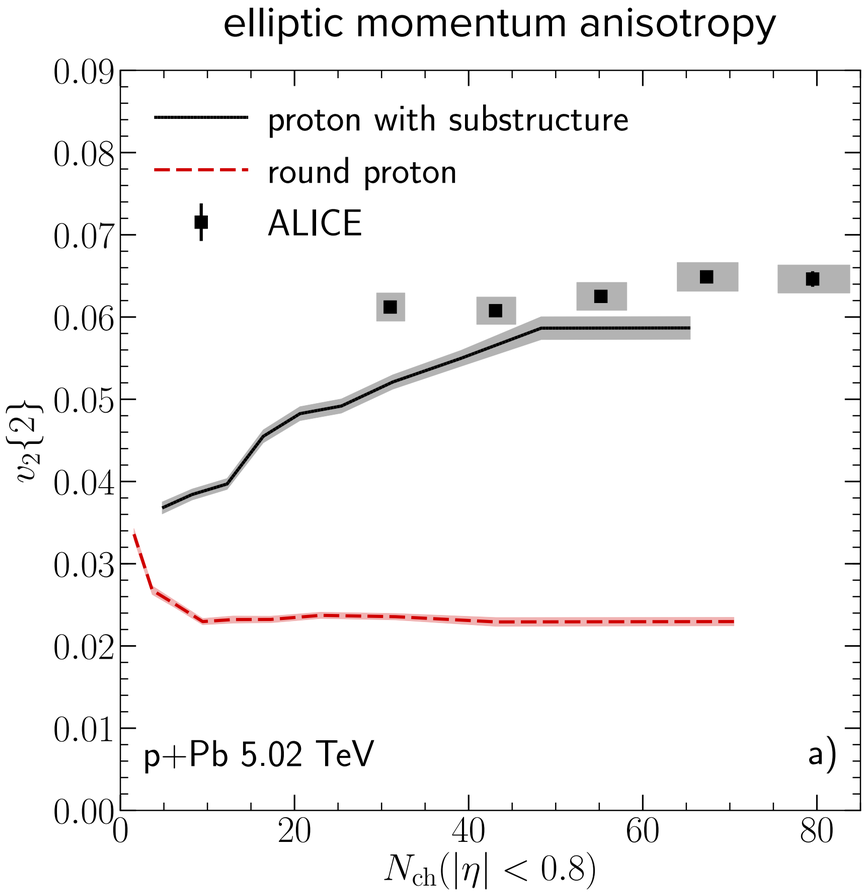

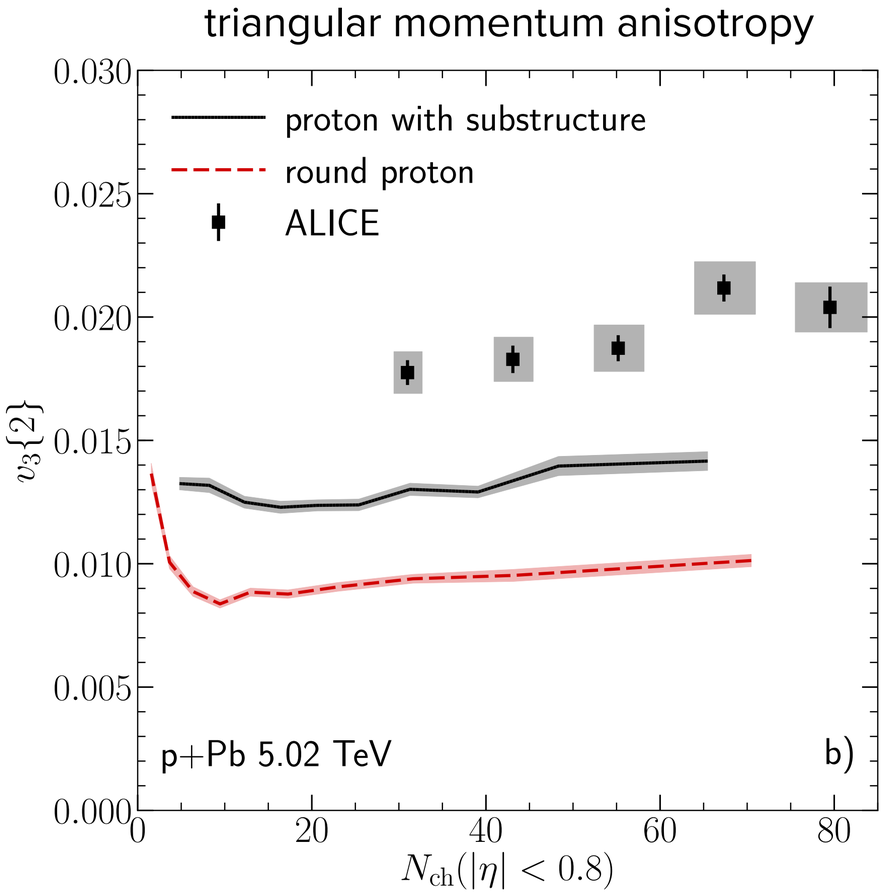

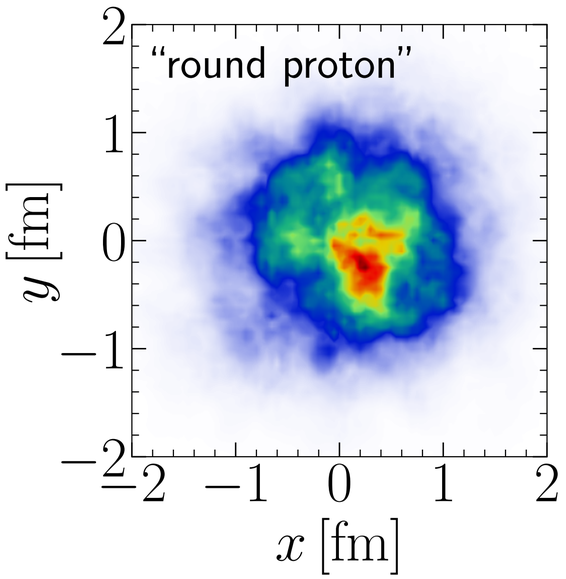

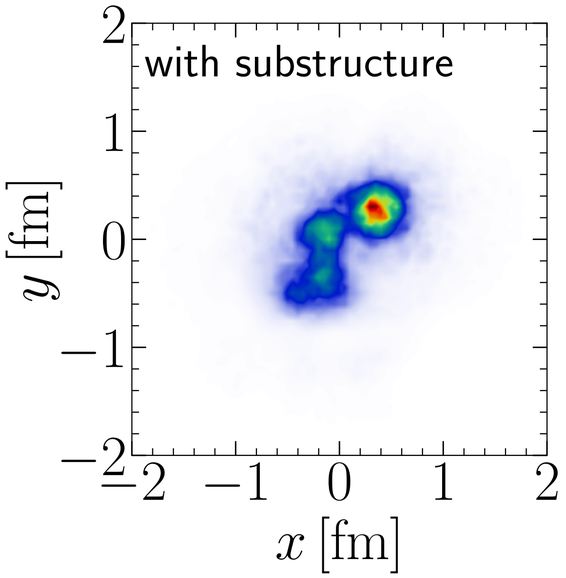

Ultraperipheral collisions (UPC)

- At an impact parameter $|b_T| > 2R_A$ nuclei are photon sources

- Photons are quasi-real $Q^2 \simeq 0$

- High energy $\gamma + \gamma$, $\gamma + p$, $\gamma + A$ at RHIC and LHC

- Focus on $\gamma + p$ and $\gamma + A$ and study diffractive production of vector mesons:

  At small *x* target is mostly gluons

$$\frac{d\sigma^{\gamma^* A \to VA}}{dt} \propto \left[xg(x, Q^2)\right]^2$$ (gluon distribution squared)

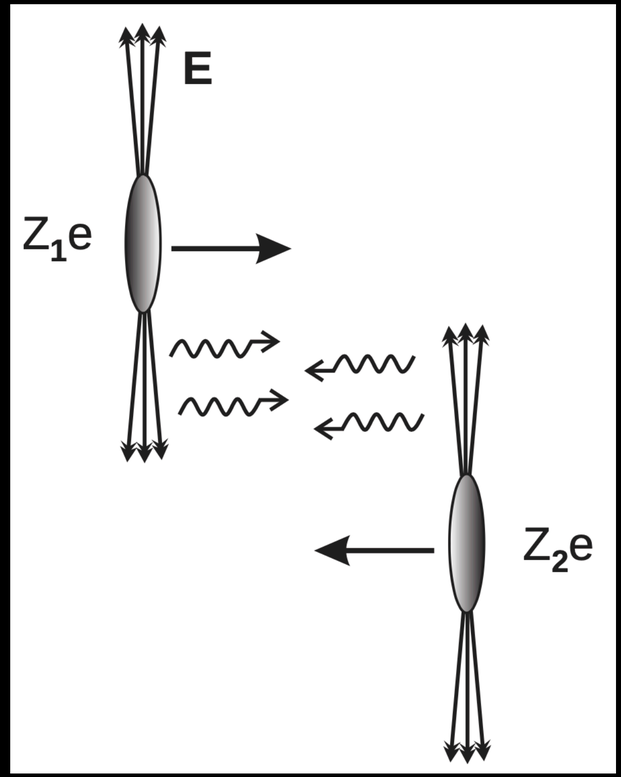

Ultraperipheral collisions (UPC)

C. A. Bertulani, S. R. Klein and J. Nystrand, Ann. Rev. Nucl. Part. Sci. 55 (2005) 271

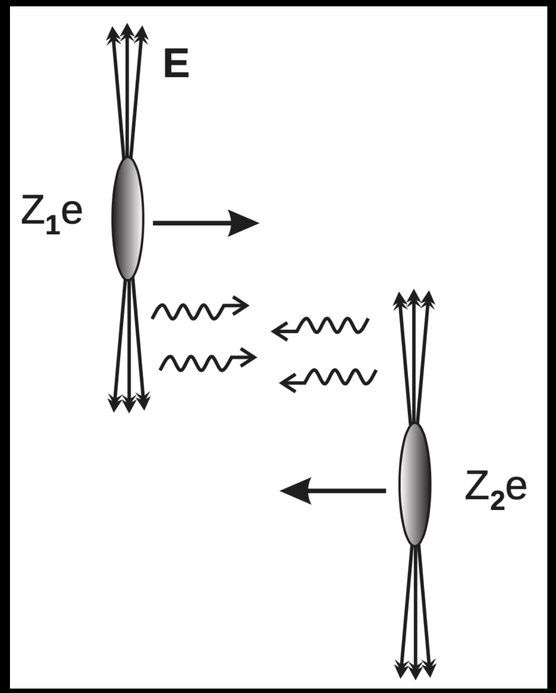

Higher energy in $\gamma + p$ than at HERA

Can study $\gamma A \rightarrow VA$ even before the EIC is built

Ignoring interference, cross section is convolution of photon flux n^{A_1} from nucleus A_1 and γA_2 cross section (and vice versa):

$$\frac{d\sigma^{AA\rightarrow J/\psi AA'}}{dt} = n^{A_2}(\omega_2)\,\sigma^{\gamma A_1}(y) + n^{A_1}(\omega_1)\,\sigma^{\gamma A_2}(-y)$$

y is the rapidity of the J/ψ

$\omega_{1/2}$ are the photon energies

Ultraperipheral collisions (UPC)

C. A. Bertulani, S. R. Klein and J. Nystrand, Ann. Rev. Nucl. Part. Sci. 55 (2005) 271

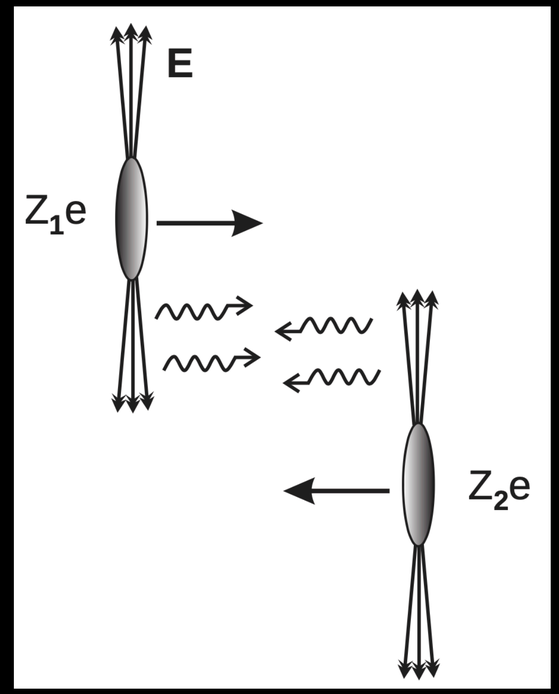

Interference is important in A+A, especially at mid-rapidity. There

$$\frac{d\sigma}{d|t|} = \frac{1}{16\pi}\int d^2\mathbf{B}\,|A_1 - A_2|^2\,\theta(|\mathbf{B}| - 2R_A)$$

Interference is destructive in A+A because of negative parity of the VM

$$\left.\frac{d\sigma^{A_1+A_2\to V+A_1+A_2}}{d|t|dy}\right|_{y=0} = 2\int d^2\mathbf{B}\,n(\omega,|\mathbf{B}|)\frac{d\sigma^{\gamma+A\to V+A}}{d|t|}[1-\cos(\boldsymbol{\Delta}\cdot\mathbf{B})]\,\theta(|\mathbf{B}| - 2R_A)$$

Center-of-mass energy dependence: $\gamma + p$

H. Mäntysaari, F. Salazar, B. Schenke, in preparation

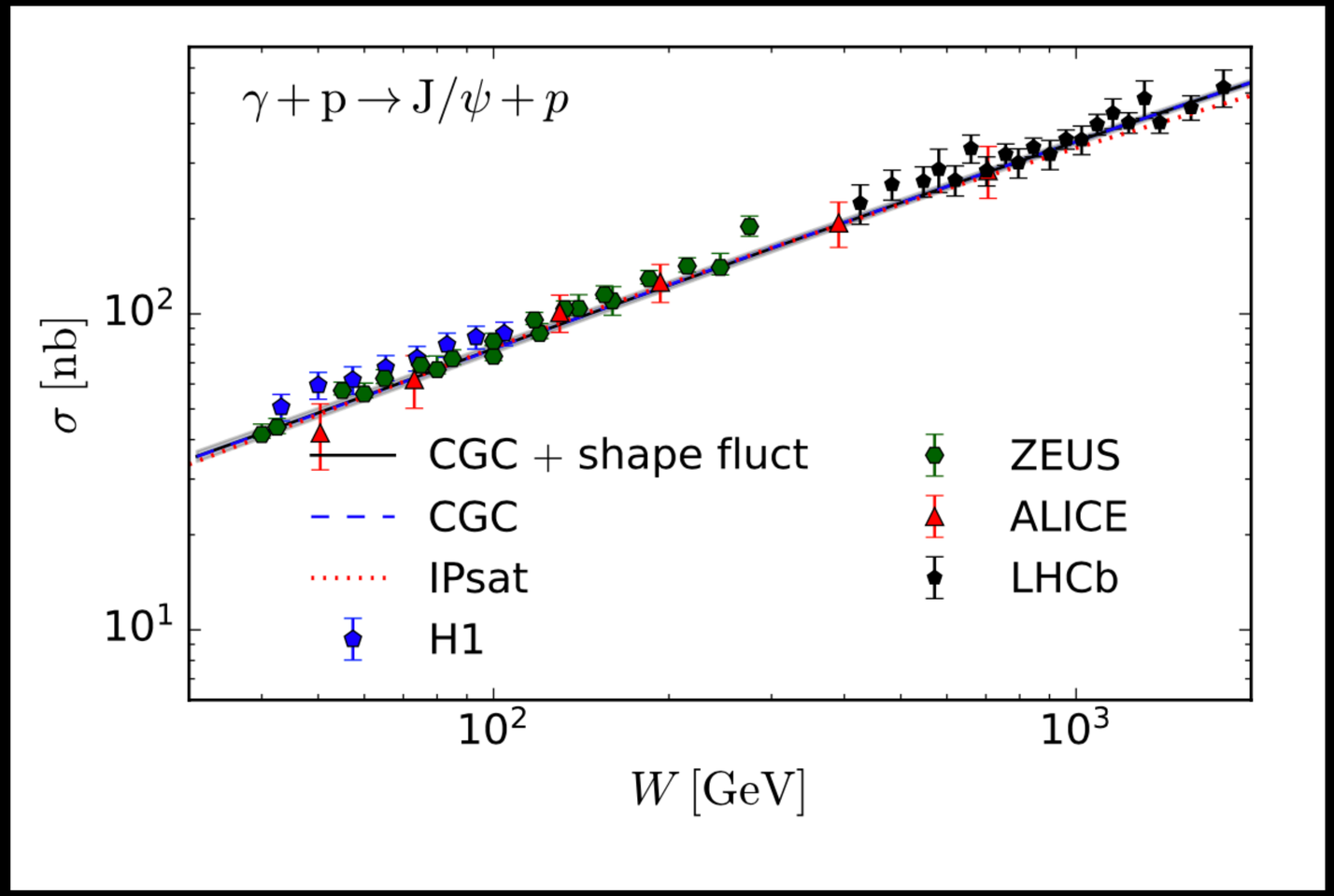

- Coherent cross section measured up to large W
- Compatible with CGC calculations, but no clear signal of saturation with proton targets

Make sure we get the normalization right in both cases: with and w/o shape fluctuations

Energy evolution of the proton size

H. Mäntysaari and B. Schenke, Phys.Rev. D98 (2018) 034013

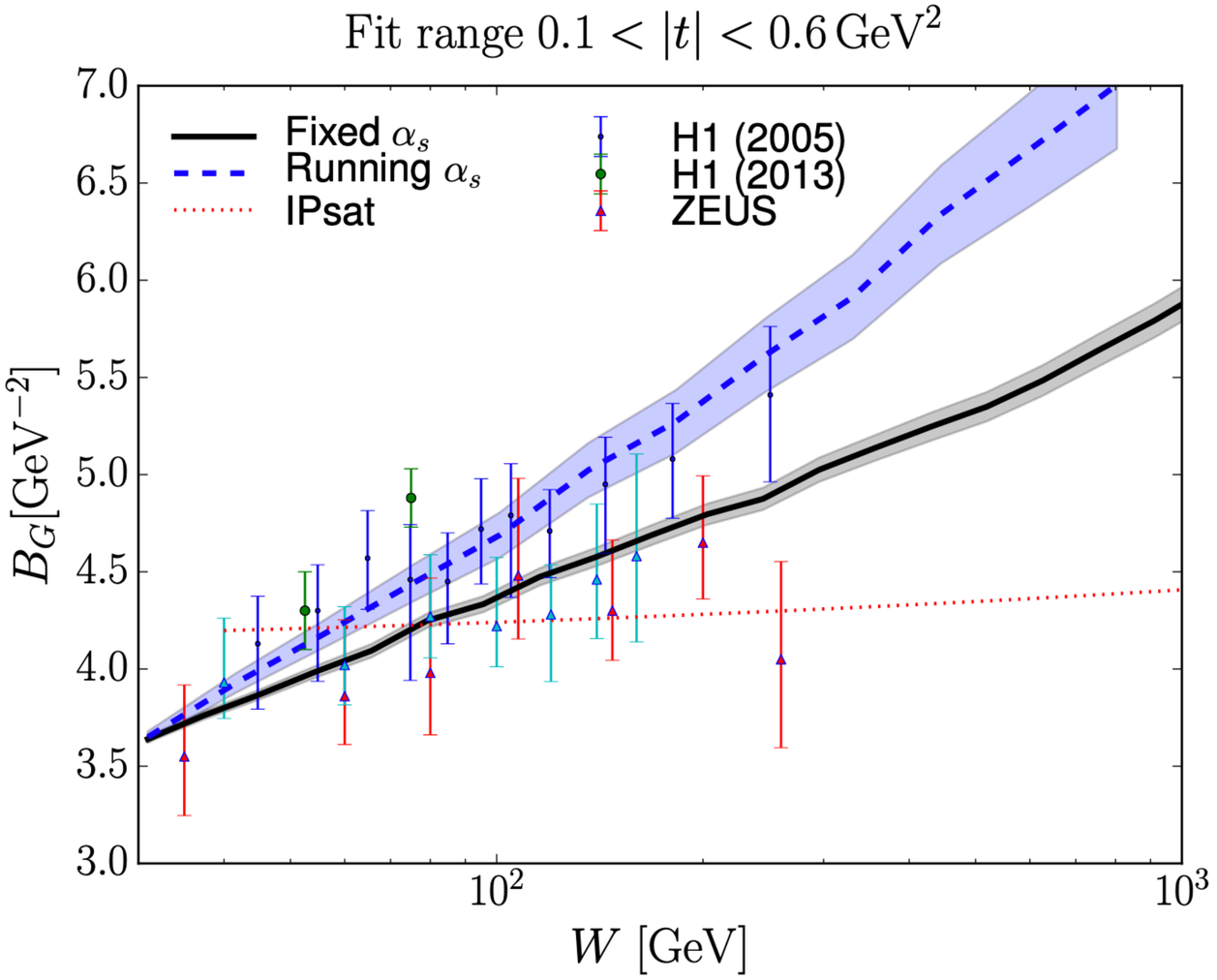

Small-x evolution describes energy evolution of the proton size

Diffractive slope shown

W=75 GeV ⟶ W=680 GeV

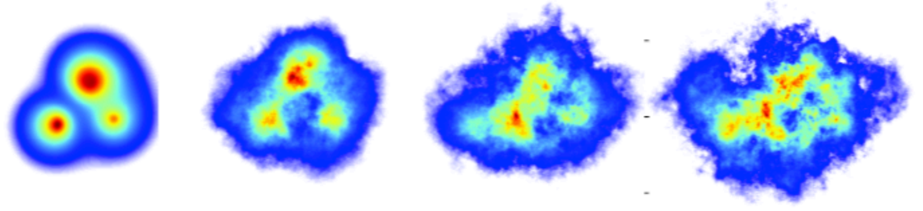

Incoherent to coherent ratio

H. Mäntysaari, B. Schenke, Phys.Rev.D 98 (2018) 3, 034013; B. Schenke, Rept. Prog. Phys. 84 (2021) 8, 082301

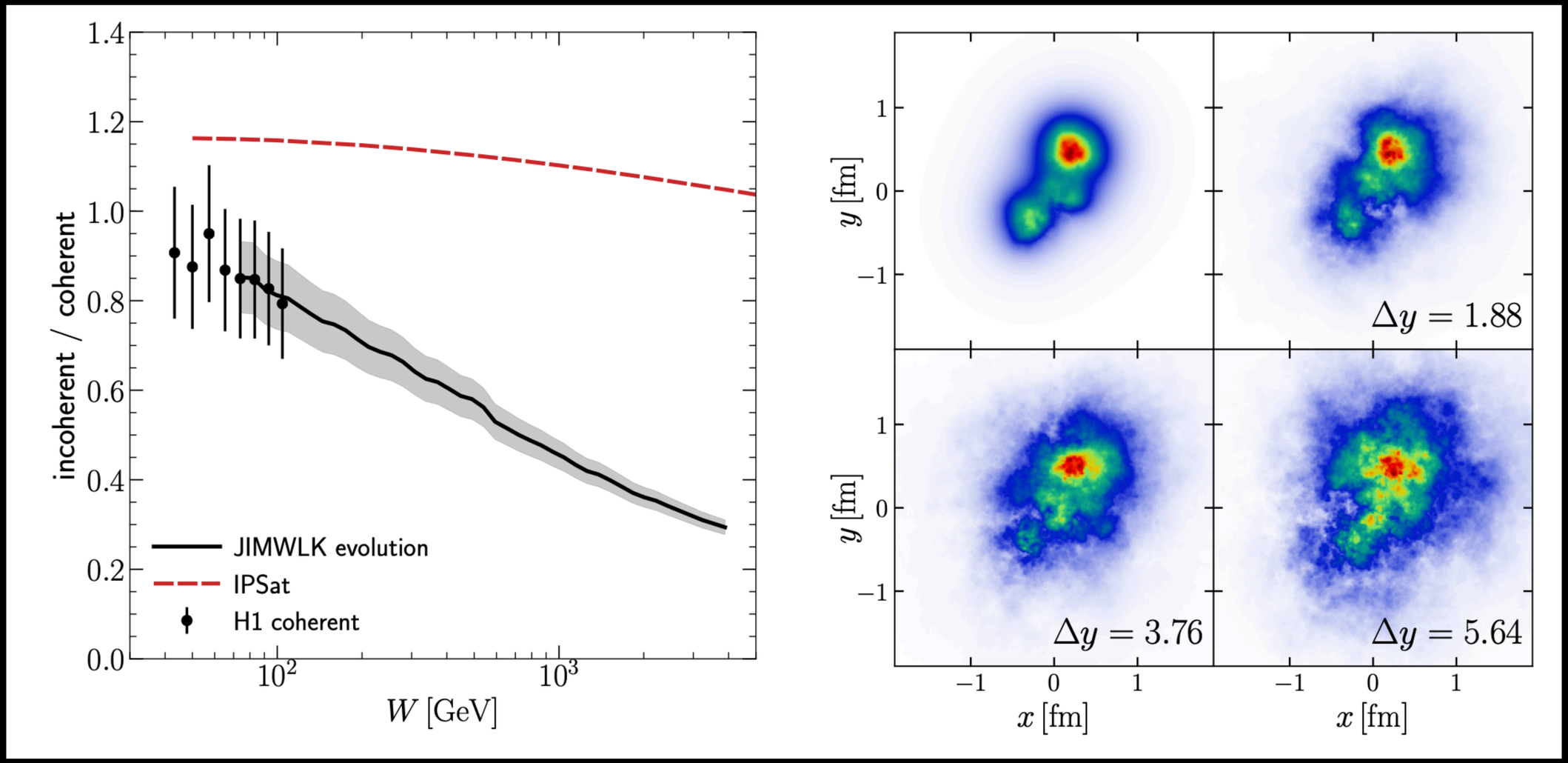

H1 collaboration, Eur. Phys. J. C73 (2013) no. 6 2466

Reduced incoherent cross section at large W?

H. Mäntysaari, B. Schenke, Phys.Rev.D 98 (2018) 3, 034013

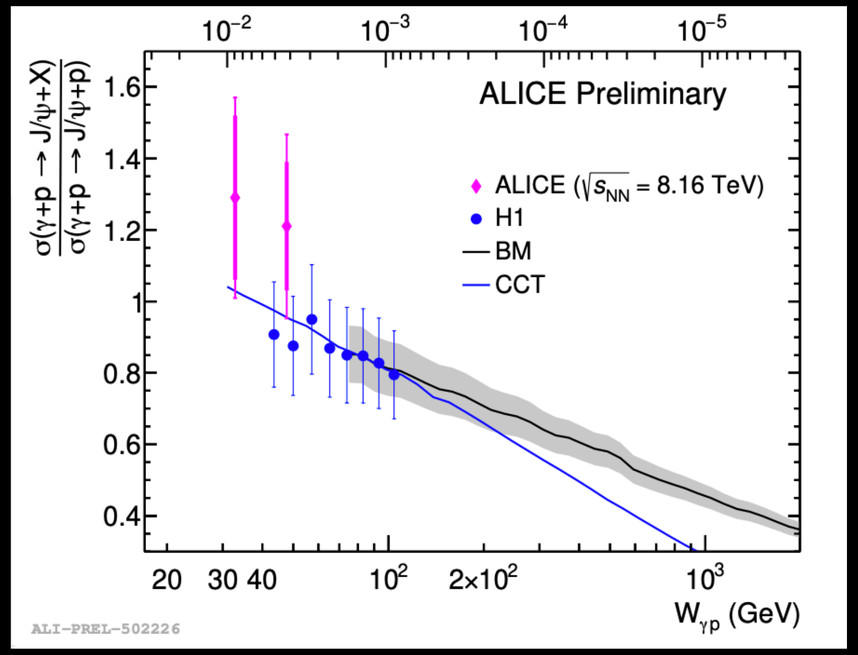

CCT: Cepila, Contreras, Takaki, 1608.07559
BM: Mäntysaari, Schenke, 1806.06783

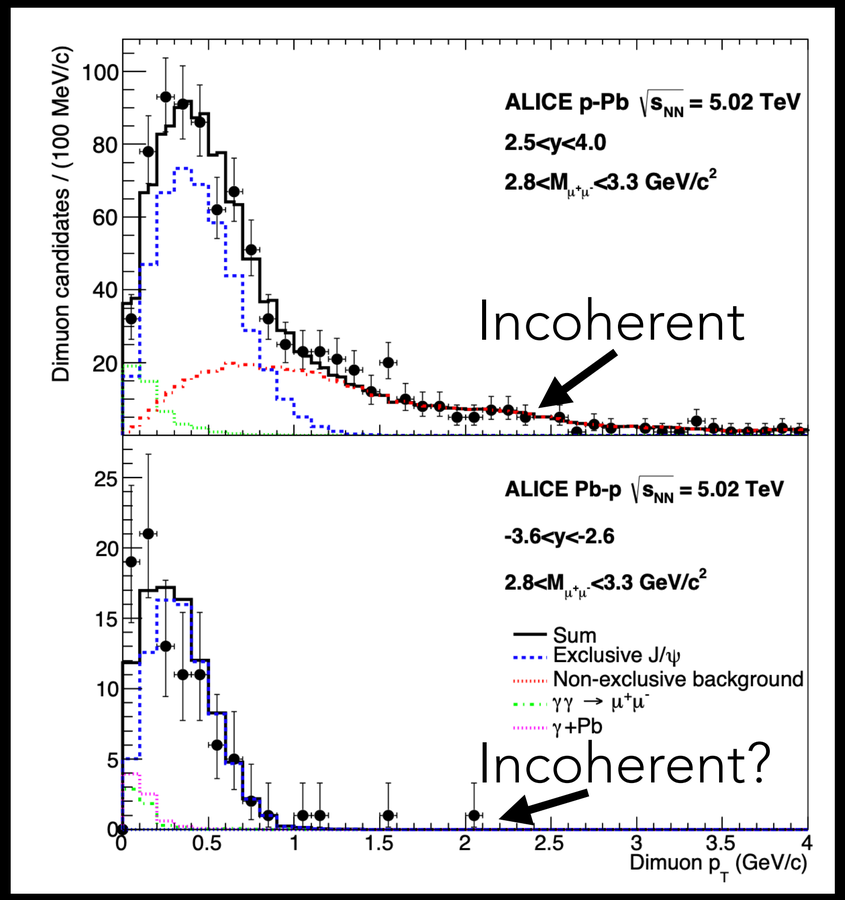

ALICE: arXiv:1406.7819 and 1809.03235

Qualitatively compatible with LHC data: Small incoherent cross section in high-energy γp scattering

Differential γ+Pb measurement

H. Mäntysaari, F. Salazar, B. Schenke, 2207.03712

Here, ALICE removed interference and photon k_T effects to get the γ+Pb cross section

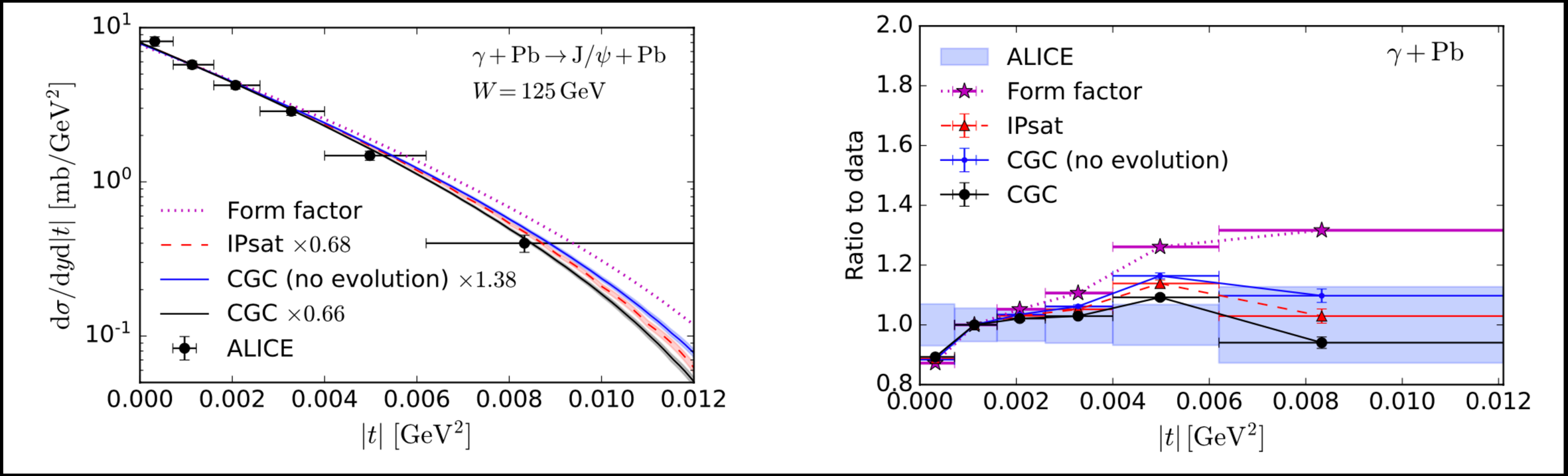

ALICE Collaboration, Phys.Lett.B 817 (2021) 136280

Saturation effects improve agreement with experimental data significantly

Saturation effects on nuclear geometry

H. Mäntysaari, F. Salazar, B. Schenke, 2207.03712

Fourier transform to coordinate space

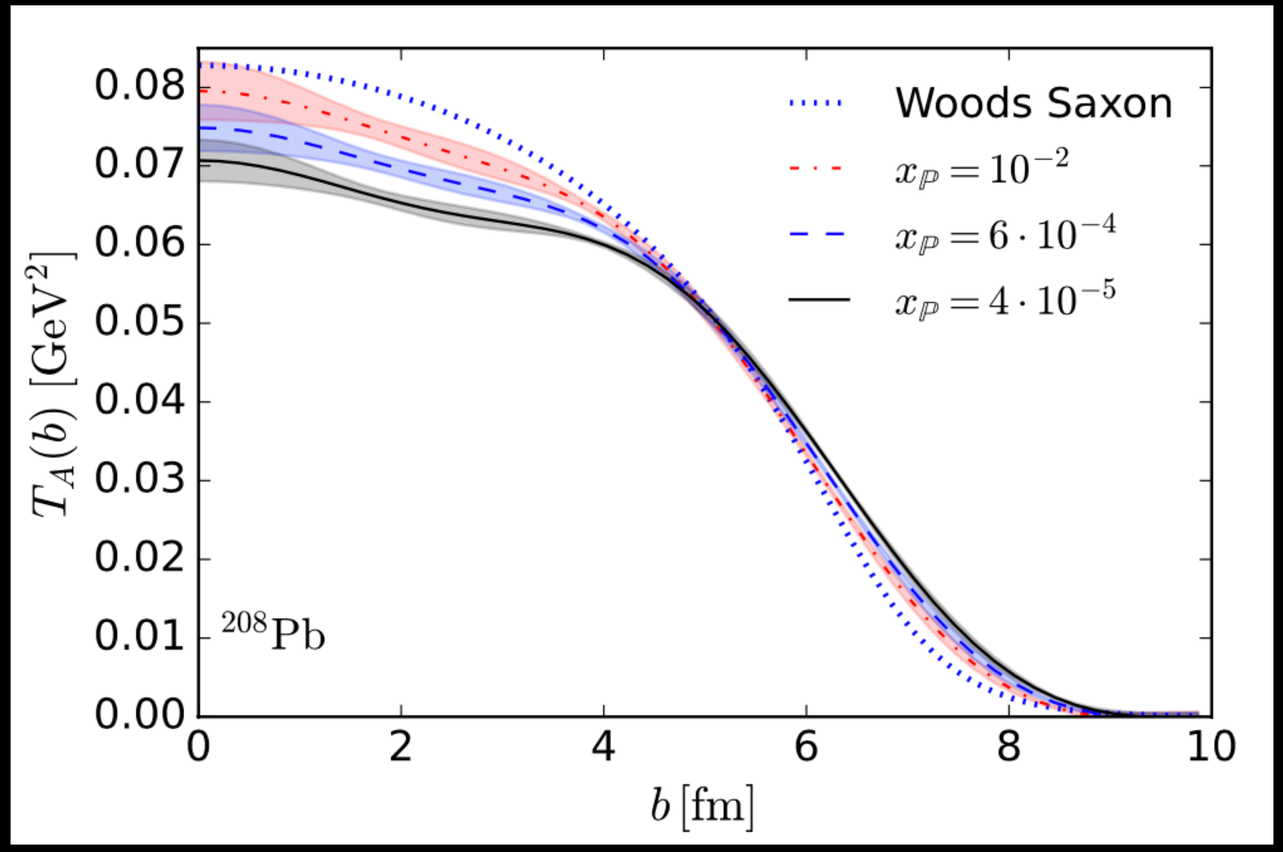

JIMWLK evolution leads to growth of the nucleus towards small x and depletion near the center (normalized so $\int d^2b T_A(b) = 208$)

|t| integrated coherent cross section

H. Mäntysaari, F. Salazar, B. Schenke, 2207.03712

Pb+Pb → Pb+Pb+J/ψ

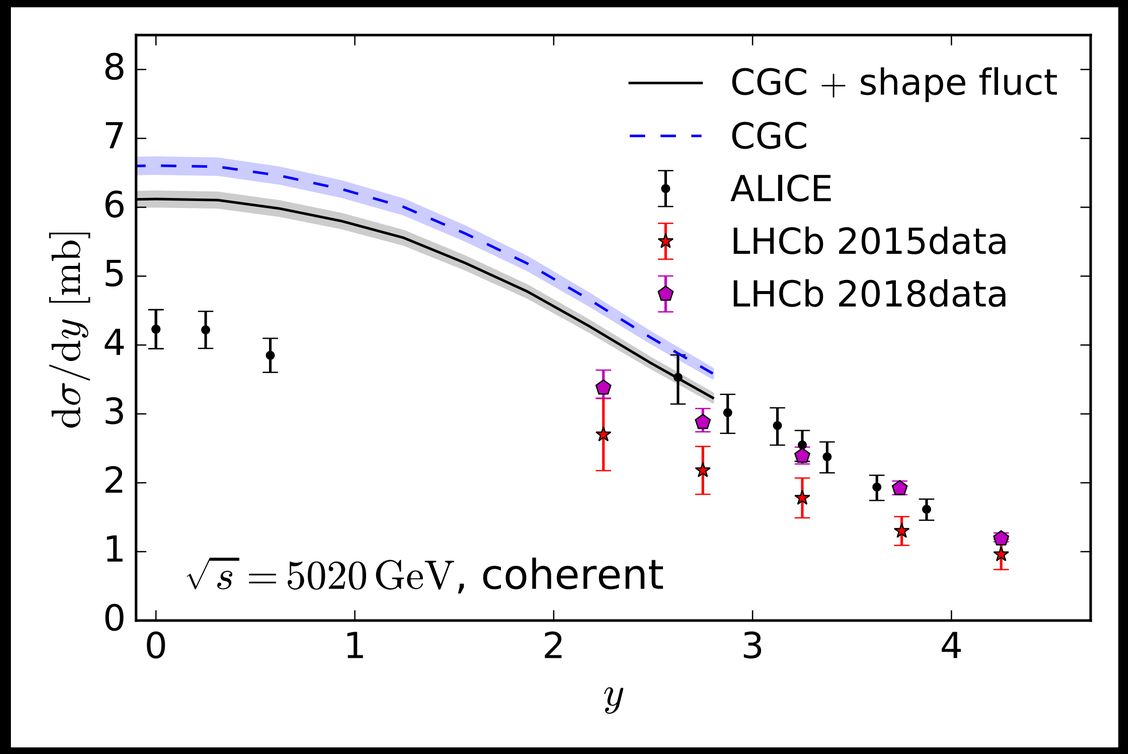

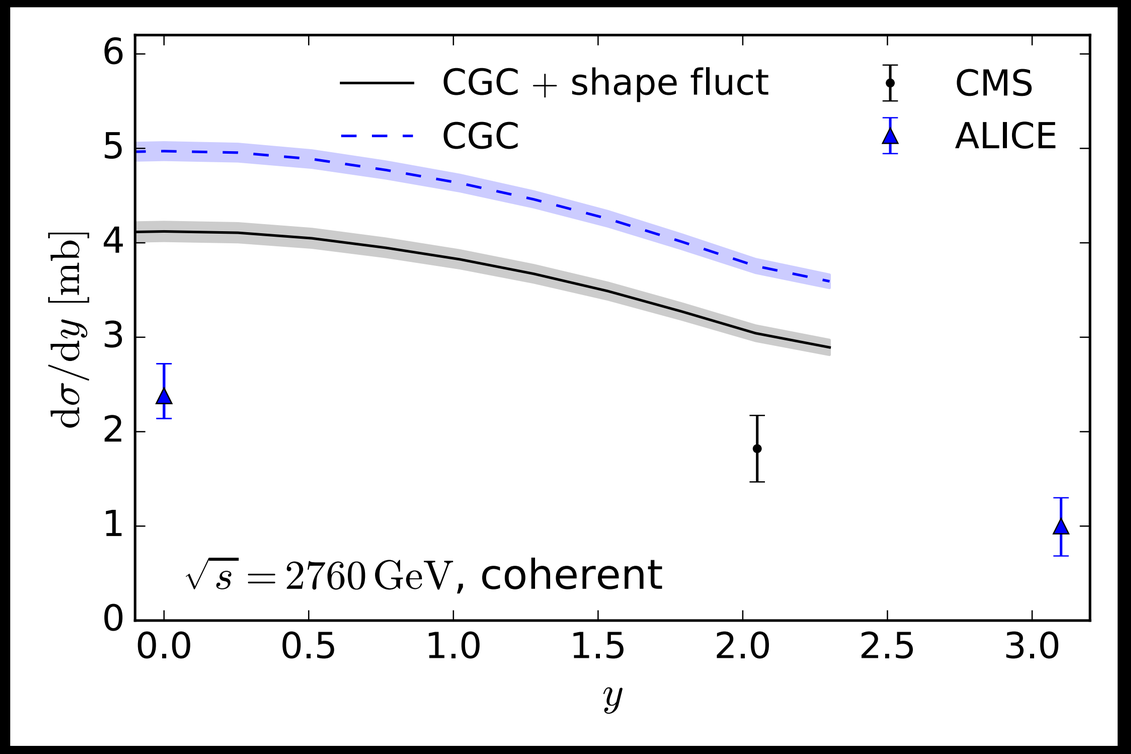

Larger suppression when including shape fluctuations: Hotter hot spots; larger local Q_s

ALICE arXiv:2101.04577; Phys. Lett. B798 (2019) 134926; Phys. Lett. B718 (2013) 1273;
Eur. Phys. J. C73 (2013) no. 11 2617; CMS, Phys. Lett. B772 (2017) 489; LHCb arXiv:2107.03223;
X. Wang, "Quarkonia production in (ultra)peripheral PbPb collisions at LHCb." Presented at DIS2022

|t| integrated incoherent cross section

H. Mäntysaari, F. Salazar, B. Schenke, 2207.03712

Pb+Pb → Pb+Pb+J/ψ

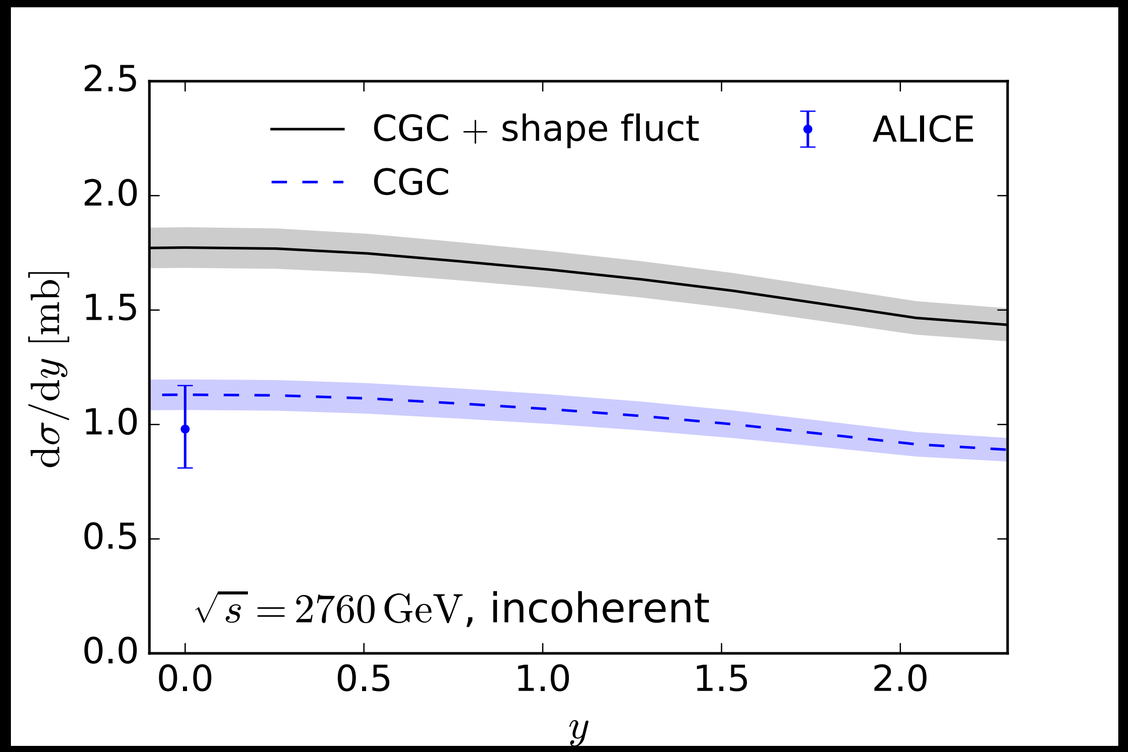

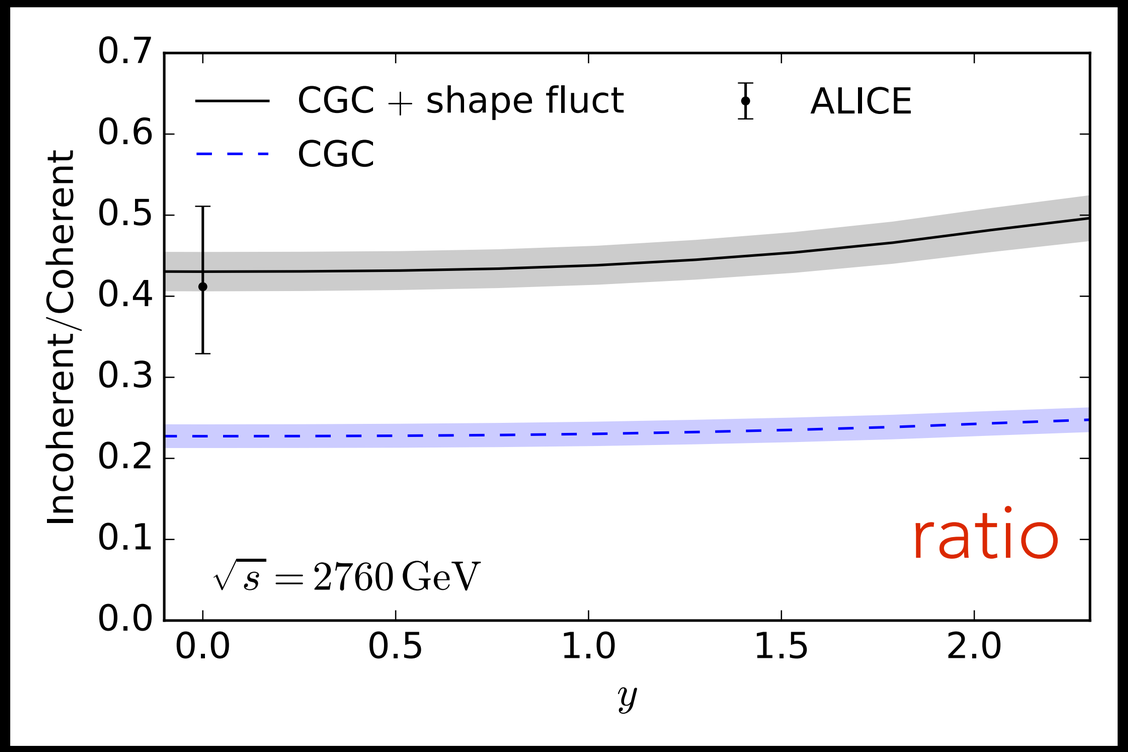

More fluctuations when including shape fluctuations → larger incoherent cross section

Ratio of coherent to incoherent well described (both coh. and incoh. overestimated)

ALICE Eur. Phys. J. C73 (2013) no. 11 2617

Pb+Pb UPCs at midrapidity

H. Mäntysaari, F. Salazar, B. Schenke, 2207.03712

ALICE Collaboration, Phys.Lett.B 817 (2021) 136280

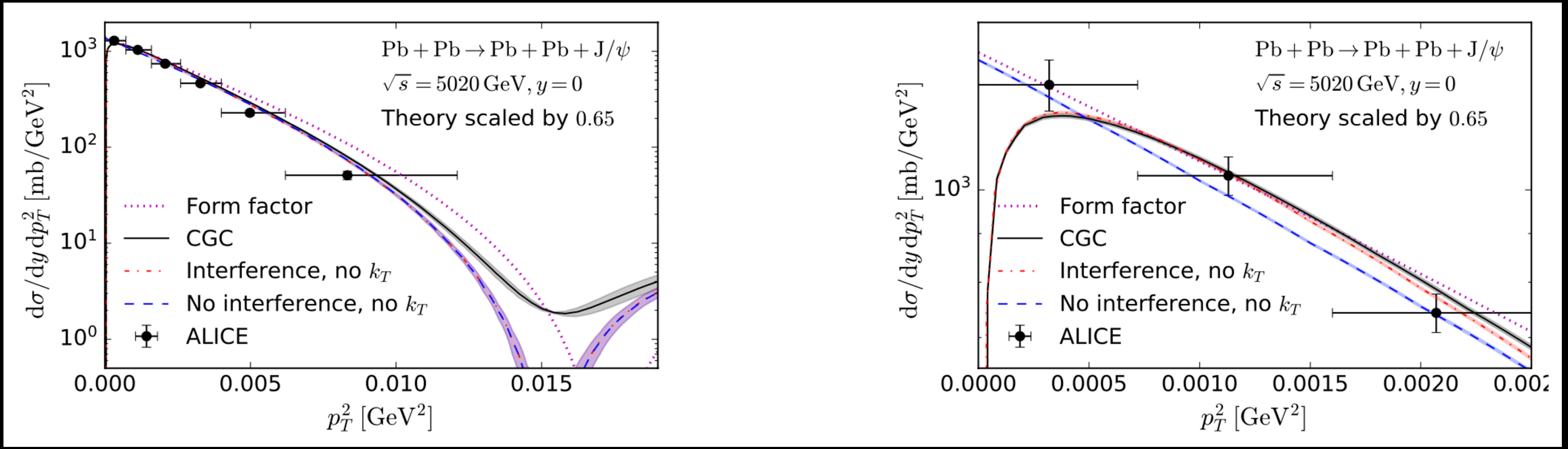

- UPC: Photon $k_T \leq 1/R_A \neq 0$k: important around dips, small effect on p_T integrated σ
- Interference (both nuclei can emit γ): $d\sigma/dp_T^2 \to 0$ when $p_T \to 0$
  Stronger effect predicted than seen in the ALICE data
- Calculated spectra not steep enough, although the ALICE γ + Pb data was well described
  ⇒ photon k_T effect included differently?
- Need a larger Pb than what we get with standard Woods-Saxon parameters

Coherent cross section away from mid rapidity

H. Mäntysaari, F. Salazar, B. Schenke, 2207.03712

LHCb Collaboration, arXiv:2206.08221

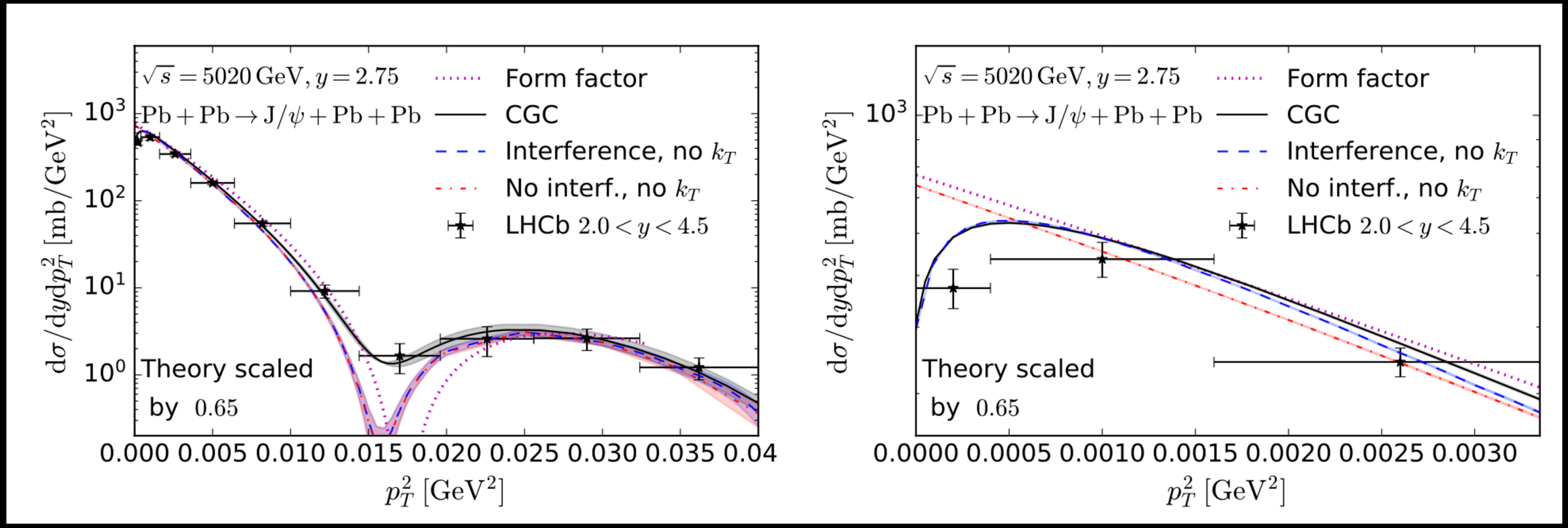

- Good agreement with LHCb data in forward region
- But note: Calculation limited to $|y| < 2.79$ to have $x > 0.01$

Effect of the nuclear size

H. Mäntysaari, F. Salazar, B. Schenke, 2207.03712

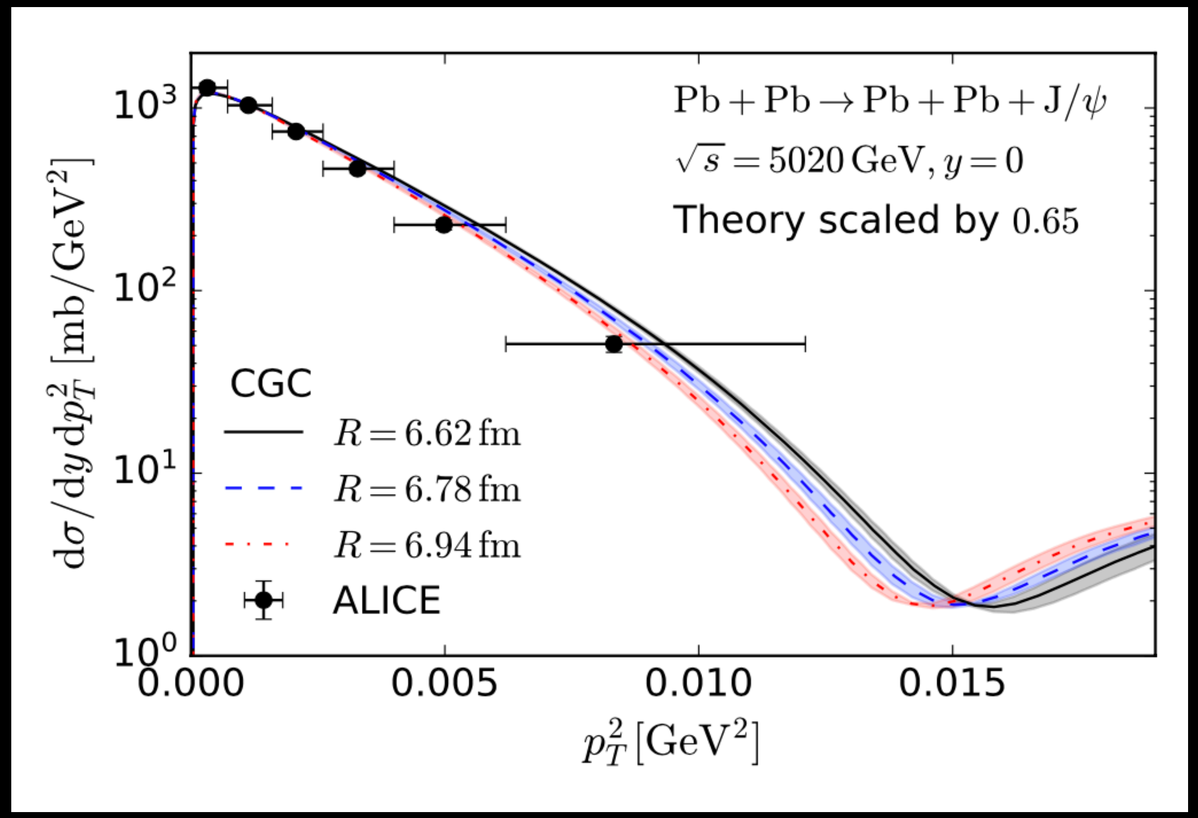

ALICE Collaboration, Phys.Lett.B 817 (2021) 136280

- Steep enough spectrum obtained with a larger nucleus
- Neutron skin effect?

STAR measurements of diffractive photo production of ρ mesons and study of interference patterns in the angular distribution of $\rho^0 \to \pi^+\pi^-$ decays
also indicate that strong-interaction nuclear radii of Au and U are larger than the charge radii
STAR Collaboration, 2204.01625

Comparing to RHIC results

H. Mäntysaari, F. Salazar, B. Schenke, 2207.03712

STAR data: W. Schmidke, Presentation at the CFNS Workshop on Photon-Induced Interactions, April 2021.

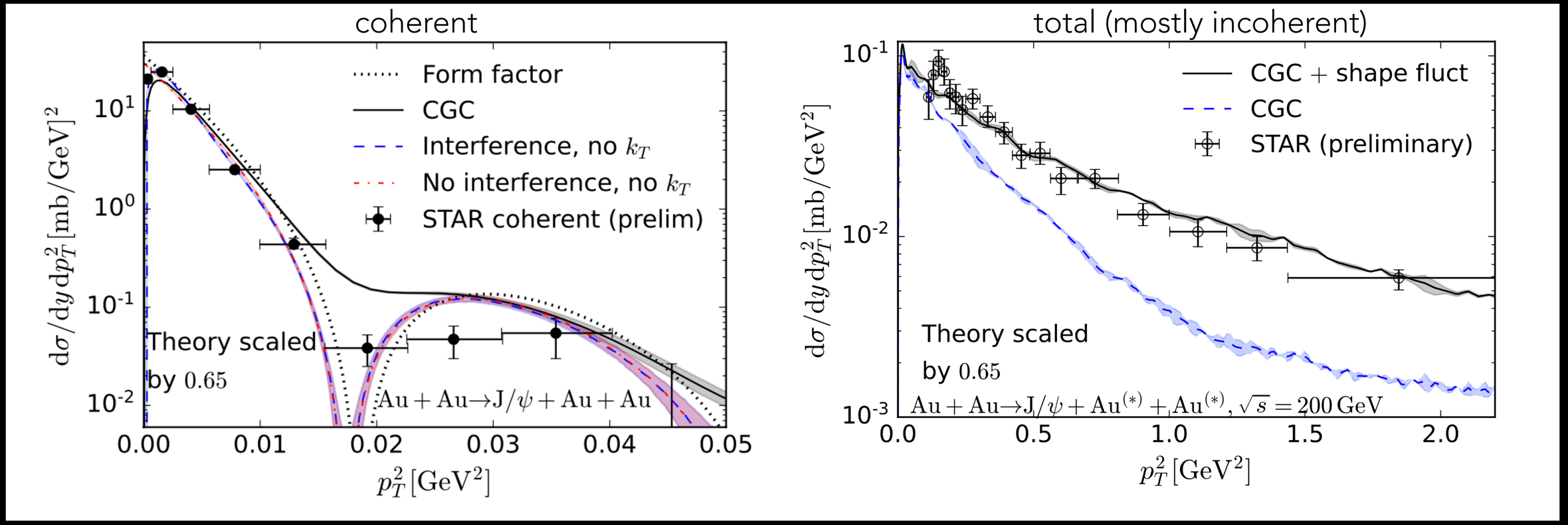

- Normalization scaled down (from HERA) same way as for comparison to ALICE data
- Inclusion of interference effect improves agreement with STAR data
- Photon k_T effect seems too strong
- Incoherent well described with subnucleon fluctuations included

Photoproduction of J/ψ in d+Au collisions at STAR

H. Mäntysaari, B. Schenke, Phys. Rev. C101, 015203 (2020)

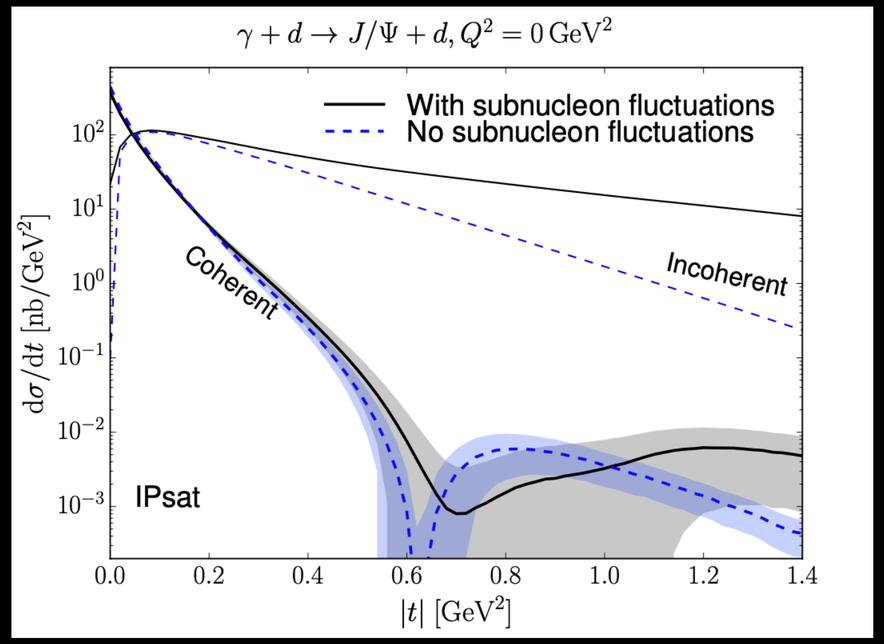

Can also access details of deuteron wave function

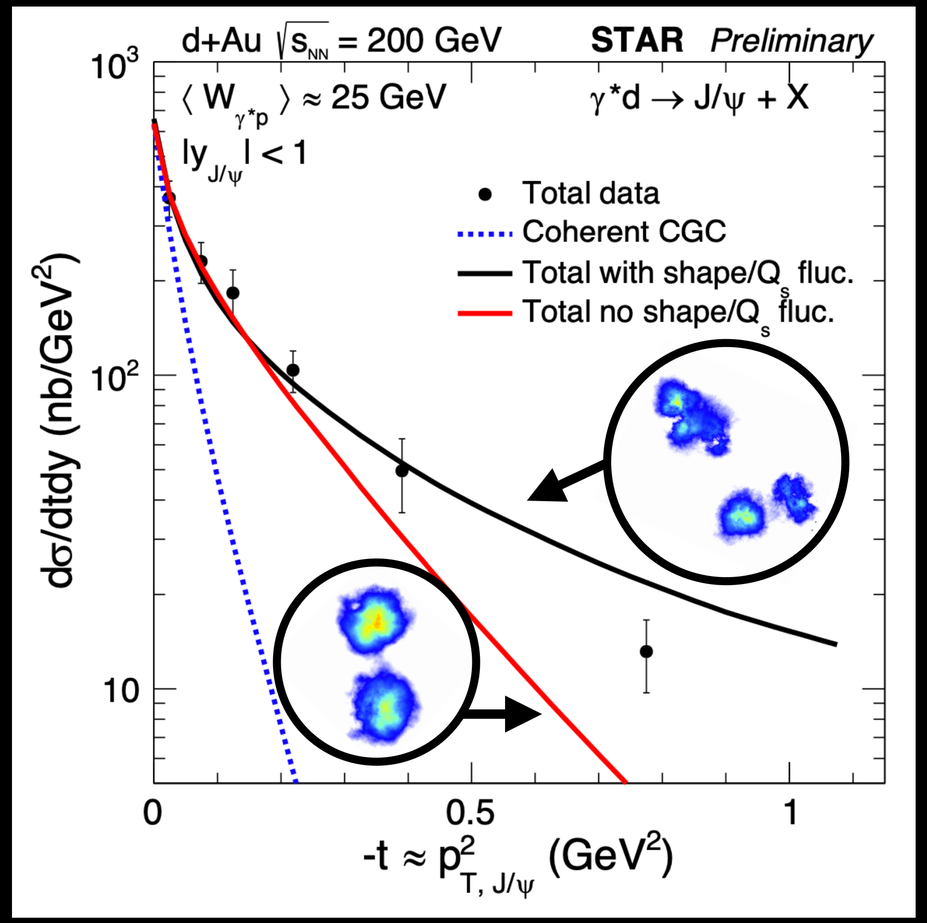

Substructure: large effect on incoherent at $|t| \gtrsim 0.25\mathrm{GeV}^2$ (as in Pb)

STAR data favors substructure

STAR Collaboration at Hard Probes 2020
PoS HardProbes2020 (2021) 100; arXiv:2009.04860

Photoproduction of J/ψ in d+Au collisions at STAR

H. Mäntysaari, B. Schenke, Phys. Rev. C101, 015203 (2020)

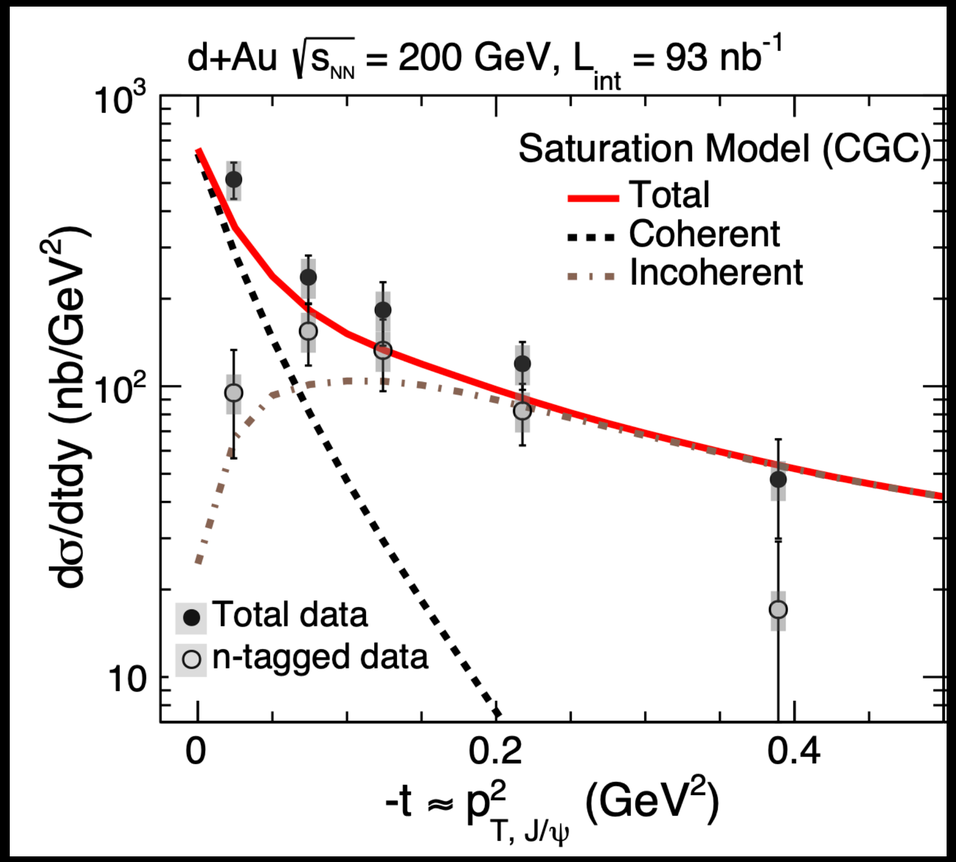

n-tagged results can be compared to incoherent cross section

STAR Collaboration, Phys. Rev. Lett. 128, 122303, e-Print: 2109.07625

3D GLASMA INITIAL STATE

B. SCHENKE, S. SCHLICHTING, PRC94, 044907 (2016)

GLUON FIELDS IN A NUCLEUS AT DIFFERENT *x*:

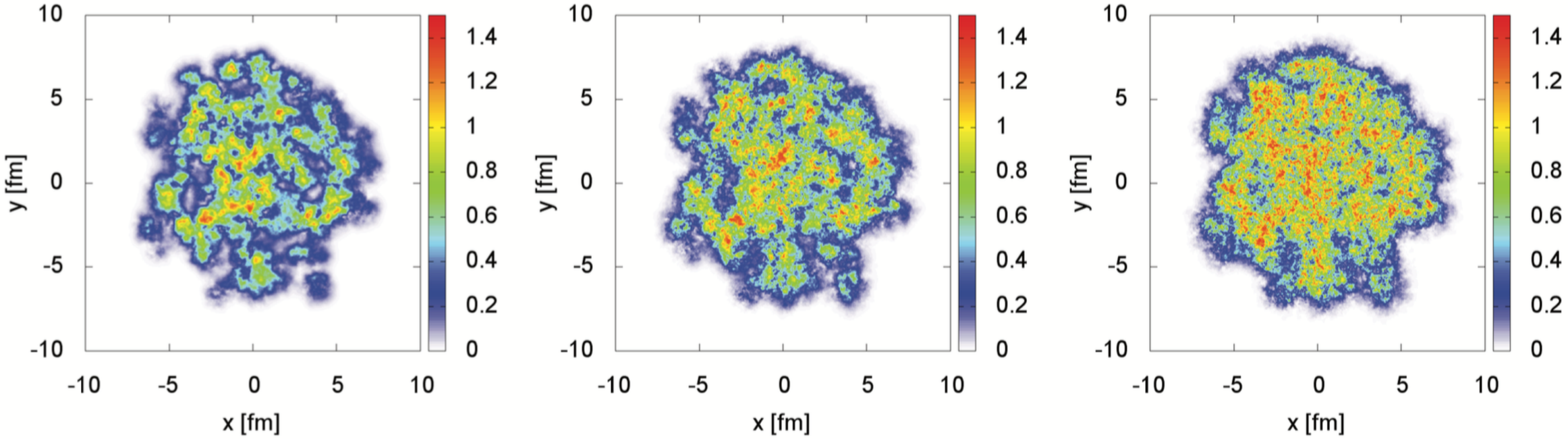

$Y = -2.4$ ($x \approx 2\times10^{-3}$) $Y = 0$ ($x \approx 2\times10^{-4}$) $Y = 2.4$ ($x \approx 1.6\times10^{-5}$)

3D GLASMA INITIAL STATE

B. SCHENKE, S. SCHLICHTING, PRC94, 044907 (2016)

- COLLIDE TWO JIMWLK EVOLVED NUCLEI

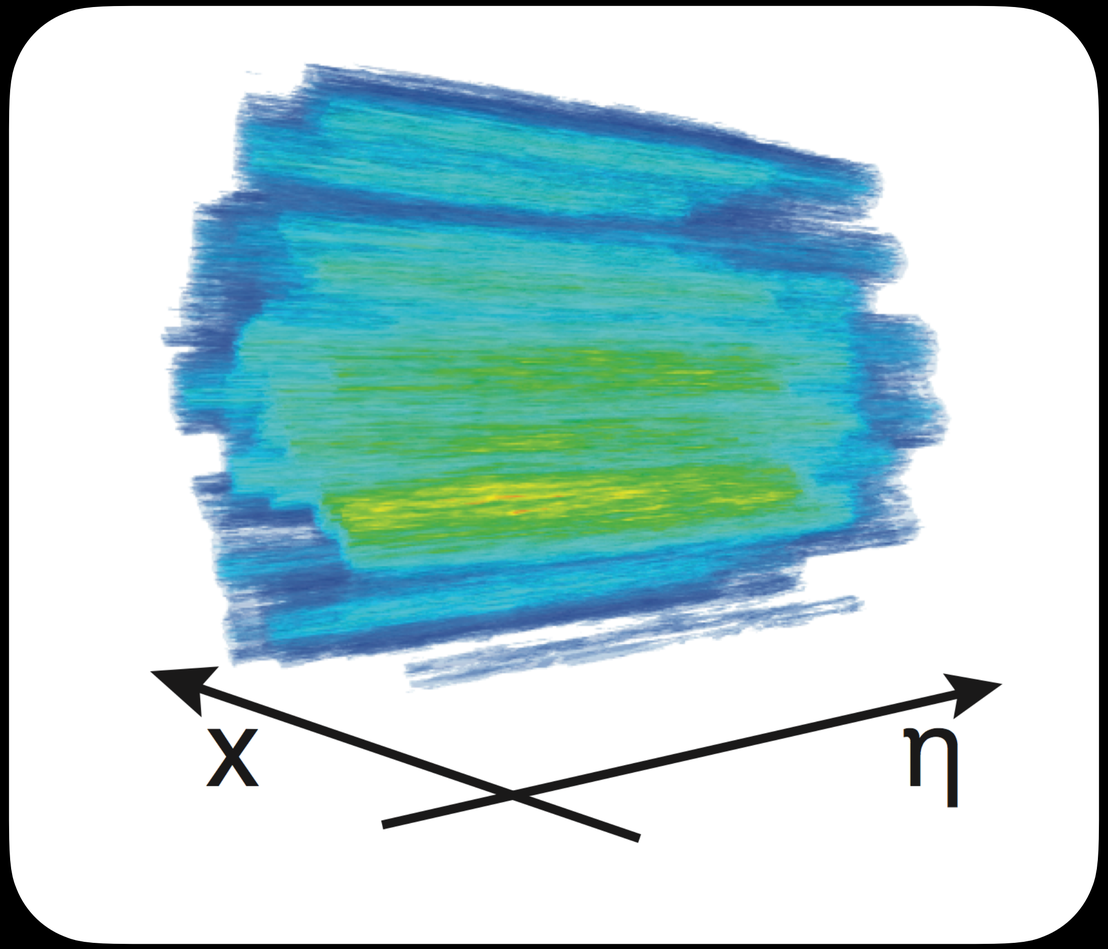

ENERGY DENSITY

GLUON RAPIDITY DISTRIBUTION

B. SCHENKE, S. SCHLICHTING, PRC94, 044907 (2016)

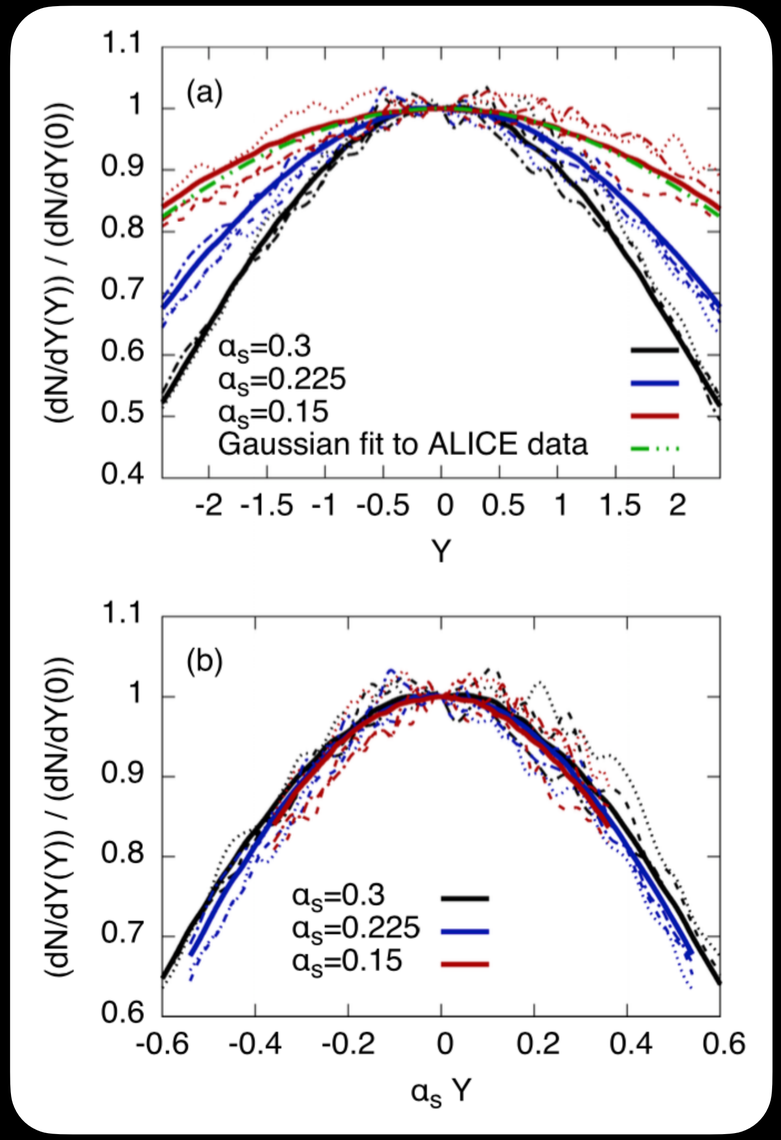

Gluon multiplicity relative to its value at Y = 0

m = 0.4 GeV

Dashed lines show results from three single events for each value of the coupling constant.

EXPERIMENTAL DATA:
ALICE, PHYS. LETT. B 726, 610 (2013)

3D GEOMETRY

B. SCHENKE, S. SCHLICHTING, PRC94, 044907 (2016)

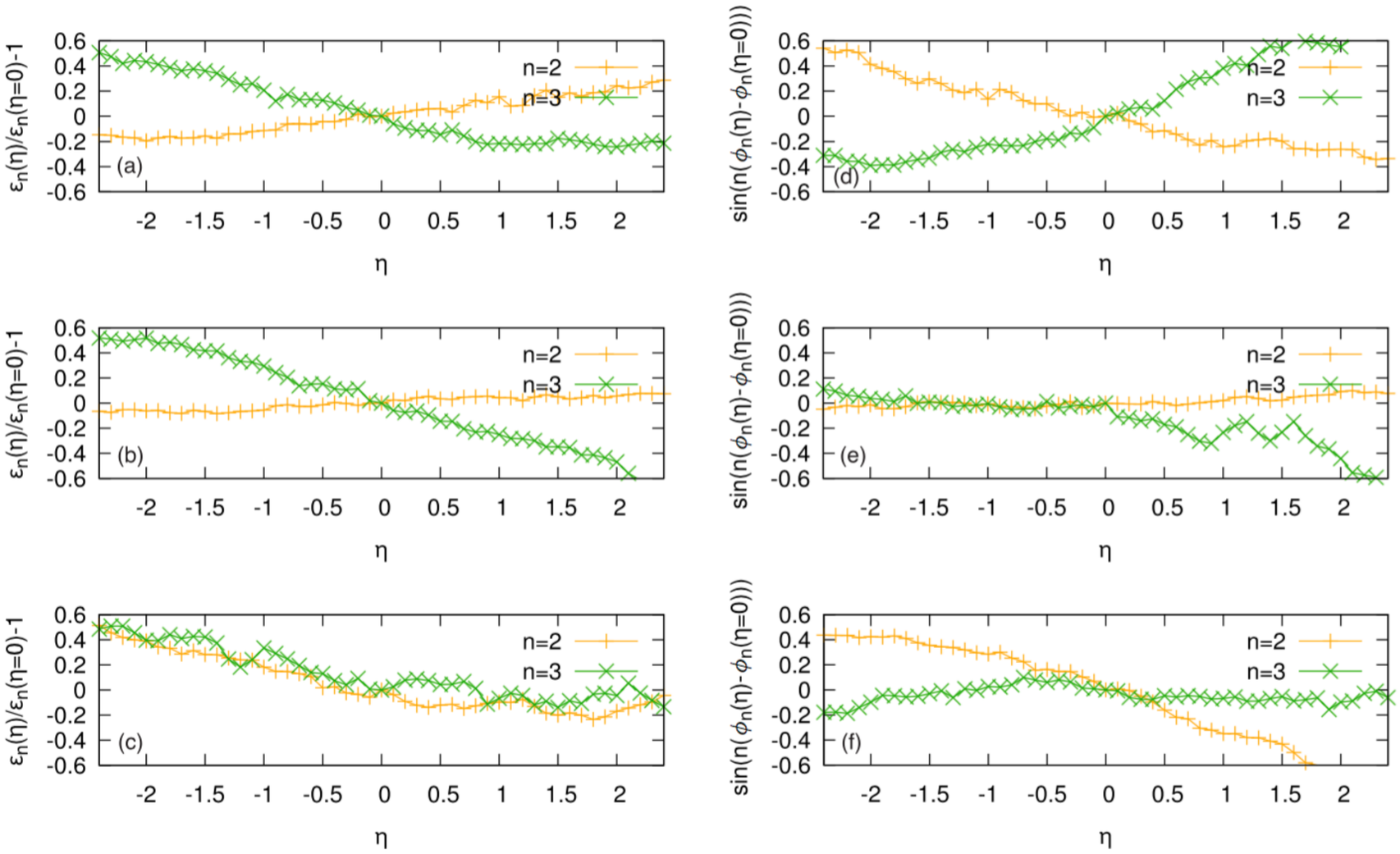

DECORRELATION MEASURE

B. SCHENKE, S. SCHLICHTING, PRC94, 044907 (2016)

$$r_n(\eta_a,\eta_b) = \frac{\langle \mathrm{Re}[\boldsymbol{\epsilon}_n(-\eta_a)\cdot\boldsymbol{\epsilon}_n^*(\eta_b)]\rangle}{\langle \mathrm{Re}[\boldsymbol{\epsilon}_n(\eta_a)\cdot\boldsymbol{\epsilon}_n^*(\eta_b)]\rangle}$$

$$= \frac{\langle \epsilon_n(-\eta_a)\epsilon_n(\eta_b)\cos\{n[\phi_n(-\eta_a)-\phi_n(\eta_b)]\}\rangle}{\langle \epsilon_n(\eta_a)\epsilon_n(\eta_b)\cos\{n[\phi_n(\eta_a)-\phi_n(\eta_b)]\}\rangle}$$

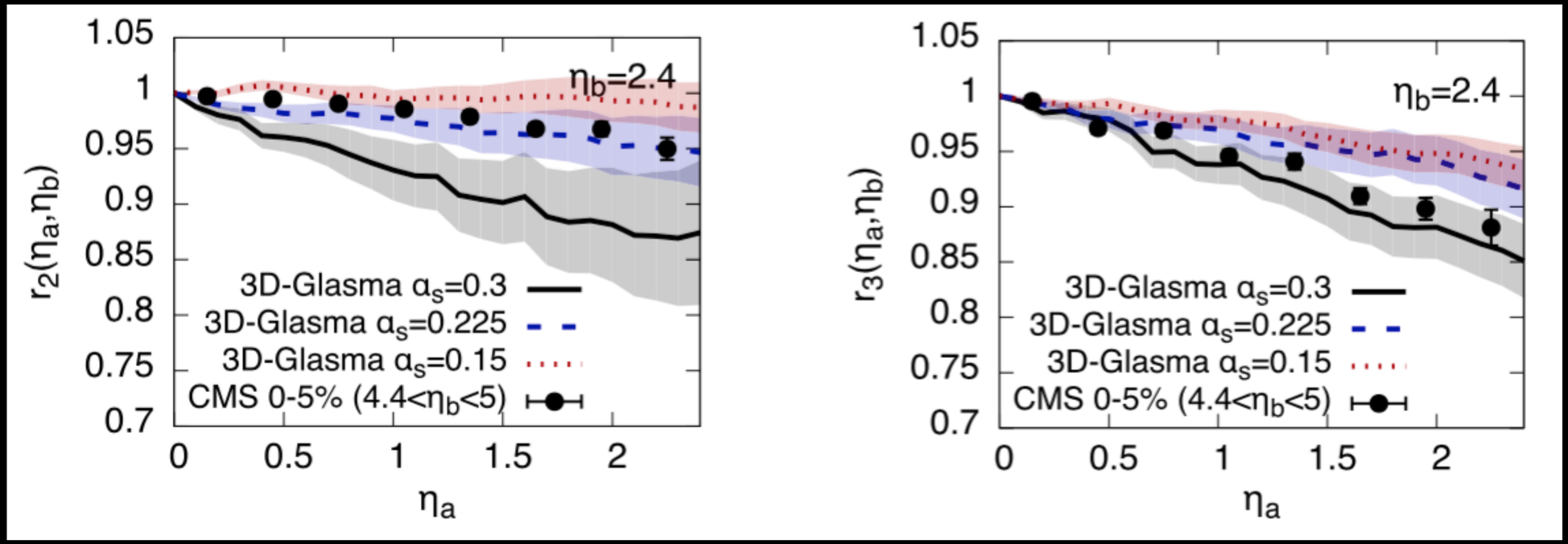

EXPERIMENTAL DATA: CMS COLLABORATION, PHYS. REV. C 92, 034911 (2015)

More theory developments

TMD-CGC correspondence

From light-like Wilson lines to transverse gauge links

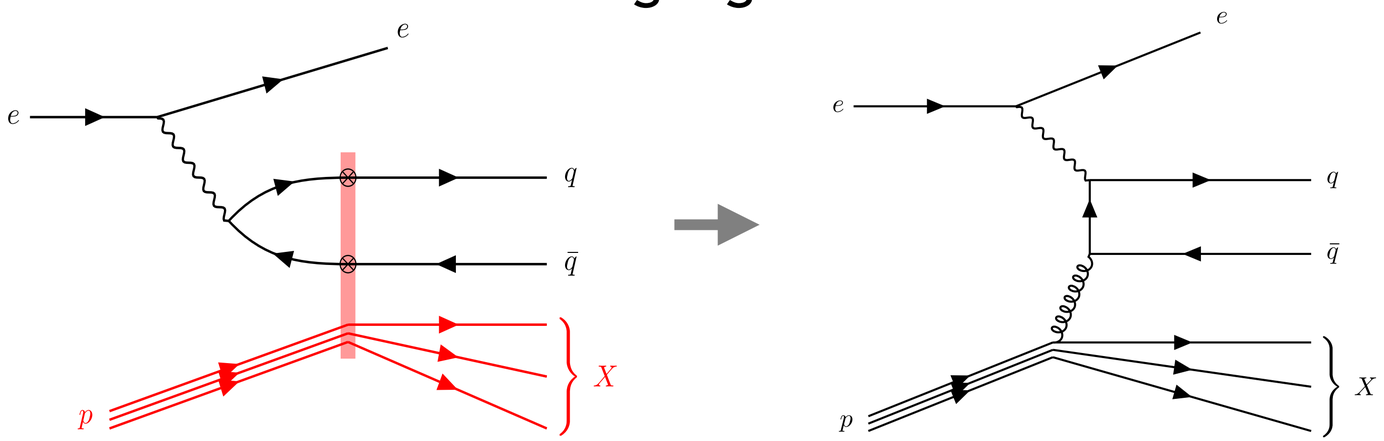

Wilson line is

$$V(\boldsymbol{z}_\perp) = \mathcal{P}\exp\left(ig\int_{-\infty}^{\infty} \mathrm{d}z^- A^{+,a}(z^-, \boldsymbol{z}_\perp)t^a\right)$$

TMD:

$$\mathbb{1} - V\left(\boldsymbol{x}_\perp\right)V^\dagger\left(\boldsymbol{y}_\perp\right) = \underbrace{ig\boldsymbol{r}_\perp^i \tilde{\boldsymbol{A}}_\perp^i}_{\text{TMD}} + \mathcal{O}\left(\boldsymbol{r}_\perp^2\right)$$

Dominguez, Marquet, Xiao, Yuan (2011)

Higher orders in r_T expansion?
Cumbersome to organize in a way which preserves explicit QCD gauge invariance for the involved operators

where $\tilde{\boldsymbol{A}}_\perp^i = \frac{i}{g}V\partial^i V^\dagger$ $\qquad \boldsymbol{r}_\perp = \boldsymbol{x}_\perp - \boldsymbol{y}_\perp$

TMD-CGC correspondence

From light-like Wilson lines to transverse gauge links

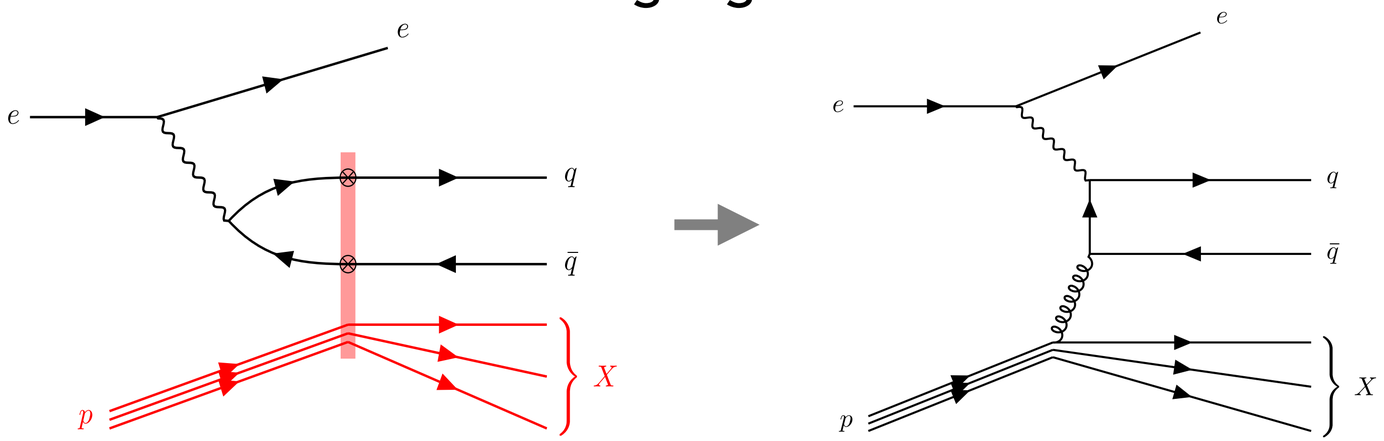

CGC: Can express dipole correlator as transverse gauge link at $x^- = -\infty$:

$$V(\boldsymbol{x}_\perp)V^\dagger(\boldsymbol{y}_\perp) = \mathcal{P}\,\exp\left[-ig\int_{\boldsymbol{y}_\perp}^{\boldsymbol{x}_\perp} \mathrm{d}\boldsymbol{z}_\perp \cdot \tilde{\boldsymbol{A}}_\perp(\boldsymbol{z}_\perp)\right]$$

Boussarie, Mehtar-Tani (2020)

Improved TMD: Then one can write:

$$\mathbb{1} - V(\boldsymbol{x}_\perp)V^\dagger(\boldsymbol{y}_\perp) = \underbrace{ig\int_{\boldsymbol{y}_\perp}^{\boldsymbol{x}_\perp} \mathrm{d}\boldsymbol{z}^i_\perp \tilde{\boldsymbol{A}}^i_\perp(\boldsymbol{z}_\perp)}_{\text{ITMD}}$$

Altinoluk, Boussarie, Kotko (2019)

$$+\underbrace{g^2\int_{\boldsymbol{y}_\perp}^{\boldsymbol{x}_\perp} \mathrm{d}\boldsymbol{z}^i_{1\perp}\int_{\boldsymbol{y}_\perp}^{\boldsymbol{z}_{1\perp}} \mathrm{d}\boldsymbol{z}^j_{2\perp}\tilde{\boldsymbol{A}}^i_\perp(\boldsymbol{z}_{1\perp})V(\boldsymbol{z}_{1\perp})V^\dagger(\boldsymbol{z}_{2\perp})\tilde{\boldsymbol{A}}^j_\perp(\boldsymbol{z}_{2\perp})}_{\text{genuine higher twists (g.h.t.)}}$$

TMD-CGC correspondence: Inclusive dijet production

TMD and ITMD as an expansion of the CGC:

$$\mathrm{d}\sigma_{\mathrm{CGC}} = \underbrace{\mathrm{d}\sigma_{\mathrm{TMD}} + \overbrace{\mathcal{O}\left(\frac{k_\perp}{Q_\perp}\right)}^{\text{kinematic}}}_{\mathrm{d}\sigma_{\mathrm{ITMD}}} + \overbrace{\mathcal{O}\left(\frac{Q_s}{Q_\perp}\right)}^{\text{genuine}}$$

Dominguez, Marquet, Xiao, Yuan (2011)

TMD valid $k_\perp, Q_s \ll Q_\perp$

back-to-back hadrons/jets and transverse momenta larger than sat scale

Hard factor — Weizsäcker-Williams gluon TMD

$$d\sigma^{\gamma^* A\to q\bar{q}X} \sim \mathcal{H}^{ij}_{\mathrm{TMD}}(\boldsymbol{P}_\perp)\, \alpha_s x G^{ij}_{\mathrm{WW}}(x, \boldsymbol{k}_\perp) + \mathcal{O}(k_\perp/P_\perp) + \mathcal{O}(Q_s/P_\perp)$$

Altinoluk, Boussarie, Kotko (2019)

Improved TMD valid $Q_s \ll Q_\perp$

transverse momenta larger than sat scale

Boussarie, Mäntysaari, Salazar, Schenke (2021)

Hard factor resums kinematic powers $k_\perp/P_\perp$

$$d\sigma^{\gamma^*_\lambda A\to q\bar{q}X} \sim \mathcal{H}^{\lambda,ij}_{\mathrm{ITMD}}(\boldsymbol{P}_\perp, \boldsymbol{k}_\perp)\, \alpha_s x G^{ij}_{\mathrm{WW}}(x, \boldsymbol{k}_\perp) + \mathcal{O}(Q_s/P_\perp)$$

TMD-CGC correspondance

Boussarie, Mäntysaari, Salazar, Schenke (2021)

$$\frac{\mathrm{d}N^{\gamma^*_\lambda + A \to q\bar{q}+X}}{\mathrm{d}^2\boldsymbol{P}_\perp \mathrm{d}^2\boldsymbol{k}_\perp \mathrm{d}\eta_1 \mathrm{d}\eta_2} = N_0^\lambda(P_\perp, k_\perp) + 2\sum_{n=1}^{\infty} N_n^\lambda(P_\perp, k_\perp)\cos(n\phi)$$

Differential yield

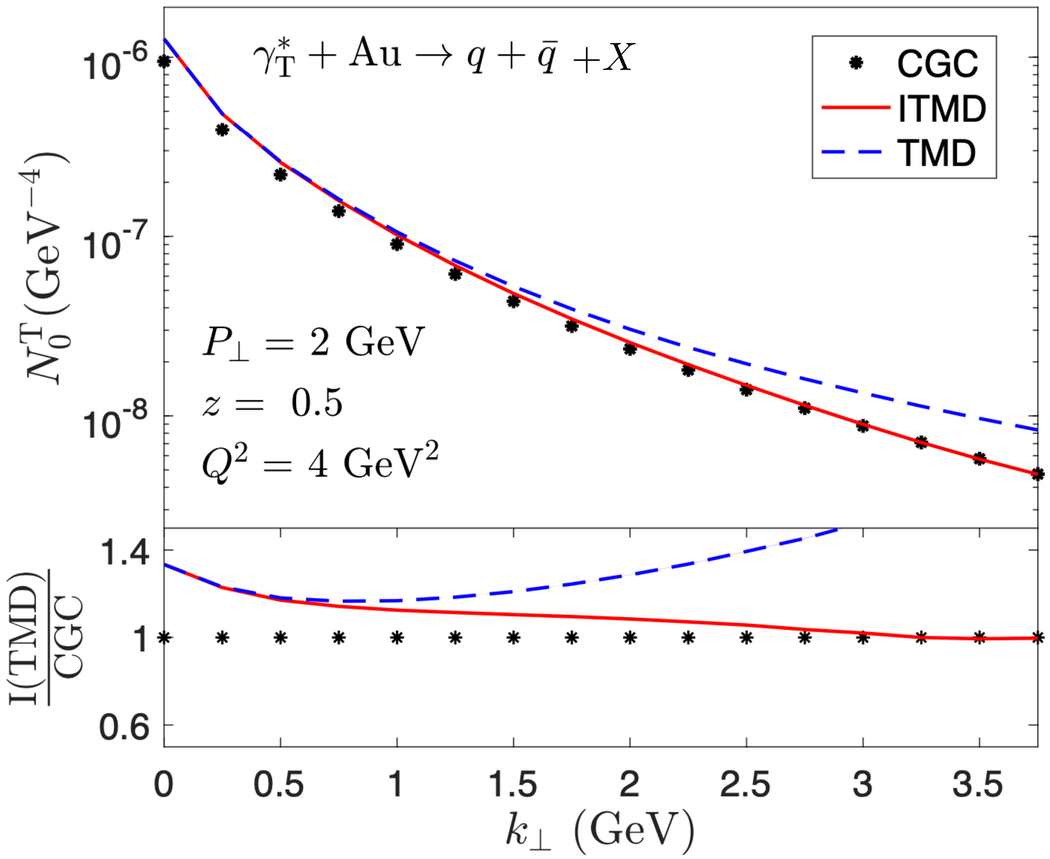

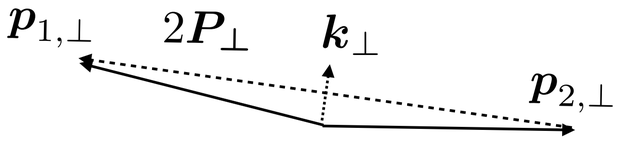

$$\phi = \phi_{\boldsymbol{P}_\perp} - \phi_{\boldsymbol{k}_\perp}$$

$$v_{2,\lambda} = \langle \cos 2\phi \rangle = N_2^\lambda / N_0^\lambda$$

$$v_{4,\lambda} = \langle \cos 4\phi \rangle = N_4^\lambda / N_0^\lambda$$

Momentum imbalance azimuthal anisotropies

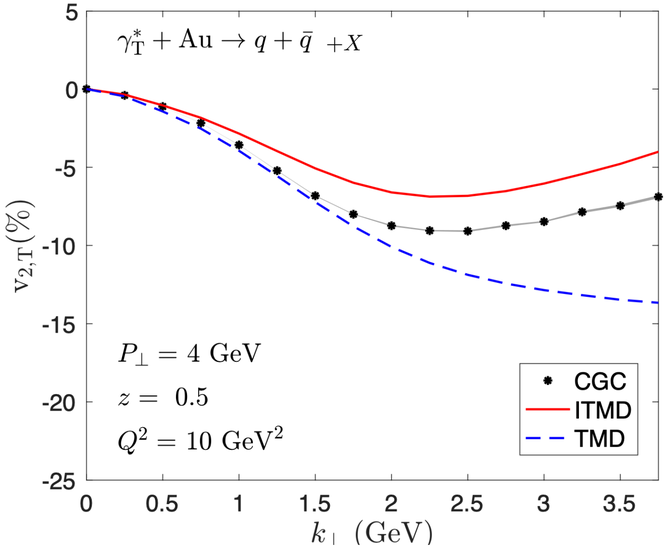

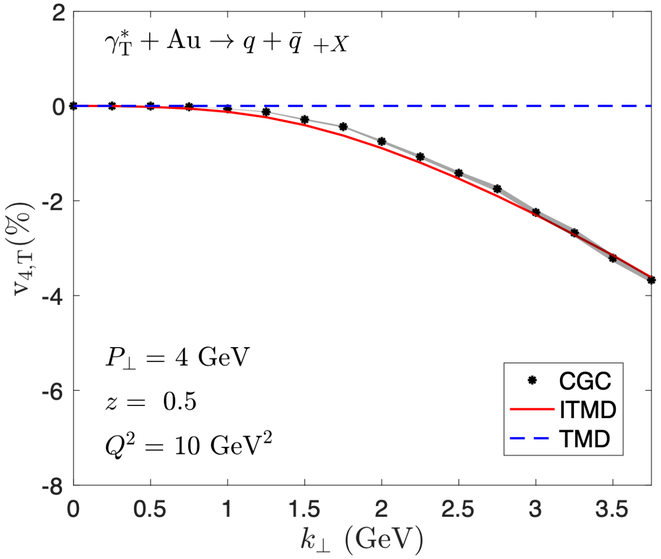

CGC shows further suppression relative to TMD in back-to-back limit

Theory developments

Calculations within the color glass condensate are moving to NLO:

NLO Impact factors for

- Fully inclusive DIS **Balitsky, Chirilli; Beuf; Hänninen, Lappi, Paatelainen**
- Semi inclusive single particle production in p+A
  Chirilli, Xiao, Yuan; Altinoluk, Armesto, Beuf, Kovner, Lublinsky; Hänninen, Lappi, Paatelainen
- Photon+dijet prodution in e+A **Roy, Venugopalan**
- Exclusive light vector meson and dijet production
  Boussarie, Grabovsky, Ivanov, Szymanowski, Wallon

NLO evolution equations

- NLL Wilson line evolution **Balitsky, Chirilli**
- NLL dipole evolution **Balitsky, Chirilli**
- NLL 3-point operator evolution **Balitsky, Grabovsky**
- NLL 4-point operator evolution **Grabovsky**
- NLL JIMWLK Hamiltonian (from 4 above results) **Kovner, Lublinsky, Mulian**

Next-to-leading order computations

Structure functions* G. Beuf, H. Hänninen, T. Lappi, H. Mäntysaari, Phys.Rev.D 102 (2020) 074028, arXiv:2007.01645

Fits to HERA data

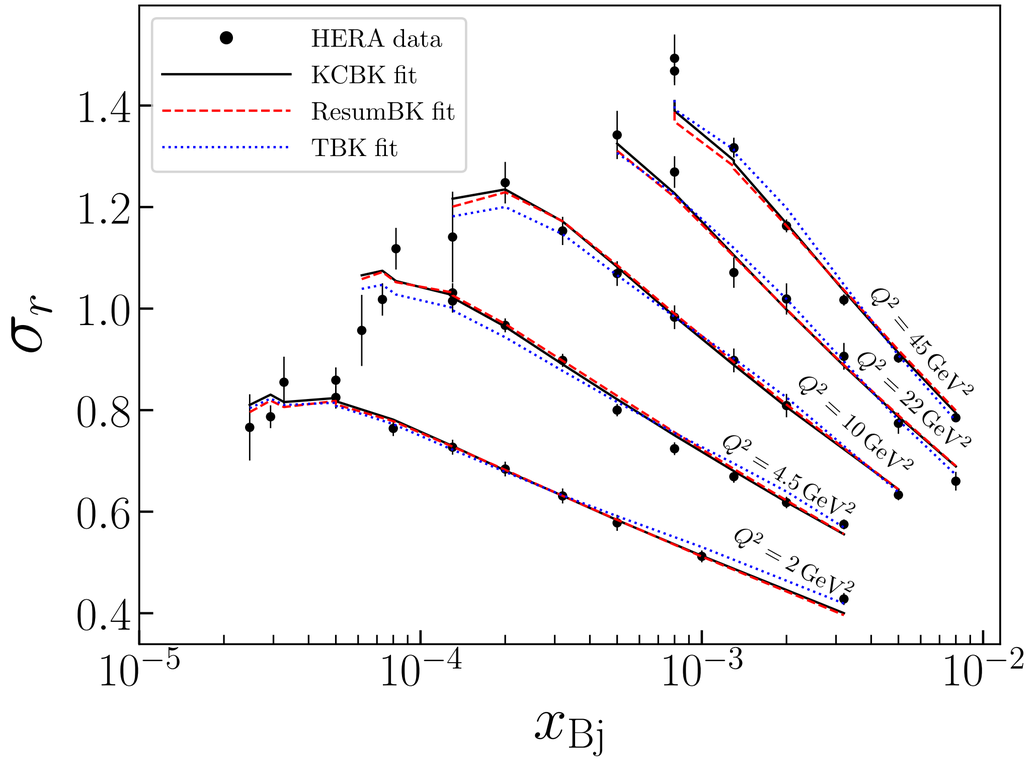

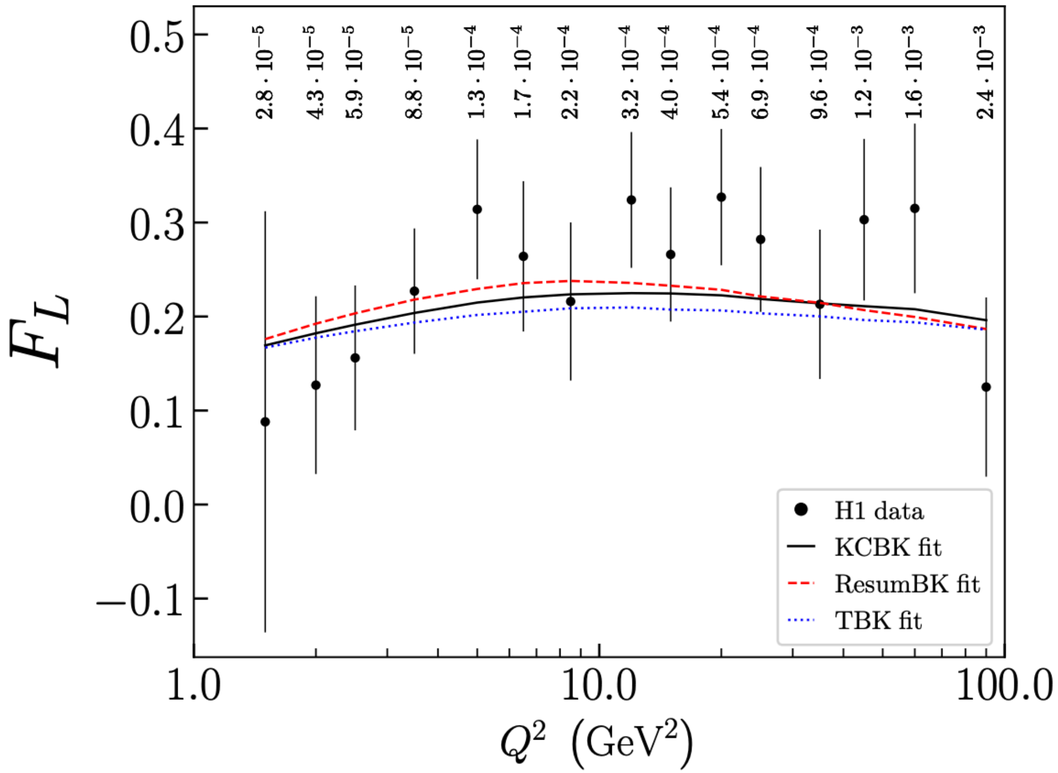

Should be extended to nuclear DIS for EIC predictions!

Study charm structure functions (less sensitive to non-perturbative physics)

* only light-quark contribution

Next-to-leading order computations

Exclusive VM production at NLO*

Mäntysaari, Penttala, Phys.Lett.B 823 (2021) 136723, 2104.02349

Including first QCD correction proportional to the coupling constant α_s, and the first relativistic correction suppressed by the quark velocity v^2

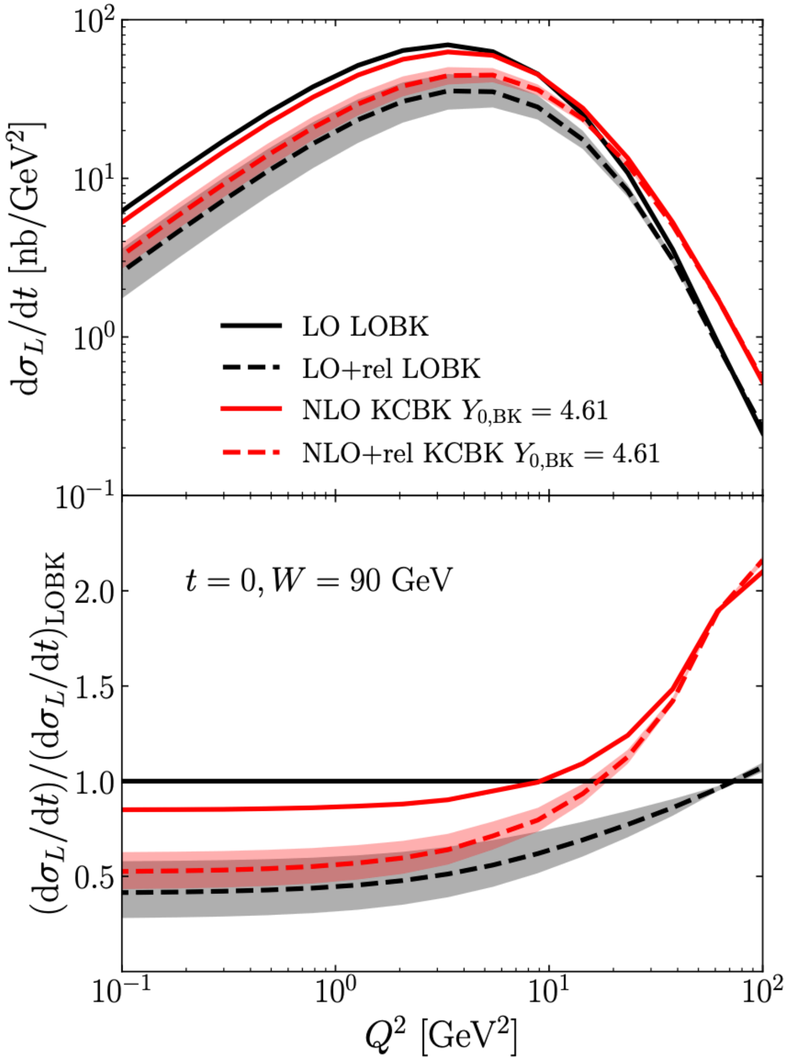

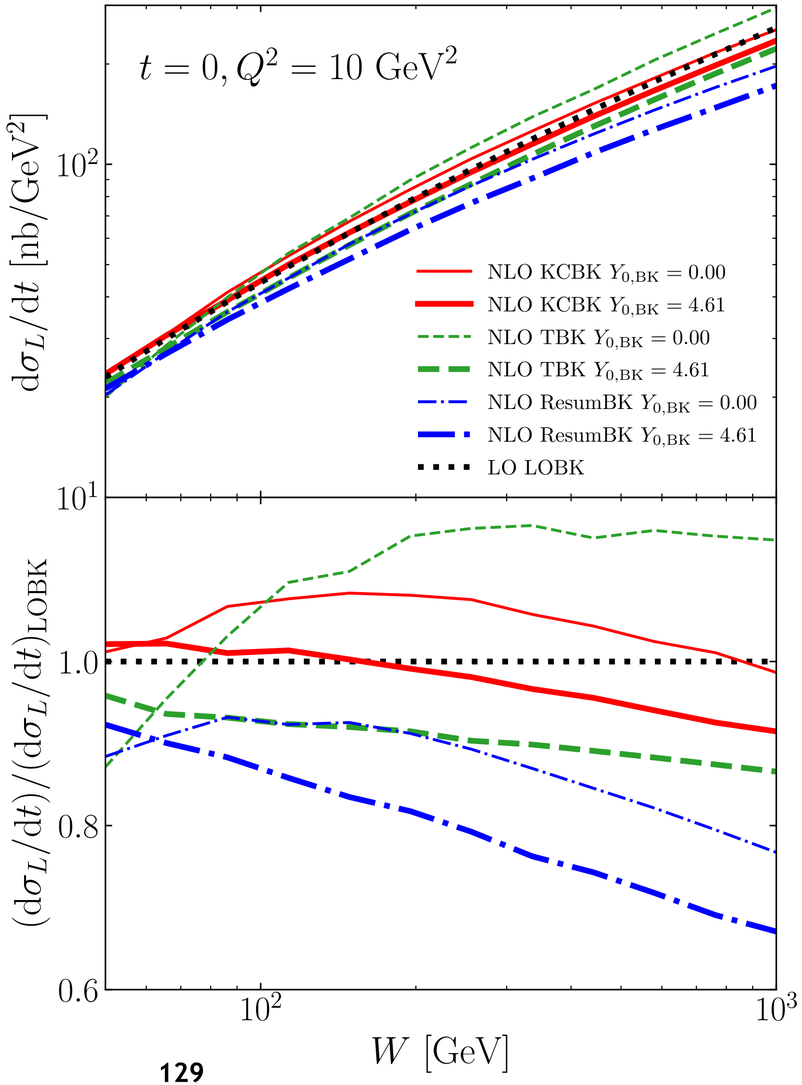

Comparison with HERA data once T pol is theoretically available

*J/Ψ electron production (only L polarization) at NLO

Next-to-leading order computations

Semi-inclusive dijet production Caucal, FS, Venugopala, *JHEP* 11 (2021) 222

Numerically tractable expressions

See also Roy, Venugopalan (2019) for photon+dijet

Computation of real and virtual contributions to dijet production

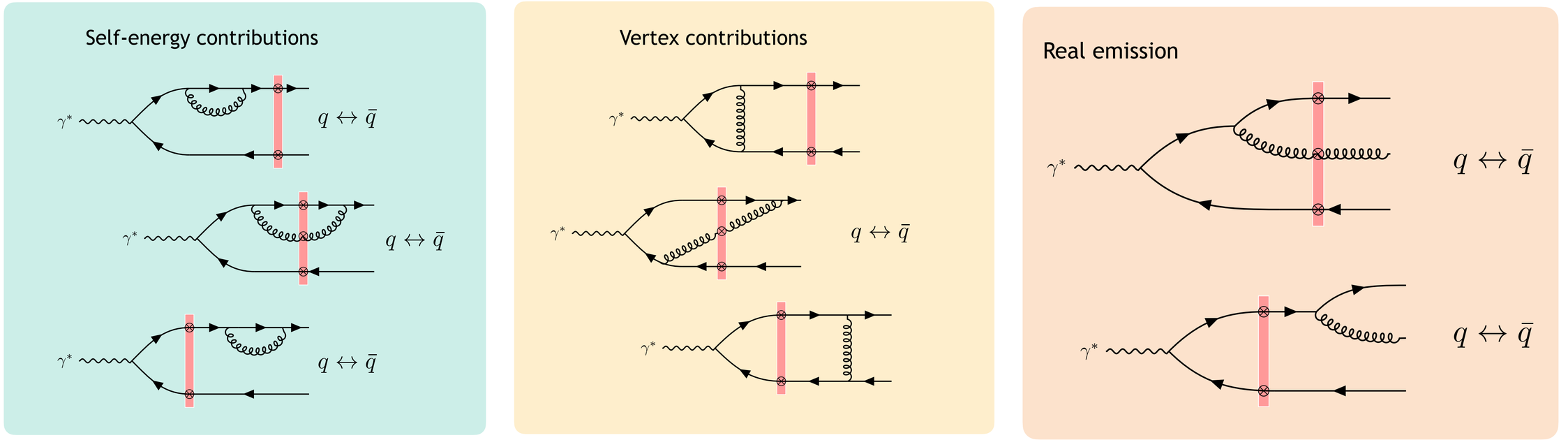

- *Cancellation of divergences: UV, soft and collinear*
- *Slow gluon divergence absorbed in redefinition of sources via Leading Log JIMWLK evolution*
- *Numerically tractable expressions for impact factor*

How large are these corrections?

Numerical results will be available in the near future!

Summary

- Gluon saturation should have imprints on many observables at high energy
- In the CGC framework light-like Wilson lines contain all relevant information
- Wilson line correlators enter all cross sections
- Can use the same framework to describe the initial state of heavy ion collisions and any process in DIS or UPCs at small x

BACKUP

Semi-inclusive DIS

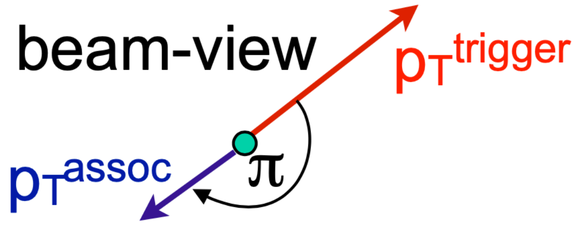

C. Marquet, B. -W. Xiao and F. Yuan, Phys. Lett. B 682 (2009) 207
L. Zheng, E.C. Aschenauer, J.H. Lee, Bo-Wen Xiao, Phys. Rev. D 89, 074037 (2014)

$$J_{eA} = \frac{1}{A^{1/3}} \frac{\sigma_{eA}^{\text{pair}} / \sigma_{eA}}{\sigma_{ep}^{\text{pair}} / \sigma_{ep}}$$

The absence of collective nuclear effects in the back-to-back pair production cross section, $\sigma_{eA}^{\text{pair}}$, corresponds to $J_{eA} = 1$

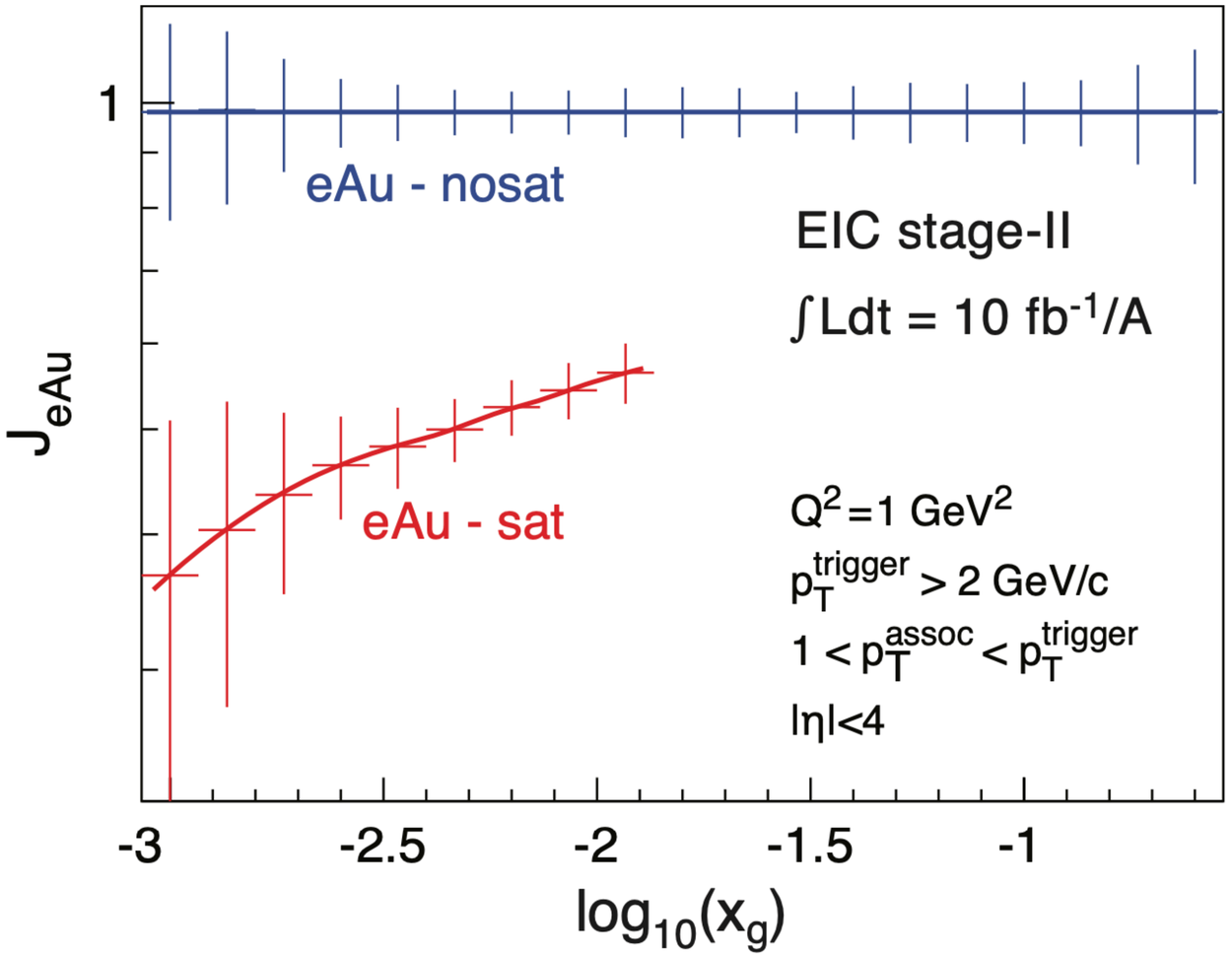

A. Accardi et al., EIC White Paper, Eur.Phys.J.A 52 (2016) 9, 268

Diffractive vector meson production

Exclusive vector meson production:
Allows measurement of momentum transfer *t*

$$\mathbf{t = (p_A - p_{A'})^2 = (p_{VM} + p_{e'} - p_e)^2}$$
$$\approx (p_T(e') + p_T(VM))^2$$

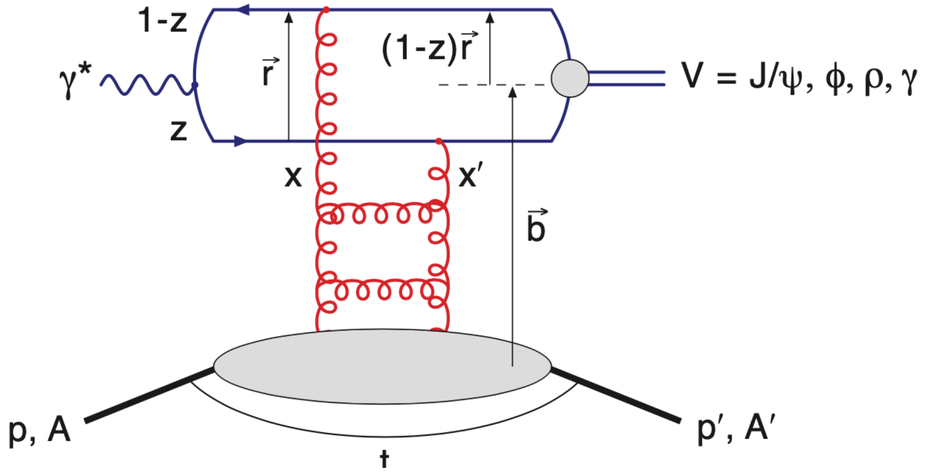

Dipole Cross-Section:

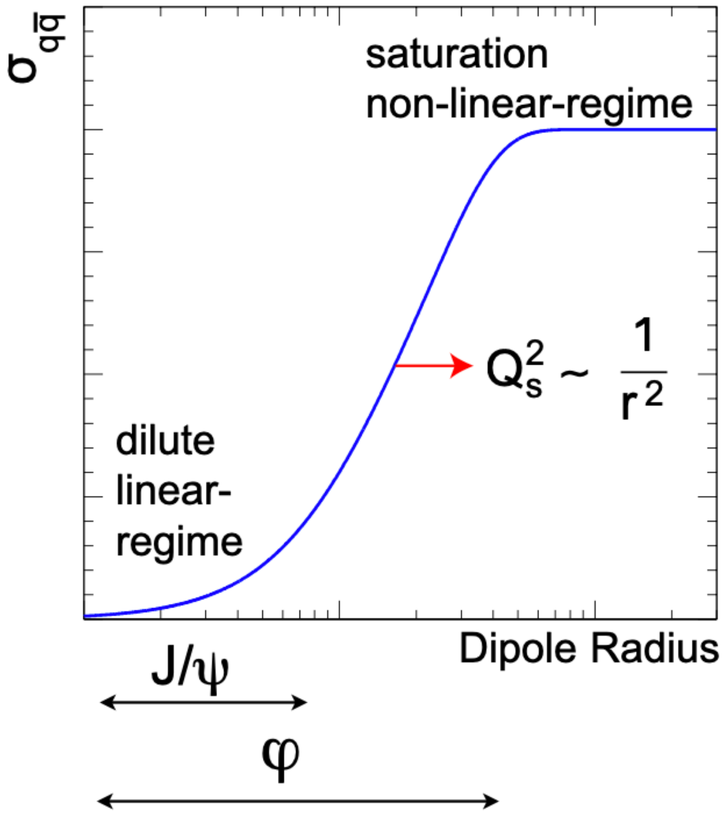

Large dipole sizes: More sensitive to saturation

Large vector meson mass and large Q^2 cut off large dipole sizes

Diffractive vector meson production

T. Toll, T. Ullrich, Phys.Rev.C 87 (2013) 2, 024913
A. Accardi et al., EIC White Paper, Eur.Phys.J.A 52 (2016) 9, 268

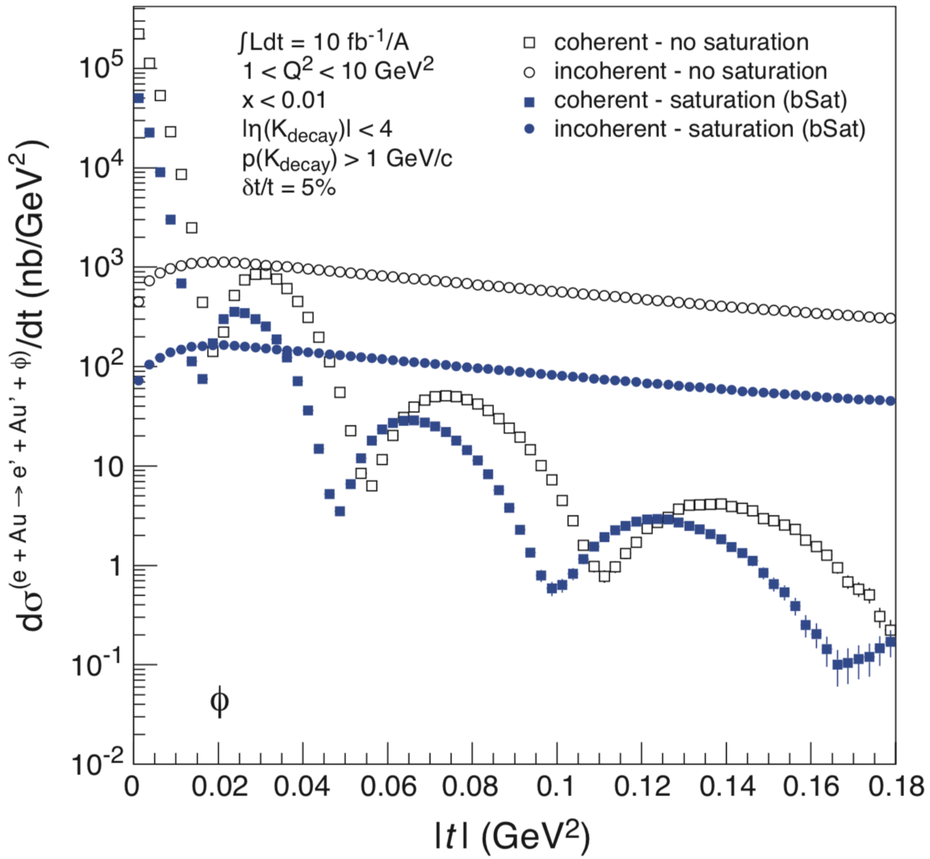

- Coherent |t|-spectrum (target stays intact) is sensitive to the average shape of the target
- Incoherent spectrum is sensitive to fluctuations

Theory developments

Calculations within the color glass condensate are moving to NLO:

NLO Impact factors for

- Fully inclusive DIS **Balitsky, Chirilli; Beuf; Hänninen, Lappi, Paatelainen**
- Semi inclusive single particle production in p+A
  Chirilli, Xiao, Yuan; Altinoluk, Armesto, Beuf, Kovner, Lublinsky; Hänninen, Lappi, Paatelainen
- Photon+dijet prodution in e+A **Roy, Venugopalan**
- Exclusive light vector meson and dijet production
  Boussarie, Grabovsky, Ivanov, Szymanowski, Wallon

NLO evolution equations

- NLL Wilson line evolution **Balitsky, Chirilli**
- NLL dipole evolution **Balitsky, Chirilli**
- NLL 3-point operator evolution **Balitsky, Grabovsky**
- NLL 4-point operator evolution **Grabovsky**
- NLL JIMWLK Hamiltonian (from 4 above results) **Kovner, Lublinsky, Mulian**

Theory developments

First numerical solutions of the Balitsky-Kovchegov (BK) evolution at NLO are becoming available. Can be implemented in fits to HERA structure function data

G. Beuf, H. Hänninen, T. Lappi, H. Mäntysaari
arXiv:2007.01645